

AWARD NUMBER: W81XWH-16-1-0411

TITLE: Targeting Mitochondrial Inhibitors for Metastatic Castrate-Resistant Prostate Cancer

PRINCIPAL INVESTIGATOR: Dr. Samuel R. Denmeade

CONTRACTING ORGANIZATION: Johns Hopkins University
BALTIMORE, MD 21205

REPORT DATE: DECEMBER 2019

TYPE OF REPORT: Final

PREPARED FOR: U.S. Army Medical Research and Materiel Command
Fort Detrick, Maryland 21702-5012

DISTRIBUTION STATEMENT: **Approved for Public Release; Distribution Unlimited**

The views, opinions and/or findings contained in this report are those of the author(s) and should not be construed as an official Department of the Army position, policy or decision unless so designated by other documentation.

REPORT DOCUMENTATION PAGE

Form Approved
OMB No. 0704-0188

Public reporting burden for this collection of information is estimated to average 1 hour per response, including the time for reviewing instructions, searching existing data sources, gathering and maintaining the data needed, and completing and reviewing this collection of information. Send comments regarding this burden estimate or any other aspect of this collection of information, including suggestions for reducing this burden to Department of Defense, Washington Headquarters Services, Directorate for Information Operations and Reports (0704-0188), 1215 Jefferson Davis Highway, Suite 1204, Arlington, VA 22202-4302. Respondents should be aware that notwithstanding any other provision of law, no person shall be subject to any penalty for failing to comply with a collection of information if it does not display a currently valid OMB control number. **PLEASE DO NOT RETURN YOUR FORM TO THE ABOVE ADDRESS.**

1. REPORT DATE DECEMBER 2019		2. REPORT TYPE FINAL		3. DATES COVERED 15AUG2016 - 14AUG2019	
4. TITLE AND SUBTITLE Targeting Mitochondrial Inhibitors for Metastatic Castrate-Resistant Prostate Cancer				5a. CONTRACT NUMBER	
				5b. GRANT NUMBER W81XWH-16-1-0411	
				5c. PROGRAM ELEMENT NUMBER	
6. AUTHOR(S) Dr. Samuel Denmeade email: denmesa@jhmi.edu				5d. PROJECT NUMBER	
				5e. TASK NUMBER	
				5f. WORK UNIT NUMBER	
7. PERFORMING ORGANIZATION NAME(S) AND ADDRESS(ES) Johns Hopkins University Baltimore, MD 21218				8. PERFORMING ORGANIZATION REPORT NUMBER	
9. SPONSORING / MONITORING AGENCY NAME(S) AND ADDRESS(ES) U.S. Army Medical Research and Materiel Command Fort Detrick, Maryland 21702-5012				10. SPONSOR/MONITOR'S ACRONYM(S)	
				11. SPONSOR/MONITOR'S REPORT NUMBER(S)	
12. DISTRIBUTION / AVAILABILITY STATEMENT Approved for Public Release; Distribution Unlimited					
13. SUPPLEMENTARY NOTES					
14. ABSTRACT The overarching challenge and focus area for this Partnering PI-Idea Development Award proposal is to rapidly develop novel therapeutic agents and validate these in pre-clinical studies needed to initiate clinical development of these agents for metastatic castrate resistant prostate cancer (mCRPC). The hypothesis of the present proposal is that an innovative and effective therapeutic approach is possible by covalently coupling niclosamide and 7 hydroxy-β-Lapachone (7OH β-Lap) analog lipophilic mitochondria toxins (MT) to human serum albumin (HSA) via a PSA specific peptide linker sequence to systemically deliver these novel agents via the blood so that these cell penetrant MTs are restrictively released only via enzymatically active PSA within extracellular fluid (ECF) at sites of mCRPC. The advantage of ECF hydrolysis is that only a fraction of cancer cells need to secrete PSA since its enzymatic activity amplifies the level of liberated cell penetrant MTs within the ECF shared by all cells within the metastatic site overcoming the problem of tumor cell heterogeneity by inducing a substantial "bystander effect".					
15. SUBJECT TERMS- NONE LISTED					
16. SECURITY CLASSIFICATION OF:			17. LIMITATION OF ABSTRACT	18. NUMBER OF PAGES	19a. NAME OF RESPONSIBLE PERSON
a. REPORT U	b. ABSTRACT U	c. THIS PAGE U			USAMRMC
			UU	11	19b. TELEPHONE NUMBER (include area code)

Table of Contents

	<u>Page</u>
1. Introduction.....	3
2. Keywords.....	3
3. Accomplishments.....	3-9
4. Impact.....	10
5. Changes/Problems.....	N/A
6. Products.....	10
7. Participants & Other Collaborating Organizations.....	11
8. Special Reporting Requirements.....	12
9. Appendices.....	12-61

Introduction

The overarching challenge and focus area for this Partnering PI-Idea Development Award proposal is to rapidly develop novel therapeutic agents and validate these in pre-clinical studies needed to initiate clinical development of these agents for metastatic castrate resistant prostate cancer (mCRPC). The hypothesis of proposal is that an innovative and effective therapeutic approach is possible by covalently coupling niclosamide and 7 hydroxy- β -Lapachone (7OH β -Lap) analog lipophilic mitochondria toxins (MT) to human serum albumin (HSA) via a PSA specific peptide linker sequence to systemically deliver these novel agents via the blood so that these cell penetrant MTs are restrictively released only via enzymatically active PSA within extracellular fluid (ECF) at sites of mCRPC. The advantage of ECF hydrolysis is that only a fraction of cancer cells need to secrete PSA since its enzymatic activity amplifies the level of liberated cell penetrant MTs within the ECF shared by all cells within the metastatic site overcoming the problem of tumor cell heterogeneity by inducing a substantial “bystander effect”.

Keywords

Metastatic castration resistant prostate cancer, mitochondria toxins, human serum albumin, PSA-activated prodrugs

Accomplishments

- **What were the major goals of the project?**

Specific Aim 1. Synthesis of HSA-coupled PSA cleavable niclosamide payload-1.

Specific Aim 2. Synthesis of HSA-coupled PSA cleavable 7OH- β -Lapachone Payload-2

Specific Aim 3. Evaluate each of HSA-couple PSA cleavable MT payloads for: 1) efficiency of PSA cleavage; 2) *in vitro* therapeutic efficacy as monotherapy vs. combinational therapy against a series of human mCRPC cell lines, 3) *in vivo* therapeutic efficacy vs. host toxicity as monotherapy vs. combinational therapy against a series of human mCRPC xenografts growing both subcutaneously and within the tibia; and 4) plasma vs. tissue biodistribution.

- **What was accomplished under these goals?**

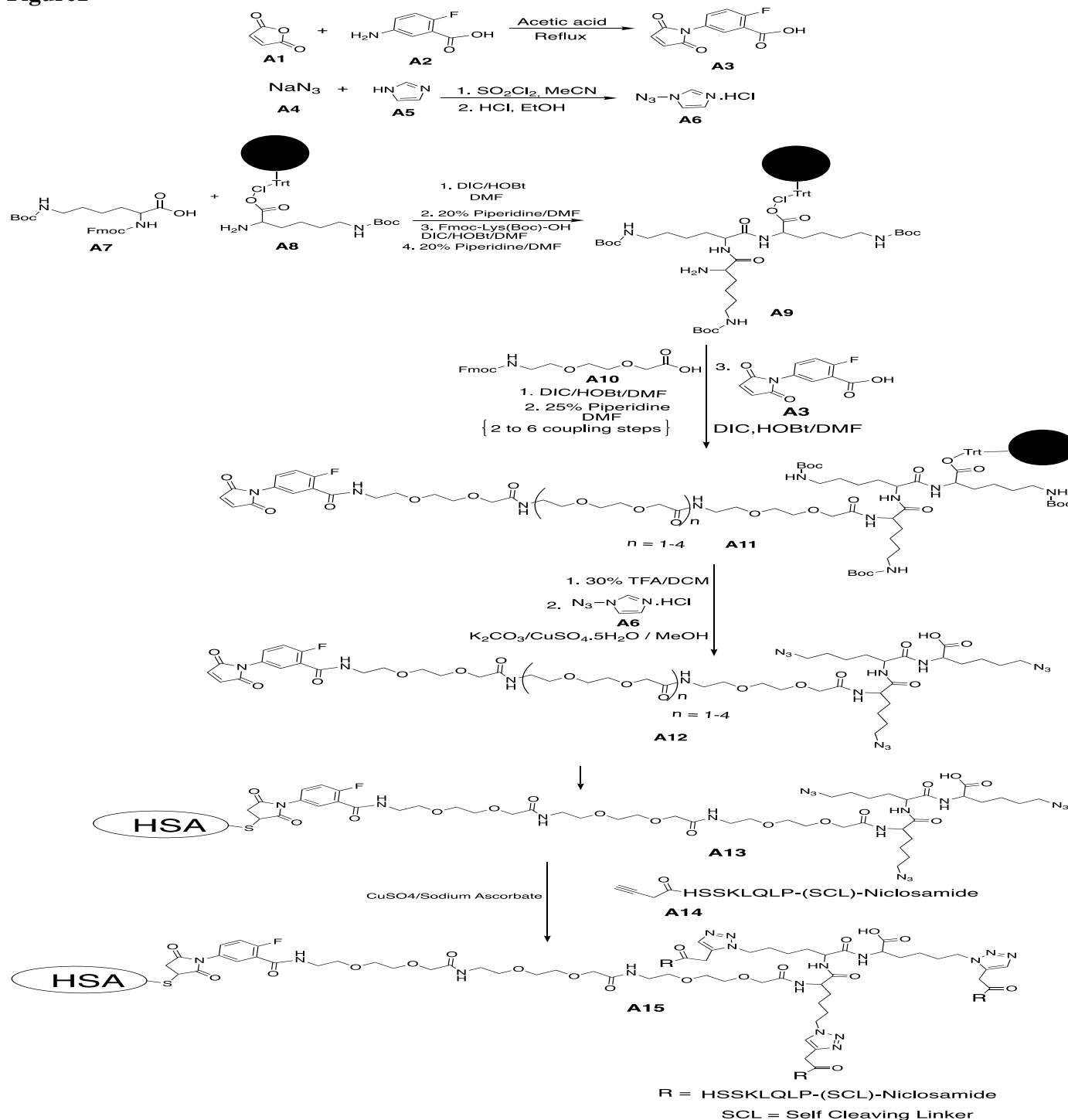
First Year accomplishments: During the first year of support we made significant progress with regard to **specific aim 1** in synthesizing a PSA activatable prodrug of niclosamide coupled to human serum albumin (HSA) to obtain the final drug-HSA conjugate (i.e. **A15 in figure 1**). This requires initial synthesis of HSSKLQLP-(SCL)-Niclosamide (i.e. **compound A14 in Figure 1**) and human serum albumin (HSA) covalently bound via its cysteine residue in position 34 to a PEG based linker ending in a trivalent azide side chain (i.e. **A13 in Figure 1**) followed by coupling of 3 molecules of **A14** per molecule of **A13** to produce **HSA-coupled payload 1 (i.e. A15 in Figure1)**. We synthesized LP-(SCL)-Niclosamide in good yield using ethylene diamine derivatives as the self-cleaving linkers (SCL) and LP as dipeptide substrate for DPPIV and have scaled up the synthesis of LP-(SCL)-Niclosamide to obtain gram quantities that have been coupled to the PSA substrate HSSKLQLP (i.e. HSSKLQLP-(SCL)-Niclosamide aka **A14 in figure 1**).

To synthesize **A13**, the stable maleimide component **A3 in Figure 1** was prepared. Also, the azide transfer reagent **A6** was prepared. Both **A3** and **A6** were synthesized in good yield, and very reproducible. They were characterized with proton and carbon-13 NMR. Using a chlorotriptyl resin solid phase support system, we synthesized the tripeptide molecule containing three lysine molecules. While the α -amino acid was protected with Fmoc, the ϵ -amino terminal of the lysine was protected with Boc. The Fmoc of the N-terminal of the tripeptide was also removed with 20% piperidine in DMF to give **A9**. The tripeptide **A9** was characterized with MALDI-MS. To the N-terminal of **A9** was coupled {2-[2(Fmoc-amino)ethoxy]ethoxy}acetic acid using DIC and HOBt as the coupling reagent. The purpose of this is to incorporate a PEG like molecule as a linker/spacer

to provide room for the coupling of the **A9** to HSA without any steric hindrance. We have used 2 to 6 units of these PEG-2 units between **A9** and the maleimide molecule **A3** so that we can investigate the effect of the length on both the coupling reaction and the kinetics of the cleavage/activation of the final bioconjugate prodrug.

To accomplish this, we began by incorporating two units of the PEG-2 derivative, {2-[2(Fmoc-amino)ethoxy]ethoxy}acetic acid, followed by Fmoc removal, and then the coupling of maleimide derivative **A3** to obtain **A11** where $n = 1$. This was followed by the deprotection of Boc with 30% TFA in dichloromethane, and the purified molecule was treated with the azide transfer reagent **A6** to obtain **A12** with $n = 1$. **A12** was characterized with MALDI-MS and HPLC. The reaction system for the **A12** synthesis is reproducible and was scaled up to obtain gram quantity as stock for conjugation to HSA.

Figure1



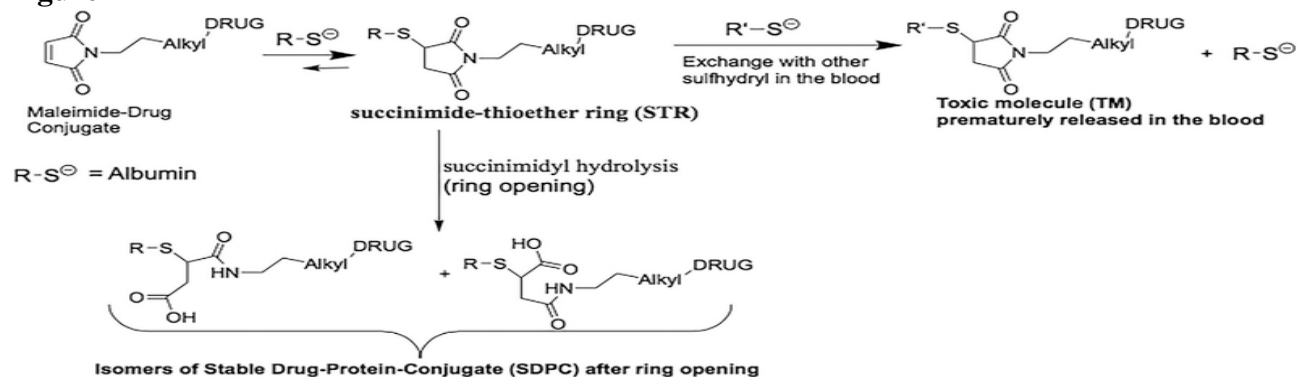
We attempted to conjugate **A12** to the Cysteine-34 of HSA to produce **A13** so that we could couple it to **A14** to produce **A15** aka **HSA-coupled PSA activated niclosamide (i.e. Payload-1)**. Unfortunately, this approach produced insufficient yield of **A13** to proceed. Based upon this discovery, an alternative approach was taken in the second year of support.

Second Year accomplishments: As an alternative approach, Boc-protected N-methyl ethylene diamine (EDA) was coupled to leucylproline (LP) dipeptide and Boc removed to produce a compound which was coupled to the critical aromatic hydroxyl group of niclosamide via an EDA-Carbamate linkage to produce LP-EDAC-niclosamide. The authenticity of this compound was documented by ^1H and ^{13}C NMR and mass spectrometry. Coupling of LP-EDAC to the hydroxyl of niclosamide prevents its anion formation thereby blocking its protonophoric ability. The LP dipeptide was chosen because when the N-terminal of L is covalently linked to the C-terminal Q in the PSA peptide to produce HSSKLQ//LP-EDAC-niclosamide, PSA efficiently hydrolyzes the peptide between Q//L releasing LP-EDAC-niclosamide. Once liberated, LP-EDAC-niclosamide is an excellent substrate for C-terminal cleavage between P and the EDAC linker by either dipeptidyl peptidase IV [DPPIV] whose expression is upregulated on the plasma membrane of prostate cancer cells, or by fibroblast activation protein (FAP) expressed by tumor infiltrating CAF/MSCs within the cancer microenvironment, as we have documented previously. Once, LP-EDAC-niclosamide is hydrolyzed, the liberated EDAC coupled intermediate undergoes **spontaneous self-cleavage** liberating niclosamide. We synthesized LP-(EDAC)-Niclosamide in good yield using ethylene diamine derivatives as the self-cleaving linkers (SCL) and LP as dipeptide substrate for DPPIV and scaled up the synthesis of LP-(SCL)-Niclosamide to obtain gram quantities.

Subsequently, we developed and validated a solid phase synthesis of a resin bound Lys-Pro-Lys-Pro-Lys peptide. The ϵ -amino group of lysine on the solid resin was protected with 1-(4,4-Dimethyl-2,6 dioxocyclohexylidene) ethyl (Dde). Fmoc-Pro-OH and Fmoc-Lys-(Dde)-OH [N-Fmoc-N'-[1-(4,4-Dimethyl-2,6 dioxocyclohexylidene) ethyl]-D-lysine] was then used for subsequent couplings. This was followed by the coupling of N-succinimidyl-PEG-3-monobromomaleimide to the α -amino group of lysine. The Dde was removed with hydrazine in solid phase and the free ϵ -amino group was reacted with N,N-Disuccinimidyl carbonate to convert it to N-succinimidyl carbamate. This activated carbamate was reacted with the free primary amine terminal of histidine, H in HSSKLQ//LP-EDAC-niclosamide with the free ϵ -amino group of lysine (K) Dde protected to form a urea conjugate. Next, the Dde group protecting the ϵ -amino of lysine was removed and the entire compound cleaved off the resin. This was purified by LC using LCMS analysis. We then attempted to couple the purified product to the cysteine 34 sulfhydryl of HSA via the monobromomaleimide to form a succinimide-thioether ring (STR).

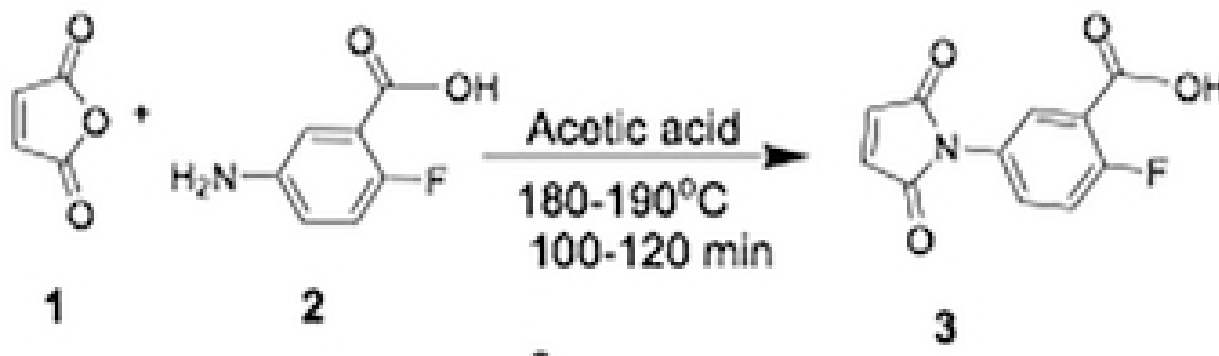
Unfortunately we found that this STR linkage, however, undergoes significant spontaneous cleavage by a retro-Michael reaction under physiologic conditions, **Figure 2**. When this reaction occurs in-vivo, it results in dose-limiting systemic toxicity as the therapeutic agent is spontaneously released to circulate in the blood forming adduct with other sulfhydryl containing species like glutathione, cysteine etc. generating a systemically toxic molecule TM, **Figure 2**. In contrast,

Figure 2



opening of the succinimide-thioether ring (succinimidyl hydrolysis) to form succinamic acid thioether results in forming a stable drug-protein-conjugate (SDPC) with a very long half-life of up to 2 years, **Figure 2**. Thus, if succinimide-thioether that is formed upon conjugation of the sulfhydryl group of HSA to maleimide is hydrolysed to the succinamic acid thioethers to form the SDPC, this eliminates the problem of poor in-vivo stability of the protein-drug conjugate. Further investigations documented that the electron withdrawing inductive effect of the N-substituent on the nitrogen of the succinimide-thioether plays a major mechanistic role in determining the rate of the succinimidyl hydrolysis to succinamic acid thioethers. Thus, in the studies performed in the **second year** of the support, synthetic pathways were developed to use 2-fluoro-5-maleimidobenzoic acid (compound 3 in **Figure 3**) for stably link compounds to the Cys-34 of albumin since it possesses the required electron

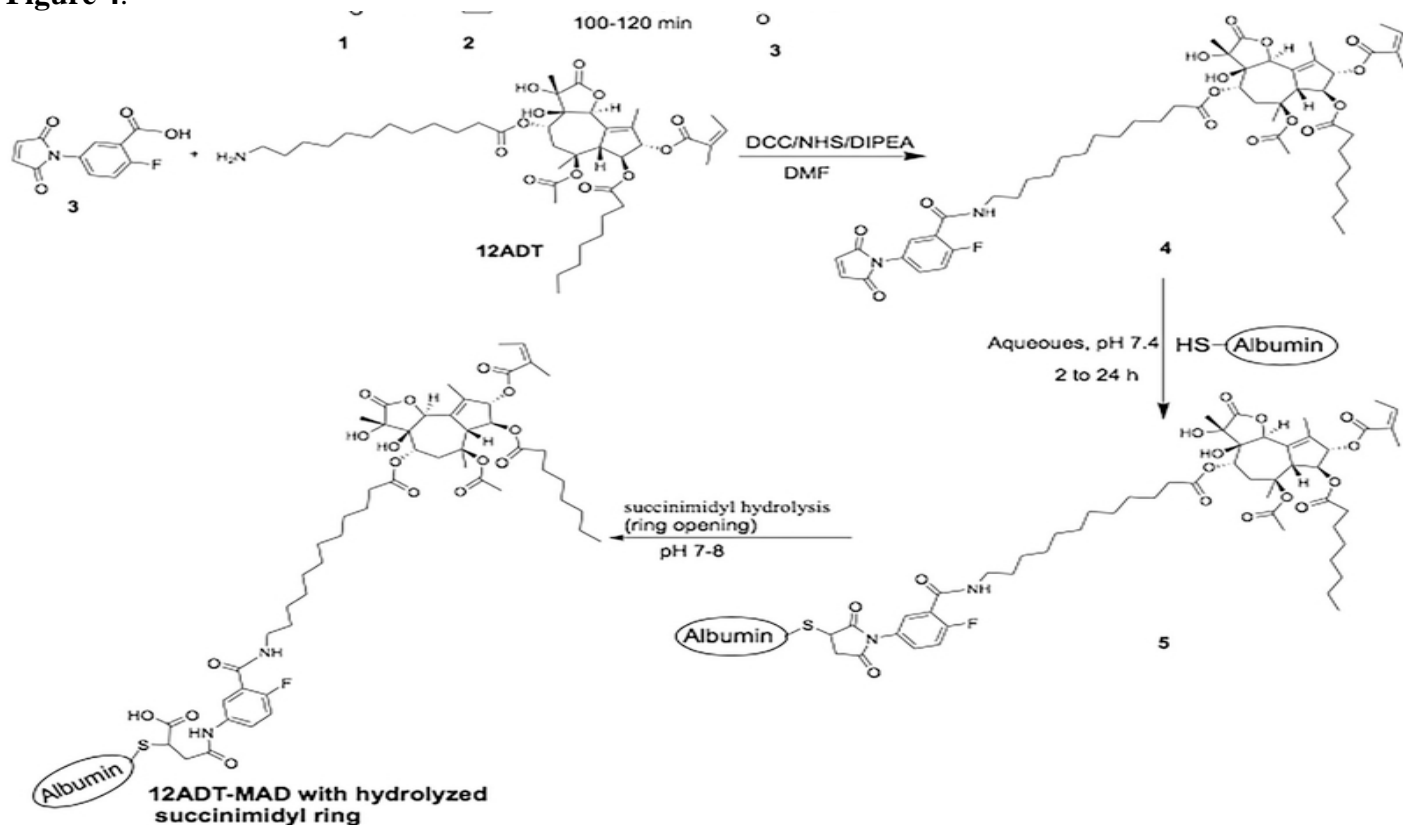
Figure 3



withdrawing inductive ability needed by combining the resonance effect of the aromatic ring and the electron withdrawing property of fluorine at para position to the nitrogen of the succinimide thioether ring.

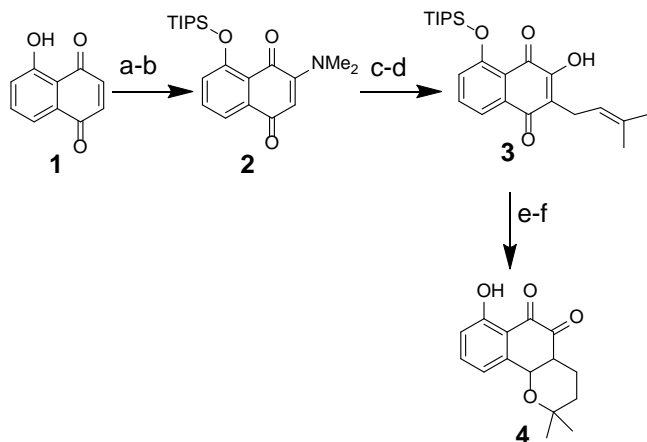
To validate this approach, a chemically modified analogue of the naturally occurring sesquiterpene γ -lactone, thapsigargin, 8-O-(12-aminododecanoyl)-8-O-debutanoyl thapsigargin (12ADT) was chosen as the initial cytotoxic drug stably coupled to albumin via such 2-fluoro-5-maleimidobenzoic (**Compound 3**) acid linkage as described in **Figure 4**. This is because 12ADT is acid stable and contains a primary amine allowing its covalent coupling via formation of a peptide bond. 12ADT is a potent inhibitor (IC_{50} 10 nM) of their endoplasmic reticulum (ER) calcium ATPase (ie, SERCA 2b) pumps and thus induces depletion of the high (ie, $>500 \mu\text{M}$) Ca^{+2} in the ER, inducing both an ER stress response and a “capacitance entrance” of extracellular Ca^{+2} in human mCRPCs producing a sustained increase in intracellular Ca^{+2} (Ca_i) to $>1 \mu\text{M}$ over the next 18–36 h. The combination of ER stress and a sustained elevation of Ca_i , eventually results in the apoptotic death of mCRPC with an LD_{50} of $<50 \text{ nM}$. An additional factor is that 12ADT’s potent killing ability is retained when coupled to single amino-acids. Using LC-MS, we documented that by 2-fluoro-5-maleimidobenzoic acid coupling to the sulfhydryl of HSA was stable for more than a month at 37° in human plasma.

Figure 4.



Based upon this validation, in the **second year** of support, we developed a solid phase synthesis on a resin for coupling HSSKLQ//LP-EDAC-niclosamide to 2-fluoro-5-maleimidobenzoic acid. Also during the **second year**, we developed a synthetic route for producing 7OH- β -Lapachone (7OH- β -Lap) as follows. The hydroxyl group of 5-hydroxy-1,4-naphthoquinone (obtained from Sigma), compound **1** in **Figure 5**, is protected with triisopropylsilyl chloride (TIPS). This is followed by reaction with dimethyl amine (DMF). The pure amino quinone formed, compound **2**, is then treated with concentration hydrochloric acid to form hydroxyl group in position 3. This is followed by reaction with 1-bromo-3-methylbut-2-ene to obtain compound **3**. This product is then treated with dilute sulfuric acid for acid catalyzed cyclization. This is then followed by deprotection of the TIPS with TBAF to obtain compound **4**, the desired product. We then developed a solid phase synthesis on a resin for coupling HSSKLQ//LP-EDAC-7OH- β -Lap to 2-fluoro-5-maleimidobenzoic acid.

Figure 5



- a) TIPSCl, Imidazole, DMF; b) NHMe_2 ; c) conc. HCl; d) 1-bromo-3-methylbut-2-ene, NaI, Et_3N , DMF; e) dil H_2SO_4 ; f) TBAF, THF

Unfortunately, the efficiency of coupling both 2-fluoro-5-maleimidobenzoate linked HSSKLQ//LP-EDAC-niclosamide and 2-fluoro-5-maleimidobenzoate linked HSSKLQ//LP-EDAC-7OH- β -Lapachone to the cysteine of HSA was too low to proceed.

Third Year accomplishments: Based upon these results, we contacted the commercial company Albumedix Ltd (Nottingham NG7 1FD, United Kingdom) which specializes upon coupling small molecule therapeutics to their recombinant produced HSA via stable sulfhydryl coupling. Beside standard recombinant HSA which contains only a single reactive sulfhydryl, this company has genetically engineered recombinant HSA with a total of 3 reactive cysteines. We have sent the company both 2-fluoro-5-maleimidobenzoate linked HSSKLQ//LP-EDAC-niclosamide and HSSKLQ//LP-EDAC-7OH- β -Lapachone for coupling and are awaiting the results with both the wild type and genetically engineered HSA.

While waiting for these results, we decided to take an additional approach via producing a non-HSA couple prodrug to overcome the solubility and non-specific toxicity of niclosamide and Lapachone. To do this, we again have taken advantage of the fact the within sites of prostate cancer are infiltrating MSCs and CAFs which express FAP on the plasma membranes. FAP is a member of the dipeptidyl peptidase (DPP) family, which has a unique requirement for a proline in the P1 position of the protease cleavage site. Amongst the family, FAP and prolyl oligopeptidase (PREP) are the only members with endopeptidase activity as the others are exclusively exopeptidases requiring a free amino terminus to recognize and cleave dipeptides from the end of a substrate. This endopeptidase activity and unique post-prolyl substrate specificity of FAP has been exploited to develop multiple FAP-targeted therapies that include prodrug. Previously, we demonstrated that intravenous (IV) administration of a FAP-activated prodrug consisting of a nine amino acid FAP peptide substrate coupled to an analog of the potent cytotoxin thapsigargin could selectively kill stromal cells within PCa xenografts leading to significant xenograft growth inhibition. Peptide-based thapsigargin prodrugs as a class require intravenous (IV) administration and have narrow therapeutic index *in vivo* in both mice and humans. In addition, it was recently recognized that PREP has similar substrate specificity, leading to a lack of specificity for many of these “targeted” agents, which complicates interpretation of these earlier studies. This led to extensive efforts to synthesize more selective FAP substrates, which has recently culminated in the development of a small molecule FAP-specific PET probe that has been safely administered to cancer patients for imaging purposes. This FAP-probe was structurally derived from a quinoline-capped dipeptide-based small molecule inhibitor, which has >80-fold selectivity over closely-related DPP family members, including PREP (IC₅₀: ~10 vs. >850 nM) with excellent plasma stability (90% mouse/100% human), oral bioavailability and a plasma half-life ($t_{1/2}$) of ~2 hrs. This orally-available small molecule inhibitor was converted to a FAP substrate by replacing the carbonitrile “warhead” with a peptide amide bond conjugated to a fluorophore to generate a probe for FAP proteolytic activity. Based on this data, we synthesized a FAP-activated analog of niclosamide by coupling this FAP-specific quinoline-capped Gly-4,4-difluoro-Pro substrate via the self-cleaving linker (SCL), para-aminobenzyl alcohol (i.e. **compound 2 in Figure 6B**) to the phenolic hydroxyl group of niclosamide, which is required for its mechanism of action (i.e. **compound 5 in Figure 6B**). Coupling to this hydroxyl inactivates niclosamide by preventing its transition between the protonated and anionic states required for translocation across the mitochondrial outer membrane. This reversible protonation allows it to cycle between the IMS and neutral cytosol; thereby, collapsing the proton gradient needed for OxPhos. FAP proteolysis leads to cyclization of the self-cleaving linker to generate this free hydroxyl group, thus “activating” niclosamide to collapse the proton gradient and induce cell death, **Figure 6B**. Based on its non-selective mechanism of action, niclosamide has nanomolar potency against all cells we have tested [Avg IC₅₀: <500nM, **Figure 6A**]. Therefore, to produce a therapeutic index based on the rationale described above, we synthesized a FAP-activated niclosamide protoxin via a straightforward 7-step synthetic scheme, **Figure 6B**. We developed an optimized LCMS protocol to accurately quantify niclosamide and the protoxin in biological matrices for biochemical and PK analyses. Using this validated assay, we have documented **FAP-specific activation of the protoxin** with an ~20-fold increase in active niclosamide over 24 hrs with no production observed with DPPIV, PREP, or in the absence of enzyme, **Figure 6C**. Importantly, as indicated above, niclosamide is non-selective once activated and toxic to all cells. Therefore, a significant bystander effect killing PCa cells is also expected once the toxin is activated in the TME. Importantly, due to its high lipophilicity, niclosamide rapidly partitions into nearby cells and does **not** “leak” out of the local TME once “activated”; thereby, efficacy *in vivo* against abiraterone-resistant CRPC

tumors, **Figure 6D**, with no evidence of toxicity technology in order to initial clinical development of this **FAP-activated niclosamide protoxin (i.e. compound 5 in Figure 6B)** for prostate cancer.

In addition, we are writing up several manuscripts for submission reporting the results of the unpublished findings and chemical synthetic pathway developed.

Figure 6E.

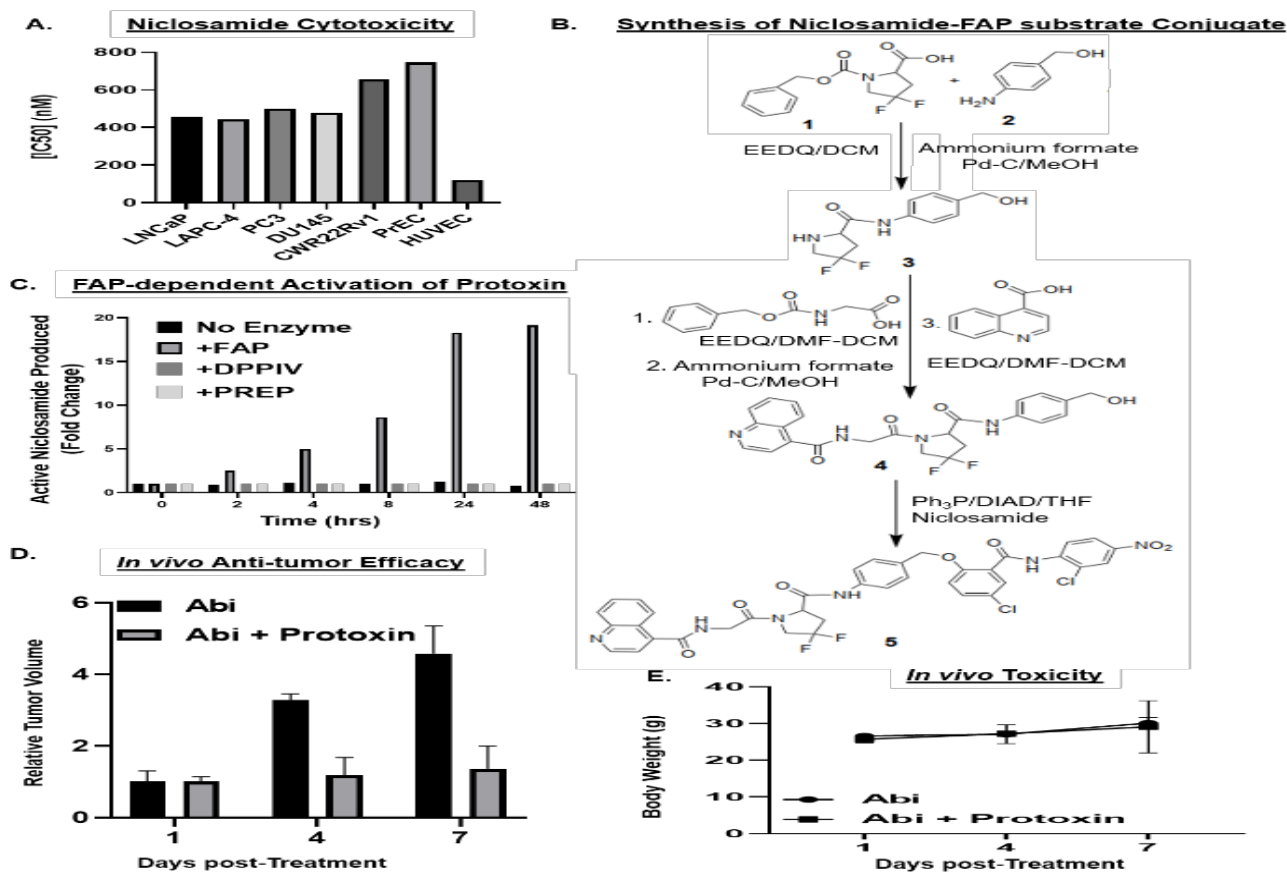


Figure 6: Synthesis and *in vitro* characterization of FAP-activated niclosamide protoxin. A) MTT assay documenting potency of niclosamide against panel of benign and malignant cells. B) Synthetic scheme for FAP-activated niclosamide protoxin. C) FAP-dependent production of active niclosamide from protoxin assessed via LCMS analysis. D) Myc-CaP-CR tumors treated with abiraterone (10 mg/kg) +/- FAP-activated protoxin (50 mg/kg). E) Body weight (g) of treated animals.

- **What opportunities for training and professional development has the project provided?**

Nothing to Report

- **How were the results disseminated to communities of interest?**

1. Akinboye ES, Rogers OC, Isaacs JT. 2-fluoro-5-maleimidobenzoic acid-linked albumin drug (MAD) delivery for selective systemic targeting of metastatic prostate cancer. *Prostate*. 2018 Jun; 78(9):655-663. doi: 10.1002/pros.23494.
2. Krueger TEG, Thorek DLJ, Denmeade SR, Isaacs JT, Brennen WN. Concise Review: Mesenchymal Stem Cell-Based Drug Delivery: The Good, the Bad, the Ugly, and the Promise. *Stem Cells Transl Med*. 2018 Sep;7(9):651-663. doi: 10.1002/sctm.18-0024

3. Brennen WN, Isaacs JT. The what, when, and why of human prostate cancer xenografts. *Prostate*. 2018 Jun; 78(9):646-654. doi: 10.1002/pros.23510.
4. Isaacs JT. Resolving the Coffey Paradox: what does the androgen receptor do in normal vs. malignant prostate epithelial cells? *Am J Clin Exp Urol*. 2018 Apr 1;6(2):55-61.
5. Akinboye ES, Brennen WN, Denmeade SR, Isaacs JT. Albumin-linked prostate-specific antigen-activated thapsigargin- and niclosamide-based molecular grenades targeting the microenvironment in metastatic castration-resistant prostate cancer. *Asian J Urol*. 2019 Jan; 6(1):99-108. doi: 10.1016/j.ajur.2018.11.004.

Impact

- **What was the impact on the development of the principal discipline(s) of the project?**
Nothing to Report
- **What was the impact on other disciplines?**
Nothing to Report
- **What was the impact on technology transfer?**
We are presently forming a company to license this technology in order to initial clinical development of this FAP-activated niclosamide protoxin (i.e. compound 5 in Figure 6B) for prostate cancer.
- **What was the impact on society beyond science and technology?**
Nothing to Report

Products

- **Journal Publications**
 1. Akinboye ES, Rogers OC, Isaacs JT. 2-fluoro-5-maleimidobenzoic acid-linked albumin drug (MAD) delivery for selective systemic targeting of metastatic prostate cancer. *Prostate*. 2018 Jun; 78(9):655-663. doi: 10.1002/pros.23494.
 2. Krueger TEG, Thorek DLJ, Denmeade SR, Isaacs JT, Brennen WN. Concise Review: Mesenchymal Stem Cell-Based Drug Delivery: The Good, the Bad, the Ugly, and the Promise. *Stem Cells Transl Med*. 2018 Sep;7(9):651-663. doi: 10.1002/sctm.18-0024
 3. Brennen WN, Isaacs JT. The what, when, and why of human prostate cancer xenografts. *Prostate*. 2018 Jun; 78(9):646-654. doi: 10.1002/pros.23510.
 4. Isaacs JT. Resolving the Coffey Paradox: what does the androgen receptor do in normal vs. malignant prostate epithelial cells? *Am J Clin Exp Urol*. 2018 Apr 1;6(2):55-61.
 5. Akinboye ES, Brennen WN, Denmeade SR, Isaacs JT. Albumin-linked prostate-specific antigen-activated thapsigargin- and niclosamide-based molecular grenades targeting the microenvironment in metastatic castration-resistant prostate cancer. *Asian J Urol*. 2019 Jan; 6(1):99-108. doi: 10.1016/j.ajur.2018.11.004.
- **Inventions, patent applications, and/or licenses**
We have submitted a Report of Invention (ROI) entitled "FAP-activated Niclosamide for the Treatment of Cancer" to the Johns Hopkins Technology Ventures [i.e. New Report of Invention Notification (JHU Reference C16229)] in order for the University to submit a US Provisional Patent application.

Participants & Other Collaborating Organizations

Name:	<i>John Isaacs</i>
Project Role:	<i>Principal Investigator</i>
Nearest person month worked:	<i>3</i>
Contribution to Project:	<i>Dr. Isaacs has coordinated/ supervised all aspects of this project on a daily basis.</i>
Funding Support:	<i>Not applicable</i>

Name:	<i>Samuel Denmeade</i>
Project Role:	<i>Partnering Principal Investigator</i>
Nearest person month worked:	<i>1</i>
Contribution to Project:	<i>Dr. Denmeade is a collaborator in coordinating supervising all aspects of this project, including the collection and analyzes of the data. He mentors Dr. Akinboye.</i>
Funding Support:	<i>Not applicable</i>

Name:	<i>Susan Dalrymple</i>
Project Role:	<i>Sr. Research Specialist</i>
Nearest person month worked:	<i>6</i>
Contribution to Project:	<i>Ms. Dalrymple performs all routine quality assurance testing on cell lines used in this study. In addition, she has coordinated all aspects of the animal studies.</i>
Funding Support:	<i>Not applicable</i>

Name:	<i>Emmanuel Akinboye</i>
Project Role:	<i>Postdoctoral Fellow</i>
Nearest person month worked:	<i>12</i>
Contribution to Project:	<i>Dr. Akinboye synthesizes all of the compounds proposed in this application. He uses ¹H and ¹³C NMR and mass spectrometry for the quality assurance for each compound. He also performs the mass spect analysis in the drug biodistribution studies.</i>
Funding Support:	<i>Not applicable</i>

Special Reporting Requirements

Partnering PI will submit his separate progress report.

Appendices

See journal articles appended below.

ORIGINAL ARTICLE

2-fluoro-5-maleimidobenzoic acid-linked albumin drug (MAD) delivery for selective systemic targeting of metastatic prostate cancer

Emmanuel S. Akinboye | Oliver C. Rogers | John T. Isaacs 

Department of Oncology, Prostate Cancer Program, The Sidney Kimmel Comprehensive Cancer Center at Johns Hopkins, The Johns Hopkins University School of Medicine, Baltimore, Maryland

Correspondence

Emmanuel S. Akinboye, Department of Oncology, Prostate Cancer Program, The Sidney Kimmel Comprehensive Cancer Center at Johns Hopkins, The Johns Hopkins University School of Medicine, Baltimore, MD 21231.
Email: eakinbo1@jhmi.edu

Funding information

DoD, Grant number: W81XWH-16-1-0410; NIH-Prostate SPORE, Grant number: P50 CA058236; Center for Scientific Review, Grant numbers: P50 CA058236, p30 CA006973

Background: The SH-group at Cys-34 of human serum albumin (HSA) is a unique and accessible functional group that can be exploited for efficient linkage of a maleimide containing cytotoxic drug derivative to albumin. The specific maleimide chemistry used for production of the maleimide-linked albumin drug (MAD) is critical, however, to minimize the plasma concentration of “free” cytotoxic drug spontaneously released from albumin carrier thus decreasing dose-limiting host toxicity while enhancing the plasma half-life from minutes to days (ie, pharmacokinetic effect) and tissue concentration of the MAD in the extracellular cellular fluid at sites of cancer (ie, EPR effect).

Methods: To accomplish this goal, a chemical synthesis was developed using 2-fluoro-5-maleimidobenzoic acid to stably link the potent cytotoxic chemically modified analogue of the naturally occurring sesquiterpene γ -lactone, thapsigargin, 8-O-(12-aminododecanoyl)-8-O-debutanoyl thapsigargin (12ADT), to Cys-34 of albumin to produce 12ADT-MAD.

Results: Using FITC-labeling, LC/MS analysis, and in vitro growth and clonogenic survival assays on a series of 6 human prostate cancer lines (LNCaP, LAPC-4, VCap, CWR22R_v1, PC3, and Du145), we documented that 12ADT-MAD is endocytosed by prostate cancer cells where it is degraded into its amino acids liberating cysteinyl-maleimide-12ADT which is both chemically stable at the acidic pH of 5.5 present in the endosome while retaining its high killing ability (IC₅₀ 50 nM) via SERCA inhibition.

Conclusions: Based upon these positive in vitro validation results, the in vivo efficacy versus host toxicity of this 12-ADT-MAD approach is presently being evaluated against a series of patient derived androgen responsive and castration resistant human xenografts in immune-deficient mice.

KEYWORDS

albumin based drug uptake, EPR effect, maleimide linkage, prostate cancer

1 | INTRODUCTION

Cancer cells are “obligate parasites” which absolutely depend on systemic nutritional support as well as metabolic cooperation with host

cells in order to produce a tumor microenvironment that can sustain their lethal growth.¹ While evolution has produced a physiology to continuously provide adequate systemic supply of nutrients through the blood to normal tissue, as cancer cells grow, they eventually exceed

the existing local blood supply, which results in the tumor microenvironment becoming acidic, hypoxic, and low in nutrients. Continued malignant growth in such a compromised (ie, stressful) microenvironment requires cancer cells to initiate autophagy to parasitize the host's energy and nutrients. In the 1920s, Warburg and the Cori's demonstrated the importance of carbohydrate metabolism and lactate generation by cancers.^{2,3} Since then, a variety of potential low molecular weight nutrients, such as fatty acids, ketone bodies, and amino acids have been identified. The first indications that plasma proteins, like albumin, might be involved in tumor autophagic nutrition were reported by Mider in the late 1940's. This report concluded that tumors act as "nitrogen traps" after comparing the protein metabolism of normal tissue and of tumor tissue.⁴ These studies demonstrate one-way passage of amino acids from the body pool to the tumor without any appreciable return and that even the stress of starvation does not release tumor protein for the body. In 1954, Babson and Winnick reported that cancer cells, unlike normal cells, utilized plasma proteins more efficiently than free leucine.⁵ Based on these findings, they concluded that tumor growth in the starving animal and in the cachectic human is driven by the cancer cell's acquired ability to trap plasma proteins and to use the degradation products (amino acids) for proliferation, a process that normal cells do not do. Later, it was shown that albumin, in order to be utilized for its amino acid content, enters cancer cells by an active process of endocytosis.^{6,7}

More recent experiments using IV injected [¹¹¹In]DTPA labeled albumin documented that large amounts of labeled albumin metabolites are retained within sites of cancer (ie, more than 20% of total injected albumin is concentrated in Dunning rat prostatic adenocarcinomas by 3 days following a single dose of radiolabeled albumin).⁸ This is significant because cancer cells must tap the energy and nitrogen resources of its host with high efficiency in order to proliferate. The required substrates, oxygen, glycolytic energy, and nitrogen must be transferred to the tumor by blood and plasma. Proteins account for 70% of the solubilized substances in plasma. Another 20% consist of a multitude of low molecular weight organic substrates (glucose, amino acids, fatty acids, urea, creatine, uric acid, glycerol) and the remaining 10% are inorganic ions. Plasma proteins are high quality nutrient and carry most of the readily available nitrogen and energy reserves of the host.⁹ Albumin is the most abundant among these proteins accounting for about 50-70% of the human plasma protein reserve. Its relevance as a metabolic reserve is demonstrated by comparing the millimolar concentrations of the amino acids in albumin with the concentration of free amino acids in plasma. Assuming a physiologic albumen concentration of 40 g/L, the concentration of amino acids that are released after complete lysosomal degradation of albumin (ie, 317 mM) exceeds the free amino acids in the plasma (ie, 2.7 mM) 117-fold.⁹ Besides providing amino acids, albumin catabolism also provides a considerable source of energy, providing a rationale for why autophagic uptake and degradation of albumin is a fundamental acquired characteristic of cancer cells.^{6,7}

While the half-life of albumin in the body is ~19 days in humans, its plasma half-life is only about 1 day.¹⁰ This is because despite tight endothelial barrier function, albumin constantly leaves the plasma via

endothelial transcytosis and enters un-degraded into the extracellular fluid throughout the body. Due to this transcytosis, albumin makes ~15 around trips from the extracellular fluid returning back to the blood via the lymphatic thoracic duct during its life-span.¹⁰ Besides transcytosis, albumin also extravasates into the extracellular fluid within sites of metastatic cancer due to a characteristic decrease in tumor endothelial barrier function which, coupled with a lack of a functional lymphatic drainage at these sites, produces a cancer specific process known as the enhanced permeability and retention (ie, EPR) effect.¹¹ We have documented that due to this malignancy driven EPR effect, a small molecule therapeutic drug bound to albumin in the blood stream is concentrated appropriately sixfold within sites of prostate cancer within 24 h of dosing.¹²

Coupling drugs to albumin in the blood is quite straightforward.¹³ This is because albumin has a modular structural organization producing a heart-shaped molecule composed of three homologous domains, each containing an A and B subdomain.¹⁴ The 1A domain contains a surface accessible cysteine at amino acid position 34 (Cys-34), Figure 1. Approximately 70% of circulating albumin in the blood stream contains the accessible Cys-34, not blocked by endogenous sulfhydryl scavenger compounds such as cysteine, homocysteine, glutathione, or nitric oxide. The concentration of these low molecular weight sulfhydryl compounds in human blood plasma in their reduced form, that is, cysteine (10-12 μ M), homocysteine (0.15-0.25 μ M), cysteinylglycine (3-4 μ M), glutathione (4-5 μ M) is low when compared to the total thiol concentration in human plasma, which is in the range 400-500 μ M.¹⁵ Thus, the free thiol group (SH) at the Cys-34 position of HSA accounts for 80-90% of the total thiol concentration in blood plasma.¹⁶ Importantly, the SH group of Cys-34 of HSA is the most

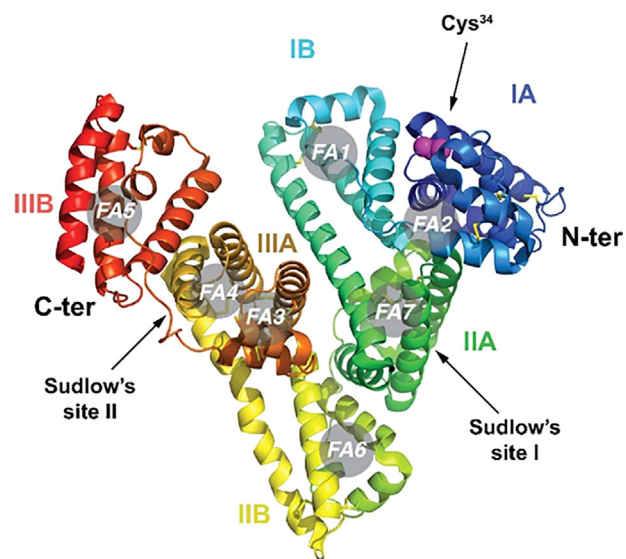


FIGURE 1 Molecular structure of human serum albumin (HSA) with an indication of its subdomains (IA, IB, IIA, IIB, IIIA, and IIIB), of the N and C termini, of Sudlow's sites I and II and of the seven fatty acid binding sites (FA1 to FA7). The side chain residues of Cys-34 are shown as purple spheres. [Color figure can be viewed at wileyonlinelibrary.com]

reactive thiol group in human plasma because of the low pK_a of Cys-34 in HSA, which is approximately seven compared to 8.5 and 8.9 for cysteine and glutathione, respectively¹⁵ at physiological pH. Taken together, the SH group of Cys-34 of HSA is a unique and accessible functional group of a plasma protein that can be exploited for in situ coupling of circulating albumin following intravenous administration of a thiol-reactive prodrug.¹³ The X-ray structure of the defatted protein structure reveals that cysteine-34 is located in a hydrophobic crevice on the surface of the protein that is approximately 10–12 Å deep.¹⁴ When HSA is complexed with long-chain fatty acids as in the X-ray structure in which seven molecules of myristic acid (ie, denoted in gray circles in Figure 1) are bound, the crevice opens up, exposing the sulfhydryl group Cys-34.¹⁷ This allows efficient coupling of this Cys-34 sulfhydryl to small molecular cytotoxic compounds containing a thiol-reactive (eg, maleimide) group which follows second-order kinetics with second-order rate constants in the range 600–2250 L mol⁻¹ min⁻¹, with the highest rate constant occurring when all of the myristic acid binding sites of albumin are saturated, as occurs in the blood.¹⁵

Thus, the SH-group at Cys-34 of HSA is a unique and accessible functional group that can be exploited for efficient linkage of a maleimide containing cytotoxic drug derivative to albumin.^{13,15} The specific maleimide chemistry used for production of the maleimide-linked albumin drug (MAD) conjugate is critical in order to minimize the plasma concentration of “free” cytotoxic drug spontaneously released from albumin carrier thus suppressing its acute host toxicity while enhancing both the plasma half-life (ie, from minutes to days) and tissue concentration of the MAD at sites of cancer (ie, EPR effect). N-alkyl maleimides are commonly used as linkers for the conjugation of the sulfhydryl group in cysteine of proteins to other therapeutic molecules to form succinimide-thioether ring. This succinimide thioether ring (STR) linkage, however, undergoes significant spontaneous cleavage by a retro-Michael reaction under physiologic conditions, Figure 2.^{18,19} When this reaction occurs in-vivo, it results in dose-limiting systemic toxicity as the therapeutic agent is spontaneously released to circulate in the blood forming adduct with other sulfhydryl containing species like

glutathione, cysteine etc. generating a systemically toxic molecule TM, Figure 2. In contrast, it has been documented that opening of the succinimide-thioether ring (succinimidyl hydrolysis) to form succinamic acid thioether results in forming a stable drug-protein-conjugate (SDPC) with a very long half-life of up to 2 years, Figure 2.²⁰ Thus, if succinimide-thioether that is formed upon conjugation of sulfhydryl group of protein to maleimide is hydrolysed to the succinamic acid thioethers to form the SDPC, this would eliminate the problem of poor in-vivo stability of the protein-drug conjugate. Further investigations have shown that the electron withdrawing inductive effect of the N-substituent on the nitrogen of the succinimide-thioether plays a major mechanistic role in determining the rate of the succinimidyl hydrolysis to succinamic acid thioethers.²⁰ Thus, in the present study, 2-fluoro-5-maleimidobenzoic acid (compound 3 in Figure 3) was used for stably linking a potent cytotoxic drug to Cys-34 of albumin since it possesses the required electron withdrawing inductive ability needed by combining the resonance effect of the aromatic ring and the electron withdrawing property of fluorine at para position to the nitrogen of the succinimide-thioether ring.^{20–22}

Selection of an “appropriate” cytotoxic drug for such 2-fluoro-5-maleimidobenzoic acid coupling to albumin is based upon the following requirements: (i) it must be chemically linkable via an acid stable bond to 2-fluoro-5-maleimidobenzoic acid; (ii) it must itself be chemically stable at the acidic pH 5.5 environment of the endosome; and (iii) it must retain its potent cytotoxicity when liberated in the endosome coupled to free cysteine. Based upon these requirements, a chemically modified analogue of the naturally occurring sesquiterpene γ -lactone, thapsigargin, 8-O-(12-aminododecanoyl)-8-O-debutanoyl thapsigargin (12ADT), Figure 3, was chosen as the initial cytotoxic drug stably coupled to albumin. This is because 12ADT is acid stable and contains a primary amine allowing its covalent coupling via formation of a peptide bond.²³ 12ADT is a potent inhibitor (IC₅₀ 10 nM) of their endoplasmic reticulum (ER) calcium ATPase (ie, SERCA 2b) pumps and thus induces depletion of the high (ie, >500 μ M) Ca⁺² in the ER, inducing both an ER stress response and a “capacitance entrance” of extracellular Ca⁺² in human mCRPCs producing a sustained increase in intracellular Ca⁺² (Ca_i)

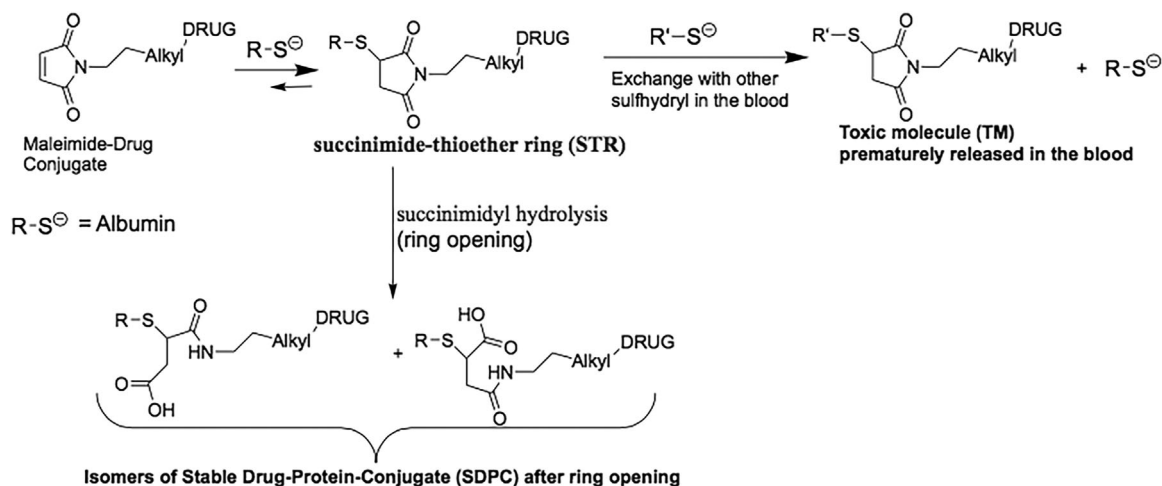


FIGURE 2 Rationale for chemical instability of N-alkyl linked maleimide-drug coupling to albumin

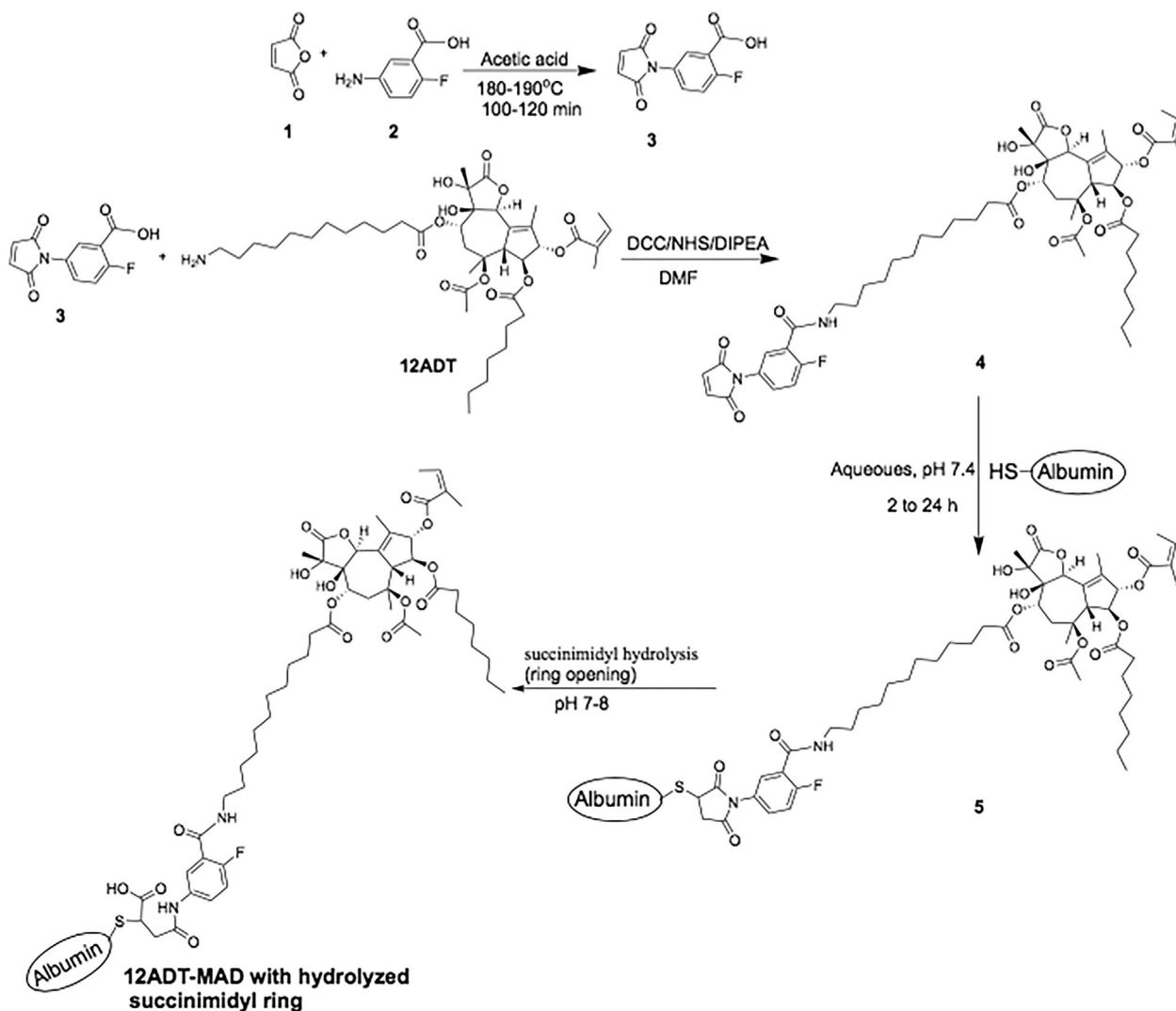


FIGURE 3 Chemical scheme for synthesizing 2-fluoro-5-maleimidobenzoic acid (compound 3), 2-fluoro-5-maleimidobenzoic acid-12ADT (compound 4), and albumin coupling to produce 12ADT-MAD (compound 5)

to $>1 \mu\text{M}$ over the next 18-36 h.²³ The combination of ER stress and a sustained elevation of Ca_i , eventually results in the apoptotic death of mCRPC with an LD_{50} of $<50 \text{ nM}$.²³ As part of this death response, AR protein expression is rapidly decreased in AR positive mCRPC cells.²⁴ In addition, 12ADT kills even multidrug resistant cells lacking apoptotic Bak and Bax proteins.²⁵ An additional factor is that 12ADT's potent killing ability is retained when coupled to single amino-acids.^{23,24,26}

2 | MATERIAL AND METHODS

2.1 | General information

All solvents and reagents used were obtained from commercial sources and used without further purification. The ^1H - and ^{13}C -NMR spectra were obtained on a Bruker Avance III 500 MHz NMR spectrometer at 500 and 125 MHz, respectively in deuterated dimethyl sulfoxide (DMSO-d_6). Chemical shifts are in δ units (ppm). MALDI-MS was done using Voyager DE-STR MALDI-TOF. Purity of the compounds was

determined with reverse phase-HPLC. The purity of all the compounds was determined to be $>95\%$.

HPLC Method 1 was used for analytical reversed-phase HPLC to determine the purity of the synthetic compounds using a Waters Delta 600 Controller equipped with a variable wavelength UV-vis detector (Waters 2487 Dual λ Absorbance Detector) set to detect at 215 and 285 nm and a Vydac 218TP54 (C18, 5 μm , 4.6 mm. i.d. X 250 mm) analytical column. The flow rate was 1.3 mL/min; mobile phase A: 5% MeCN, 95% water and 0.1% TFA. Mobile phase B: 100% MeCN, 0.1% TFA. Gradient: 0-2 min 100% mobile phase A; 2-20 min gradual change to 100% mobile phase B; 20-25, 100% mobile phase B; 25-27 min gradual change to 100% mobile phase A; 27-30 min, 100% mobile phase A. Injection volume: 100 μL .

HPLC Method 2 was used for preparative purification of compounds 4 and 6. Flow rate: 25 mL/min; mobile phase A: 5% MeCN, 95% water and 0.1% TFA. Mobile phase B: 100% MeCN, 0.1% TFA gradient: 0-4.0 min, 100% mobile phase A; 4.0-20.0 min gradual change to 100% mobile phase B; 20.0-20.5 min 100% mobile phase B;

20.5–21.0 min, sharp change to mobile phase A; 21.0–24.0 min mobile phase A. Injection volume: 1.0 mL.

2.2 | Synthesis of 2-fluoro-5-maleimidobenzoic acid-12ADT (compound 4)

Thapsigargin was purified from *Thapsia garganica* seeds and 12 ADT analogue synthesized as described in detail previously.²² Synthesis was performed as summarized in the synthetic scheme shown in Figure 3. To obtain a stable HSA coupled 12ADT through the Cys-34 of albumin, we utilized 2-fluoro-5-maleimidobenzoic acid derivative, compound 3. This compound was synthesized as previously reported,^{23,24} but with modifications that facilitate a more efficient isolation and purification for large scale synthesis, as presented in Figure 3. To accomplish this synthesis, 5-amino-2-fluorobenzoic acid (5.0 g, 1 molar equivalent) and maleic anhydride (4.7 g, 1.5 molar equivalent) were separately dissolved in 100 mL acetic acid. The maleic anhydride clear solution was gradually added to the clear solution of 5-amino-2-fluorobenzoic acid and a slurry was formed. The mixture was placed in oil bath for refluxing and it became a clear, homogenous brown liquid upon heating. It was then refluxed at 180–190°C for 2 h. Solvent and all volatiles were evaporated from the mixture by using rotary evaporator to give a pale brown powdery precipitate. This crude product precipitate was then triturated in water, filtered and residue washed with water. The residue was air dried to afford 2-fluoro-5-maleimidobenzoic acid, compound 3 (5.94 g, 78.4% yield). ¹H NMR (500 MHz, DMSO-*d*₆) 7.20 (1H, s), 7.46 (1H, t, *J* = 10.0 Hz), 7.60–7.65 (1H, m), 7.87 (1H, dd, *J* = 3.0 Hz, 6.5 Hz), 13.35–13.65 (1H, br s); ¹³C NMR (125 MHz, CDCl₃) 118.5, 120.5, 127.9, 130.5, 133.5, 135.1 (2C), 159.2, 161.5 (2C), 164.8. HPLC purity 98.4%.

To obtain compound 4, purified compound 3 (300 mg, 1.277 mmol, 2.5 molar equivalent to 12ADT) was dissolved in 20 mL DMF. This was followed by the addition of N-hydroxysuccinimide (NHS) (293.7 mg, 2.554 mmol; 2 molar equivalent to 3) and dicyclohexylcarbodiimide (DCC) (527 mg, 2.558 mmol; 2 molar equivalent to 3). The reaction mixture was stirred at room temperature for 3 h and then filtered. The filtrate was added to a solution of 12ADT (397 mg, 0.5103 mmol; 1 molar equivalent to compound 3) in DMF and 5 molar equivalent of N,N-diisopropylethylamine (DIPEA). The reaction mixture was stirred at room temperature and monitored with MALDI-MS for indication of the mass of the desired product. The reaction was stopped after stirring for 2 h and solvent was evaporated completely. The crude product was then purified using preparative HPLC (method 2) to give N-aryl-maleimide-12ADT, compound 4. Yield: 57%, brown powder; MALDI-MS *m/z* 1018.33, [(C₅₃H₇₁FN₂O₁₅ + Na)⁺, calcd. 1018.14), HPLC *t_R* is 12.5 min and purity is 97.8%.

2.3 | Kinetics of 2-fluoro-5-maleimidobenzoic acid-12ADT (compound 4) coupling to HSA

To determine its coupling kinetics, a mixture of 10 mM of compound 4 in phosphate buffered saline (PBS) pH 7.4 containing 100 μM solution of HSA was incubated for various time spans up to 24 h at 37°C. The

mixture was then centrifuged at 18 000g for 15 min to remove any precipitate. Supernatants were then assayed using Ellman's reagent (G-Biosciences cat# BC87) according to manufacturer's instructions to determine the amount of free HSA cysteine in each solution. Samples were read at 412 nm and free thiol concentration was determined using an extinction coefficient of 14,140 M⁻¹ cm⁻¹.

2.4 | Production of 12ADT-MAD (compound 5)

A total of 10 mM solution of compound 4 was prepared in DMSO and an aliquot of this was diluted with fetal bovine serum (FBS) to 100 μM. This was incubated at 4°C, room temperature, and 37°C to obtain the optimum reaction condition. Reactions at room temperature and 37°C were monitored over a 2 h period and the reaction at 4°C were monitored over a 24 h period. Since FBS contains ~400 μM albumin, all compound 4 added was expected to covalently react with albumin in FBS. To determine this, at each time point 100 μL aliquot was taken and added to 300 μL of acetonitrile and the mixture was vortexed and centrifuged at 13 000 rpm for 6 min. The supernatant obtained was analyzed by analytical HPLC and MALDI-MS to determine the presence of unreacted compound 4.

2.5 | Synthesis of cysteinyl-2-fluoro-5-maleimidobenzoic acid-12ADT (compound 6)

Synthesis was performed as summarized in the synthetic scheme shown in Figure 4. To obtain compound 6, 30 mg (0.0301 mmol) of compound 4 was dissolved in 3.5 mL DMF and to this was added 3.5 mL acetone and 50 μL of DIPEA. This clear solution was then added gradually to a solution of L-cysteine (43.7 mg, 0.3612 mmol) in 2.5 mL PBS, pH 8 buffer solution. The homogenous mixture was incubated at 40–50°C for 5 min and then stirred at room temperature for 2 h. The crude product was purified using preparative HPLC (method 2) to give compound 6. Yield: 82%, pale brown powder; MALDI-MS *m/z* 1139.94, [(C₅₆H₇₈FN₃O₁₇S + Na)⁺, calcd. 1139.29), HPLC *t_R* is 15.5 min and purity is 96.7%.

2.6 | Fluorescent-labeling of human serum albumin (HSA)

Human serum albumin (recombinant expressed in rice) was purchased from Sigma-Aldrich, Saint Louis, MO (Sigma cat#A9731) and reconstituted in PBS. To covalently couple a fluorescent label to the reactive lysines of HSA, NHS-fluorescein (Thermo Fisher, Rockford, IL, cat# 46410), dissolved in DMSO, was mixed in 10-fold excess with the HSA at a pH of 7.4. This reaction took place at room temperature for 2 h in the dark. To quickly assess the efficiency of the reaction, the labeled protein was passed through a dye removal column (Thermo Fisher cat# 22858) according to manufacturer's recommendations and the effluent was analyzed by absorbance at 450 and 280 nm. For microscopy and cell based assays, all labeled HSA preparations were purified using a AKTAprime Plus FPLC System (GE 11001313) using a HiLoad Superdex 200 PG (GE 28989335) column with PBS pH 7.4 as the buffer. One milliliter fractions were collected and screened using A280, A450, and SDS PAGE for the presence of relevant amounts of

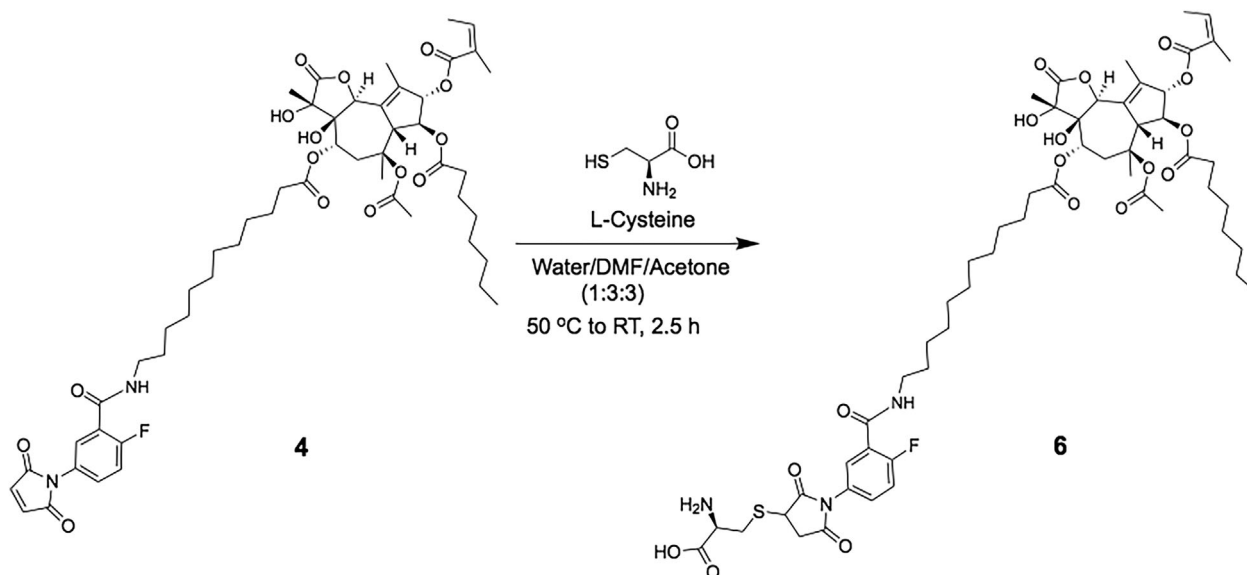


FIGURE 4 Chemical scheme for synthesizing cysteinyl-2-fluoro-5-maleimidobenzoic acid-12ADT (compound 6)

labeled HSA. Positive fractions were pooled and sterile filtered for downstream purposes.

2.7 | Cell lines and cell culture assays

The culture conditions and media for all of the human prostate cancer lines used in these studies (ie, LNCaP, LAPC-4, VCaP, CWR22Rv1, PC-3, DU-145) are as described previously.^{23,24} All lines were mycoplasma negative using the MycoSensor PCR Assay kit (Agilent Technologies, La Jolla, CA) and genetically authenticated within the last 6 months using STR profiling performed by the Johns Hopkins Genetic Resource Core Facility. Cell viability at various times post exposure to test compounds was determined using trypan blue exclusion as previously described.²³ The dose-response ability of test compounds to kill prostate cancer cells was determined using a clonogenic survival assay as described previously,²³ with the results expressed as the nmol/L concentration needed to lose 50% of the clonogenic ability (ie, LD₅₀) after 48 h of exposure to the test compound. In addition, MTT growth assays performed as described previously²⁷ were used to confirm the clonogenic results. SERCA pump inhibition, expressed as the concentration needed to inhibit 50% of the enzymatic activities (IC₅₀ value) and the change in the intracellular Ca⁺² concentration were determined as previously described.²³

2.8 | Fluorescence imaging

To assess cell uptake of HSA, cells were plated at confluency in 6-well plates and treated with 500 nM fluorescent HSA constructs for various time points. The media was then removed and cells were washed with PBS three times. Cells were then fixed with methanol and stained with ProLong™ Diamond Antifade Mountant with DAPI (Thermo Fisher cat# P36962). Cells were then imaged using a Nikon C1si True Spectral Imaging Confocal Laser Scanning Microscope System. All images were analyzed using ImageJ software.

2.9 | Cellular production of cysteinyl-2-fluoro-5-maleimidobenzoic acid-12ADT (compound 6) from 12ADT-MAD

LNCaP cells were incubated with 500 nM 12ADT-MAD in RPMI-1640 media containing 10% fetal bovine serum for 24 h and then the media removed and the cells washed, trypsinized, and centrifuged. Cell pellets containing 10⁷ cells were homogenized using a hand held glass homogenizer (Kimble Kontes size 22) in 1 mL of Complete Protease inhibitor (Roche Diagnostics, Indianapolis, IN) buffer. This whole homogenate was deproteinated with the addition of 3 volumes of acetonitrile containing 0.1% Formic acid (CH₃CN/0.1% FA) and after mixing, samples were centrifuged at 15 000 RPM × 5 min. Resulting supernatant and calibration standards of Cysteinyl-maleimide-12ADT were separately analyzed by liquid chromatography coupled to a quadrupole mass spectrometer (LC/MS/MS) (Applied Biosystems ABI 3000 triple quadrupole MS).

3 | RESULTS

3.1 | Kinetics of 2-fluoro-5-maleimidobenzoic acid 12ADT (compound 4) coupling with HSA

Initially, the kinetics of coupling 2-fluoro-5-maleimidobenzoic acid (compound 3) to the sulfhydryl group of a low molecular weight compound (ie, 2-mercaptoethanol) was evaluated. When compound 3 was incubated with excess 2-mercaptoethanol (10 molar equivalent) in DMSO-d₆ and the reaction was monitored using ¹H-NMR. Within 30 min, complete disappearance of the peak corresponding to the maleimide peak at 7.20 and the presence of the peaks that indicate the expected Michael addition reaction and the formation of succinimide-thioether (indicated by peaks at 2.95 [1H, m], 3.31 [1H, m], 4.18 [1H, m]) were observed. These results prove that just like the common

N-alkyl-maleimide derivative, 2-fluoro-5-maleimidobenzoic acid also undergo fast Michael addition reaction with sulfhydryl group to form succinimide-thioether. Based upon these positive results, the kinetics of 2-fluoro-5-maleimidobenzoic acid 12ADT (compound 4) coupling to HSA was tested. These studies documented that within 30 min, there was >95% loss of albumin associated free sulfhydryl.

3.2 | Rapid cellular uptake of 2-fluoro-5-maleimido-benzoic acid coupled human serum albumin (HSA)

HSA was fluorescein-labeled via n-linkage to a series of lysines using standard techniques and FPLC purification. An aliquot of the fluorescently labeled HSA was coupled via Cys-34 to 2-fluoro-5-maleimido-benzoic acid (ie, compound 3). A variety of human prostate cancer cells were incubated in tissue culture with 500 nM of either the fluorescein-HSA with unreacted Cys-34 (ie, fluorescein-HSA) or fluorescein-HSA-maleimide coupled proteins and at various times, the cultures were washed, methanol fixed, counter-stained with DAPI to identify nuclei which are blue, and examined for green fluorescein-albumin using

confocal microscopy. Unexpectedly, but significantly, only the 2-fluoro-5-maleimidobenzoic acid coupled fluorescein-labeled HSA is rapidly (ie within minutes) internalized producing both punctate endosomal and diffuse cytoplasmic staining, with little uptake of the green fluorescein-HSA with unreacted Cys-34 even after 4 h, Figure 5A. Western blot analysis demonstrated that >90% of the fluorescein-label in the cytoplasmic fraction is associated with small peptides and free fluorescein-labeled-lysine consistent with albumin degradation in the endosome. This is consistent with earlier studies documenting that endothelial cells transcytose unmodified albumin without degrading it, but albumin in which Cys-34 is capped with gold is taken up and degraded by the cells into its amino acids.²⁸ Such selective cellular uptake of fluorescein-HSA-2-fluoro-5-maleimidobenzoic acid is not toxic to prostate cancer cells as documented by its lack of growth inhibitory ability even after 5 days of exposure at 10 μ M, Figure 5B.

These data document that when Cys-34 in albumin is "capped," the protein is "recognized" differently than unmodified albumin and is phagocytized and degraded into its free amino-acids by cancer cells. Thus by capping albumin with a 2-fluoro-5-maleimidobenzoic acid

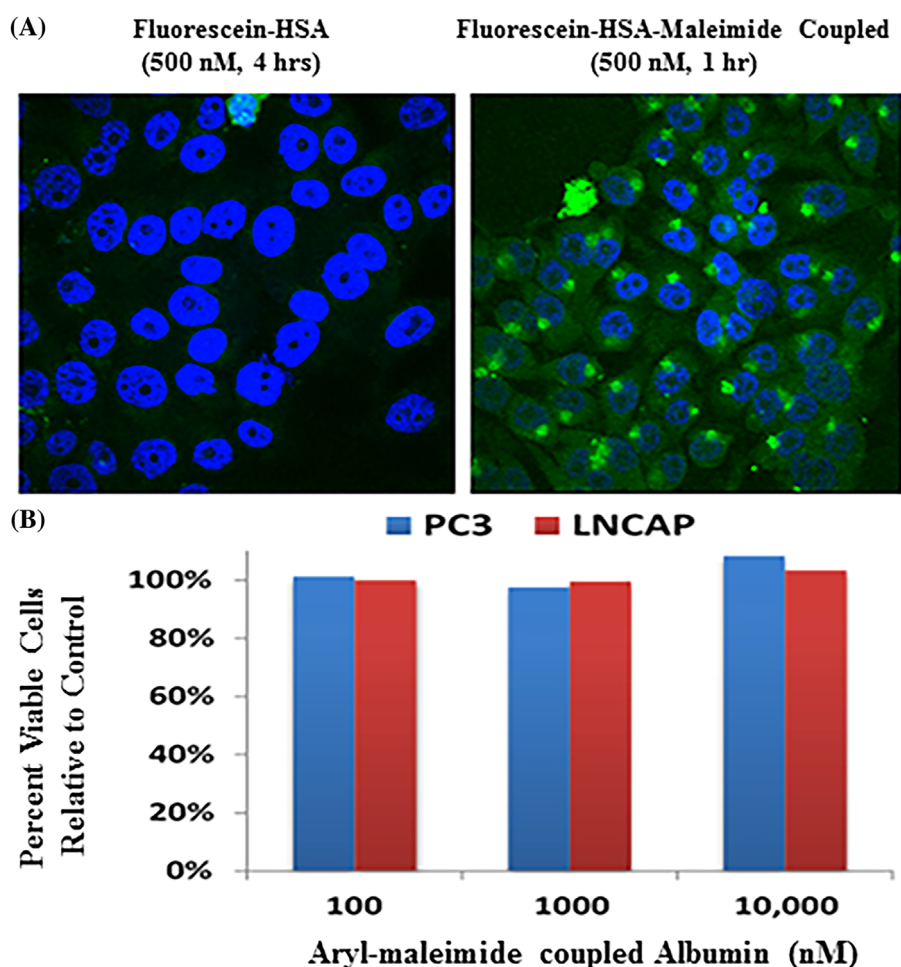


FIGURE 5 A, Differential uptake by PC-3 human prostate cancer cells of 500nM FITC-HSA at 4 h vs 500 nM FITC-HSA-maleimide at 1 h. Blue fluorescence is due to DAPI staining of DNA and Green fluorescence is due to fluorescein-HSA-maleimide uptake. B, Dose-Response of LNCaP and PC-3 human prostate cancer cells to 5 day of fluorescein-HSA-maleimide as evaluate percent viability compared to untreated control cells. [Color figure can be viewed at wileyonlinelibrary.com]

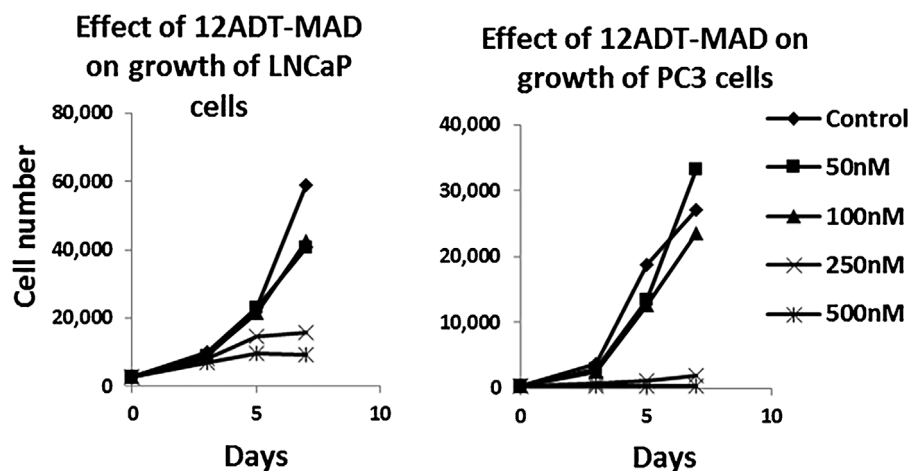


FIGURE 6 Kinetics of the dose response toxicity of 12ADT-MAD to LNCaP and PC-3 human prostate cancer cells

coupled cytotoxic drug, we hypothesize that the resultant resulting maleimide-linked albumin drug (MAD) can selectively concentrate in the extracellular fluid (ECF) at sites of metastatic prostate cancer due to the combination of an enhanced serum half-life and tumor specific EPR effect. Once in the tumor ECF, MAD is taken up by the cancer cells and degraded within endosomes to liberate its cytotoxic moiety.

3.3 | Kinetics of coupling of 2-fluoro-5-maleimidobenzoic acid-12ADT to albumin in situ in serum to produce 12ADT-MAD

There are two possible methods to produce 12ADT-MAD (compound 5) for therapeutic systemic delivery. The first is to couple 2-fluoro-5-maleimidobenzoic acid-12ADT (compound 4) with albumin directly ex vivo as presented in Figure 3 and then purify the 12ADT-MAD for subsequent intravenous injections. Alternatively, since we have documented that the rate of coupling to albumin is so rapid, compound 4 could be injected intravenously allowing coupling in the blood to the high (~400 μ M) albumin concentration producing 12ADT-MAD in situ, as long as there are no serum components which either compete for or inhibit such coupling. To test for this possibility, the kinetics of such in situ coupling was evaluated by incubating 100 μ M of compound 4 with fetal bovine serum containing ~400 μ M albumin at 37°C. These results documented that coupling of compound 4 with albumin produces compound 5 rapidly in the serum (ie, >90% of the compound 4 is covalently linked to albumin within 5 min with essentially no free non-protein bound compound 4 being detectable after 30 min).

3.4 | Therapeutic efficacy of 12ADT-MAD against prostate cancer cells

The dose response cytotoxicity of 12ADT-MAD (compound 5) was evaluated against a series of six human prostate cancer lines (LNCaP, LAPC-4, VCap, CWR22R_v1, PC3, and Du145). These results demonstrated that cell death is extensively induced in all lines with IC₅₀ values ranging from 100 to 250 nM. Figure 6 presents representative data for

the PC3 and LNCaP cell lines. Importantly, therapeutic response is totally dependent upon the 12ADT as part of the MAD since the albumin coupled aryl-maleimide without the 12ADT has no growth inhibitory ability, Figure 5B. Using fluorescein labeling and LC/MS, we documented that 12ADT-MAD is endocytosed by prostate cancer cells where it is degraded into amino acids liberating cysteinyl-maleimide-12ADT (compound 6). Compound 6 was separately documented to be chemically stable at the acidic pH of 5.5 in the endosome and to retain potent killing ability (IC₅₀ < 50 nM) for prostate cancer cells. This cell killing is due to its SERCA inhibition (IC₅₀ 20 nM) inducing an ER stress response and a “capacitance entrance” of extracellular Ca⁺² in the prostate cancer cells causing an increase in intracellular Ca⁺² (Ca_i) to >1 μ M producing apoptotic death.

4 | DISCUSSION

Based upon these positive in vitro validation results, the in vivo dose-response efficacy versus host toxicity of this 12ADT-MAD approach is presently being evaluated against a series of patient derived androgen responsive and castration resistant human xenografts in immune-deficient mice. As part of this testing, we are comparing the dose-response of anti-tumor efficacy versus host toxicity of intravenously injected ex vivo synthetically produced 12ADT-MAD versus in situ generated 12ADT-MAD produced by intravenous injection of 2-fluoro-5-maleimidobenzoic acid-12ADT. These future studies will thus define which approach is optimal for clinical translation.

ACKNOWLEDGMENTS

we would like to acknowledge the Department of Defense Prostate Cancer Research Program, Award No W81XWH-16-1-0410, NIH-Prostate SPORE; Grant number: P50 CA058236. Also we wish to thank the Cell Imaging Facility supported by the SKCCC CCSG (P30 CA006973) for their services and assistance; the Mass Spectrometry and Proteomics Core facility of the Johns Hopkins School of Medicine

for the Mass Spec analysis; and Johns Hopkins School of Medicine Pharmacology Department for the H and C-13 NMR analysis.

ORCID

John T. Isaacs  <http://orcid.org/0000-0002-3854-4658>

REFERENCES

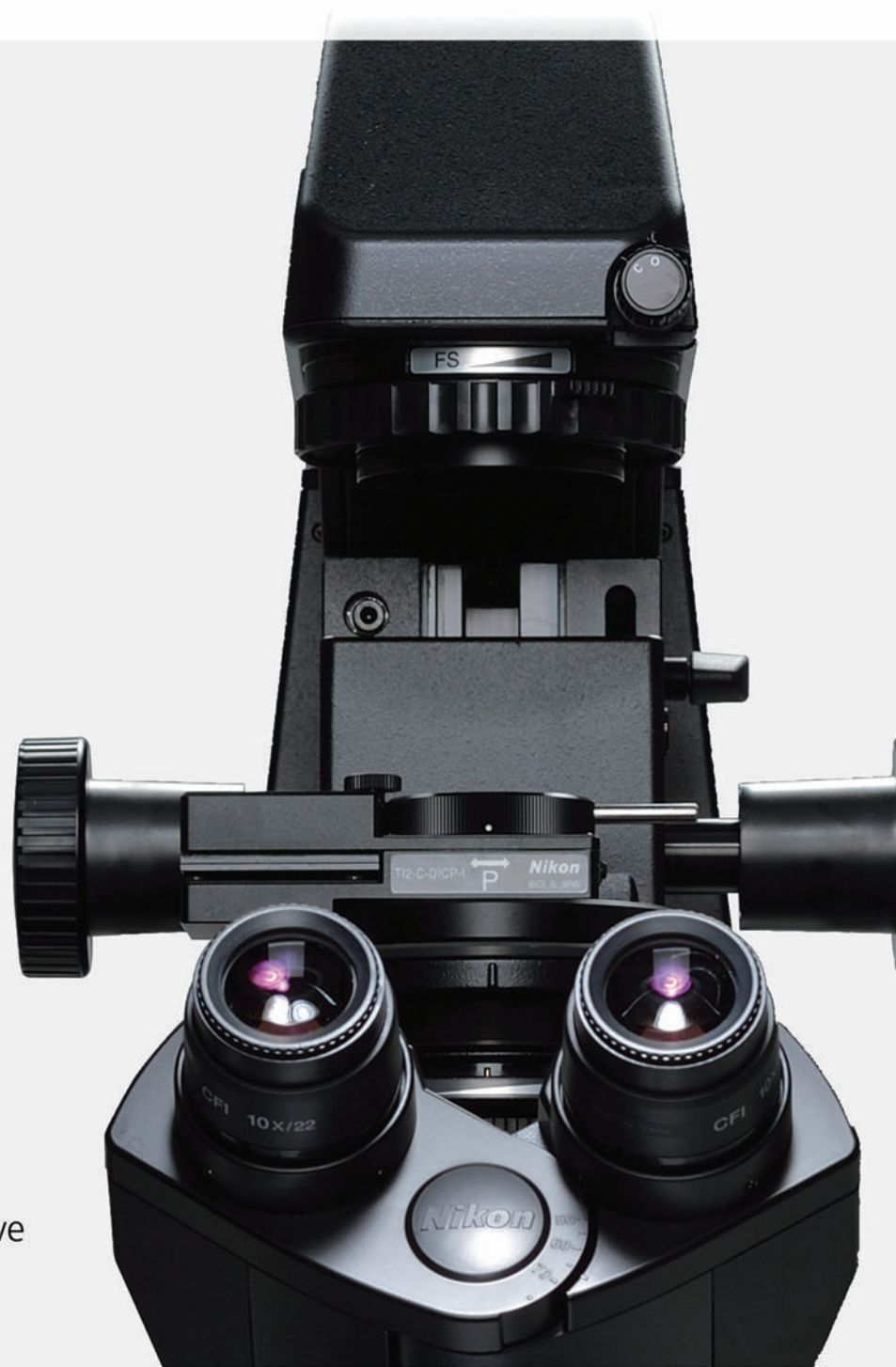
- Martinez-Outschoorn UE, Pestell RG, Howell A, et al. Energy transfer in "parasitic" cancer metabolism: mitochondria are the powerhouse and Achilles' heel of tumor cells. *Cell Cycle*. 2011;10:4208–4216.
- Warburg O, Wind F, Negelein E. The metabolism of tumors in the body. *J Gen Physiol*. 1927;8:519–530.
- Cori CA, Cori GT. The carbohydrate metabolism of tumours. *J Biol Chem*. 1925;65:397–405.
- Mider GB. Some aspects of nitrogen and energy metabolism in cancerous subjects: a review. *Cancer Res*. 1951;11:821–829.
- Babson AL, Winnick T. Protein transfer in tumor-bearing rats. *Cancer Res*. 1954;14:606–611.
- Commisso C, Davidson SM, Soydaner-Azeloglu RG, et al. Macropinocytosis of protein is an amino acid supply route in Ras-transformed cells. *Nature*. 2013;497:633–637.
- Davidson SM, Jonas O, Keibler MA, et al. Direct evidence for cancer-cell-autonomous extracellular protein catabolism in pancreatic tumors. *Nat Med*. 2017;23:235–241.
- Stehle G, Wunder A, Schrenk HH, Hartung G, Heene DL, Sinn H. Albumin-based drug carriers: comparison between serum albumins of different species on pharmacokinetics and tumor uptake of the conjugate. *Anticancer Drugs*. 1999;10:785–790.
- Stehle G, Sinn H, Wunder A, et al. Plasma protein (albumin) catabolism by the tumor itself—implications for tumor metabolism and genesis of cachexia. *Crit Rev Oncol Hematol*. 1997;26:77–100.
- Sleep D, Cameron J, Evans LR. Albumin as a versatile platform for drug half-life extension. *Biochim Biophys Acta*. 2013;1830:5526–5534.
- Matsumura Y, Meada H. A new concept for macromolecular therapeutics in cancer chemotherapy: mechanism of tumor-tropic accumulation of proteins and antitumor agent Smancs. *Cancer Res*. 1986;46:6387–6392.
- Isaacs JT, Dalrymple SL, Rosen DM, Hammers H, Olsson A, Leanderson T. Anti-cancer potency of tasquinimod is enhanced via albumin-binding facilitating increased uptake in the tumor microenvironment. *Oncotarget*. 2014;5:8093–8106.
- Kratz F. A clinical update of using albumin as a drug vehicle—a commentary. *J Control Release*. 2014;190:331–336.
- Bhattacharya AA, Grüne T, Curry S. Crystallographic analysis reveals common modes of binding of medium and long-chain fatty acids to HSA. *J Mol Biol*. 2000;303:721–732.
- Kratz F, Warnecke A, Scheuermann K, et al. Probing the cysteine-34 position of endogenous Serum albumin with thiol-binding doxorubicin derivatives: improved efficacy of an acid-sensitive doxorubicin derivative with specific albumin-binding properties compared to that of the parent compound. *J Med Chem*. 2002;45:5523–5533.
- Ogasawara Y, Mukai Y, Togawa T, Suzuki T, Tanabe S, Ishii K. Determination of plasma thiol bound to albumin using affinity chromatography and high performance liquid chromatography with fluorescence detection: ratio of cysteinyl albumin as a possible biomarker of oxidative stress. *J Chromatogr B Anal Technol Biomed Life Sci*. 2007;845:157–163.
- Gryzunov YA, Arroyo A, Vigne JL, et al. Binding of fatty acids facilitates oxidation of cysteine-34 and converts copper-albumin complexes from antioxidants to prooxidants. *Arch Biochem Biophys*. 2003;413:53–66.
- Alley SC, Benjamin DR, Jeffrey SC, Okeley NM, Meyer DL, Sanderson RJ, and Senter P D. Contribution of linker stability to the activities of anticancer immunoconjugates. *Bioconjugate Chem*. 2008;19:759–765.
- Shen BQ, Xu K, Liu L, et al. Conjugation site modulates the in vivo stability and therapeutic activity of antibody-drug conjugates. *Nat Biotechnol*. 2012;30:184–189.
- Fontaine SD, Reid R, Robinson L, Ashley GW, Santi DV. Long-term stabilization of maleimide-thiol conjugates. *Bioconjugate Chem*. 2015;26:145–152.
- Christie RJ, Fleming R, Bezabeh B, et al. Stabilization of cysteine-linked antibody drug conjugates with N-aryl maleimides. *J Control Release*. 2015;220:660–670.
- De Figueiredo RM, Oczipka P, Frohlich R, Christmann M. Synthesis of 4-maleimidobutyric acid and related maleimides. *Synthesis*. 2008;8:1316–1318.
- Denmeade SR, Jakobsen CM, Janssen S, et al. Prostate-specific antigen-activated thapsigargin prodrug as targeted therapy for prostate cancer. *J Natl Cancer Inst*. 2003;95:990–1000.
- Vander Griend DJ, Antony L, Dalrymple SL, et al. Amino acid containing thapsigargin analogues deplete androgen receptor protein via synthesis inhibition and induce the death of prostate cancer cells. *Mol Cancer Ther*. 2009;8:1340–1349.
- Janssen K, Horn S, Niemann MT, Daniel PT, Schulze-Osthoff K, Fischer U. Inhibition of ER Ca²⁺ pump forces multidrug-resistant cells deficient in Bak and Bax into necrosis. *J Cell Sci*. 2009;122:4481–4491.
- Denmeade SR, Mhaka AM, Rosen DM, et al. Engineering a prostate-specific membrane antigen-activated tumor endothelial cell prodrug for cancer therapy. *Sci Transl Med*. 2012;4:140ra86.
- Uzgare AR, Isaacs JT. Enhanced redundancy in Akt and mitogen-activated protein kinase-induced survival of malignant versus normal prostate epithelial cells. *Cancer Res*. 2004;64:6190–6199.
- Schnitzer JE, Bravo J. High affinity binding, endocytosis, and degradation of conformationally modified albumins. *J Biol Chem*. 1993;268:7562–7567.

How to cite this article: Akinboye ES, Rogers OC, Isaacs JT. 2-fluoro-5-maleimidobenzoic acid-linked albumin drug (MAD) delivery for selective systemic targeting of metastatic prostate cancer. *The Prostate*. 2018;78:655–663. <https://doi.org/10.1002/pros.23494>



Nikon Bioimaging Lab

Let us do the imaging for you.



The Nikon Bioimaging Lab is a state-of-the-art facility located in Cambridge, Massachusetts, that provides advanced technologies to support the burgeoning regenerative medicine and biotech sector.


For more information, visit www.microscope.healthcare.nikon.com/bioimaging-lab



Nikon Instruments Inc. ■ www.microscope.healthcare.nikon.com ■ nikoninstruments@nikon.net



Concise Review: Mesenchymal Stem Cell-Based Drug Delivery: The Good, the Bad, the Ugly, and the Promise

TIMOTHY E. G. KRUEGER,^a DANIEL L. J. THOREK,^{b,c} SAMUEL R. DENMEADE,^{c,d} JOHN T. ISAACS,^{c,d} W. NATHANIEL BRENNEN^c 

Key Words. Mesenchymal stem cell • Cell-based therapy • Drug delivery • Homing • In vivo cell tracking • Cell size

^aDepartment of Pharmacology and Molecular Sciences, Johns Hopkins University School of Medicine, Baltimore, Maryland, USA;

^bDepartment of Radiology and Radiological Science, Johns Hopkins University School of Medicine, Baltimore, Maryland, USA;

^cDepartment of Oncology at the Sidney Kimmel Comprehensive Cancer Center (SKCCC) at Johns Hopkins, Baltimore, Maryland, USA;

^dDepartment of Urology, James Buchanan Brady Urological Institute, Johns Hopkins University School of Medicine, Baltimore, Maryland, USA

Correspondence: W. Nathaniel Brennen, Ph.D., Johns Hopkins University School of Medicine, 1650 Orleans Street, CRB-1, Rm 1M46, Baltimore, Maryland 21287, USA. Telephone: (410) 502-6021; e-mail: wbrenne2@jhmi.edu

Received February 2, 2018; revised May 15, 2018; accepted for publication May 30, 2018; first published August 2, 2018.

<http://dx.doi.org/10.1002/sctm.18-0024>

This is an open access article under the terms of the Creative Commons Attribution-NonCommercial-NoDerivs License, which permits use and distribution in any medium, provided the original work is properly cited, the use is non-commercial and no modifications or adaptations are made.

ABSTRACT

The development of mesenchymal stem cells (MSCs) as cell-based drug delivery vectors for numerous clinical indications, including cancer, has significant promise. However, a considerable challenge for effective translation of these approaches is the limited tumor tropism and broad biodistribution observed using conventional MSCs, which raises concerns for toxicity to nontarget peripheral tissues (i.e., the bad). Consequently, there are a variety of synthetic engineering platforms in active development to improve tumor-selective targeting via increased homing efficiency and/or specificity of drug activation, some of which are already being evaluated clinically (i.e., the good). Unfortunately, the lack of robust quantification and widespread adoption of standardized methodologies with high sensitivity and resolution has made accurate comparisons across studies difficult, which has significantly impeded progress (i.e., the ugly). Herein, we provide a concise review of active and passive MSC homing mechanisms and biodistribution postinfusion; in addition to in vivo cell tracking methodologies and strategies to enhance tumor targeting with a focus on MSC-based drug delivery strategies for cancer therapy. *STEM CELLS TRANSLATIONAL MEDICINE* 2018;7:651–663

SIGNIFICANCE STATEMENT

As excitement for mesenchymal stem cell-based therapies, and synthetic biology approaches in general, continues to build and as these therapies increasingly undergo evaluation in the clinic, this review represents a sobering reminder of the broad biodistribution and poor homing efficiency to most target tissues observed using current methodologies, thereby justifying the need for enhanced targeting strategies to potentiate efficient and effective clinical translation of these strategies.

INTRODUCTION

There is enormous enthusiasm regarding the potential for cell-based therapies to treat a diverse array of pathological indications as the technology to engineer cells with specific attributes is maturing and entered clinical testing in some cases. This has been most visible with the emergence of chimeric antigen receptor (CAR) T-cells, although multiple other cell types are also in active development as platforms for synthetic biology approaches. Among the most promising of these engineered cell platforms are mesenchymal stem cells (MSCs). MSCs are defined analytically and functionally based upon positive (CD73, CD90, and CD105) and negative (CD45, CD34, CD14/CD11b, CD19/CD20/CD79 α , and HLA-DR) cell surface markers, plastic adherence, and the ability to

differentiate into osteoblasts, adipocytes, and chondrocytes. However, it should be noted this definition leaves room for significant phenotypic diversity, and these minimal criteria clearly define a heterogeneous population of cells with implications for clinical development [1].

Despite this heterogeneity, MSCs have numerous advantages that potentiate their clinical translation. These properties include their ease of isolation from multiple tissues, ex vivo expansion capacity, multipotent differentiation potential, immunomodulatory functions, ability to be manipulated or genetically modified, and immune-evasive or -privileged status, which permits use in an allogeneic setting. Although initial trials were premised on the ability of MSCs to repair damaged tissue

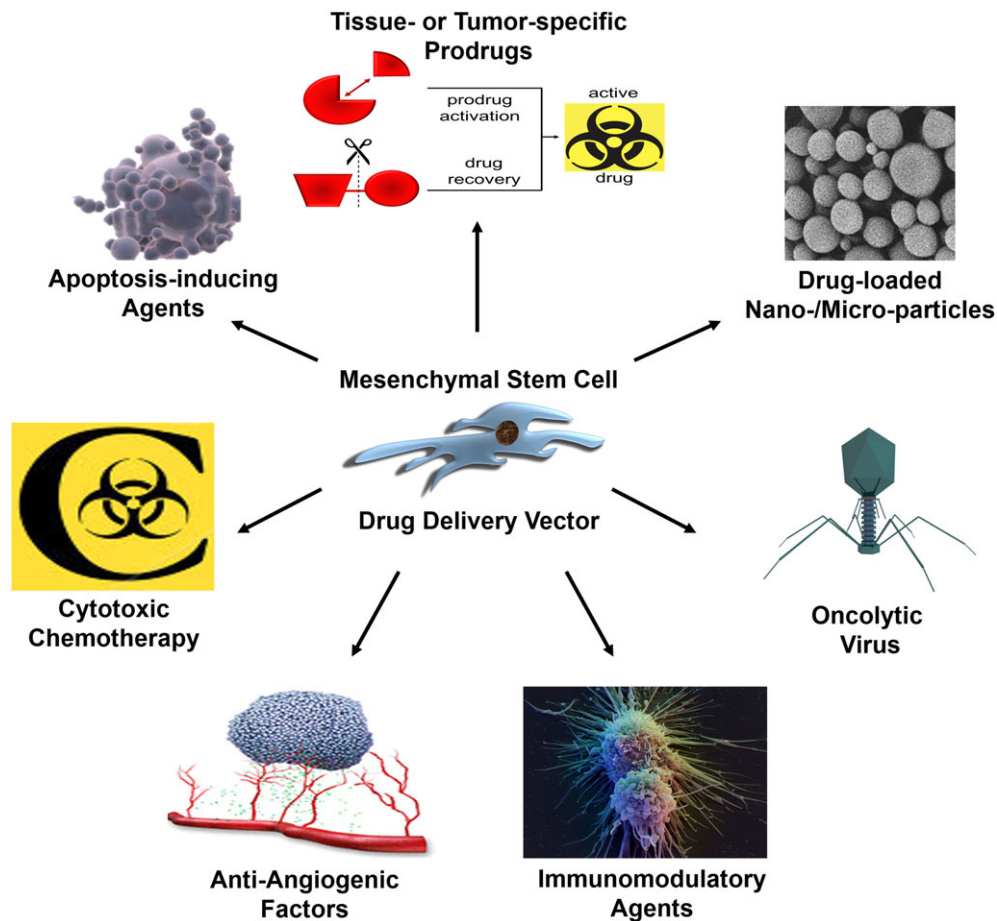


Figure 1. Mesenchymal stem cell (MSC)-based drug delivery strategies. The tumor tropism of MSCs can be exploited to deliver a wide variety of therapeutic agents for the treatment of cancer, such as apoptosis-inducing agents, cytotoxic chemotherapy, anti-angiogenic factors, immunomodulatory agents, oncolytic viruses, drug-loaded nanoparticles/microparticles, and tissue- or tumor-specific prodrugs.

via cell replacement, more recent clinical development has focused on their potent paracrine and immune regulatory functions [2]. Significant efforts have also been made to exploit the innate ability of MSCs to traffic to sites of inflammation, including those present in cancer, to deliver a variety of therapeutic interventions, including apoptosis-inducing agents, cytotoxic chemotherapy, drug-loaded nanoparticles/microparticles, tumor- or tissue-specific prodrugs, immunomodulatory agents, oncolytic viruses, and anti-angiogenic factors (Fig. 1; Table 1) [3–5].

These efforts have culminated in more than 1,000 completed or ongoing clinical trials using MSCs across many disorders with varying degrees of success. The clinical benefits of repurposing MSCs for the treatment of diverse clinical indications are challenged by evolving techniques to improve cell function, localization, and tracking following systemic infusion. A significant limitation for many of these strategies has been the lack of robust MSC homing to target tissues [6]. It has been posited that MSCs primarily ‘act at a distance’ via exosomes, polarization of phagocytic monocytes, and other paracrine effects [7–11], which may partially overcome poor targeting and broad biodistribution of systemically infused MSCs, particularly when coupled with exosome targeting strategies [9, 12]. However, increased activity directly in target tissue would likely be of significant benefit for many

applications, especially for those using MSCs as cell-based drug delivery vectors; wherein limiting toxicity to peripheral nontarget tissues is of critical importance. Factors that influence MSC homing are multifactorial; these include culture conditions during ex vivo expansion, tissue source, population heterogeneity, cell size, and species-specific differences in affinities for cognate receptor–ligand pairs when using xenogeneic models. The breadth of these factors necessitates that we focus this review on passive homing mechanisms related to cell size and mechanical entrapment, whereas others have recently been reviewed elsewhere [13]. A central limitation in evaluating and improving MSC homing has been a lack of robust quantification and widespread adoption of standardized methodologies with high sensitivity and resolution across models and disease states. Herein, we summarize MSC homing mechanisms and biodistribution postinfusion, in vivo cell tracking methodologies, and strategies to enhance tumor targeting with a focus on MSC-based drug delivery strategies for cancer therapy.

MSC HOMING MECHANISMS

The mechanisms for cellular trafficking via systemic circulation were first characterized for leukocyte homing to sites of inflammation, which involves a multistep adhesion and extravasation cascade. Given the role of MSCs in regulating the

Table 1. Classes and examples of MSC-based anti-cancer agent drug delivery strategies

Anti-cancer strategy	Common agents	Mechanism of action	Advantages	References
Oncolytic viruses	Adenovirus; Measles virus; Herpes simplex virus	Viruses infect, replicate in, and lyse tumor cells	Amplification of anti-tumor effect with multiple rounds of infection; Selective replication in tumor cells	[75–78, 98]
Tumor- or tissue-specific prodrugs	CD + 5-FU; Hsv-tk + Ganciclovir; PSA-activated thapsigargin peptide	Cytotoxic drug metabolites induce cell death by inhibiting DNA synthesis (5-FU, ganciclovir) or by inducing ER stress (thapsigargin)	Selective drug activation in tumor microenvironment	[79–84]
Immunomodulatory agents	IL-2; IL-12; Interferon-β; CX3CL1	Lymphocyte activation and induction of tumor-specific T-cell responses; Direct induction of tumor cell differentiation and growth arrest	Endogenous signaling molecules; Potential direct and indirect effects on tumor growth; Synergy with other immunotherapies	[73, 89–92]
Apoptosis-inducing agents	TRAIL	Direct induction of apoptosis via death receptors	Currently in clinical trials; Endogenous signaling molecule	[93–97]
Cytotoxic chemotherapy	Paclitaxel; Doxorubicin	Induction of cell death via inhibition of microtubule depolymerization (paclitaxel) or topoisomerase II function (doxorubicin)	FDA-approved chemotherapeutic drugs	[68]

Abbreviations: CD, cytosine deaminase; 5-FU, 5-fluoruracil; Hsv-tk, herpes simplex virus-thymidine kinase; PSA, prostate specific antigen; TRAIL, TNF-related apoptosis-inducing ligand.

overall immune response [14–16], it is unsurprising that MSCs are thought to use similar mechanisms to migrate toward inflammatory cues emanating from sites of tissue damage including the tumor microenvironment [13, 17–19]. Nitzsche et al. provide a thorough review of the important molecular determinants of MSC homing at each step of this migratory cascade [19].

‘Passive Homing’, Cell Size, and Mechanical Entrapment

Despite evidence that MSC homing is mediated by specific receptor–ligand pairs, passive entrapment of MSCs in the tumor or sites of injury occurs at least partially as a result of increased vascular permeability and mechanical entrapment in these microenvironments. An important distinction between

MSCs and lymphocytes is their size (Fig. 2), with cell diameters ranging from 15–30 μm versus 4–12 μm, respectively [20–22]. It is often unappreciated that relatively small increases in cell diameter translate into significant increases in cell volume, because this value increases as the cube of the radius. This larger cell size, particularly following ex vivo culture [23], leads to passive arrest of MSCs in small diameter vessels such as terminal arterioles, capillaries, and postcapillary venules as a result of mechanical entrapment. Indeed, the vast majority of MSCs infused intravenously (IV) are rapidly cleared from the blood and found within the capillary beds of the lungs within minutes of injection [24–28]. In both humans and animal models, this rapid entrapment is followed by clearance from the lungs and accumulation in the liver and spleen over subsequent hours to days [24–28]. Recent evidence suggests this “redistribution” may be a function of nonclassical phagocytic monocytes engulfing cellular debris (and tracking labels) from apoptotic MSCs entrapped in the lungs [10, 11].

Mechanical entrapment in the lungs results from the fact that pulmonary capillaries are ~10–15 μm in diameter, a phenomenon termed the pulmonary ‘first-pass effect’ [20, 21, 29, 30]. Previous studies using microspheres have documented that objects ≥10 μm in diameter are highly susceptible to this effect [21], and particles <1 μm are necessary to ensure complete dispersion through the smallest capillaries [30]. Importantly, endogenous MSCs in the bone marrow are smaller in size (~10 μm) [23], which enable efficient trafficking via systemic circulation. Similar to lymphocytes, MSCs are thought to increase in size once activated (mimicked during ex vivo culture) within sites of inflammation and tissue damage.

Although cellular deformability can facilitate passage of larger cells through smaller vessels to some degree [23, 31], there is a physical limit to this property that is necessary to maintain cell viability and prevent vessel occlusion. Intra-arterial (IA) infusions can circumvent the first-pass effect to provide one pass through systemic circulation and exposure to peripheral tissues before entering the lungs. However, mechanical entrapment may still be a dominant driver of MSC biodistribution (Fig. 2). In one study,

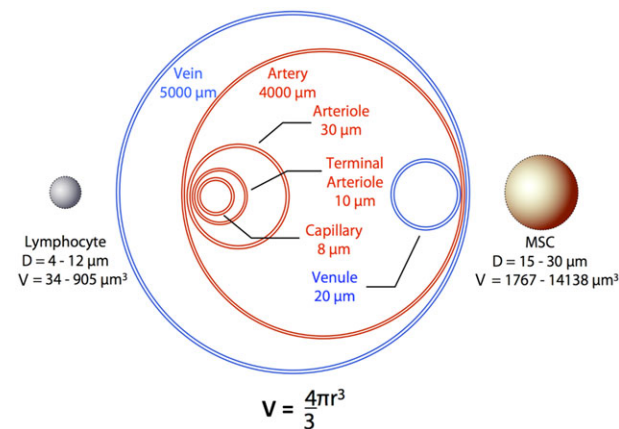


Figure 2. Mechanical barriers to MSC trafficking via systemic circulation. The large cell size of MSCs, particularly following ex vivo expansion, is a significant physical barrier that prevents efficient and complete dispersion through small vessels in the vascular network. This severely limits access of exogenously introduced MSCs to many target tissues, including tumors. Abbreviations: D, diameter; MSC, mesenchymal stem cell; V, volume.

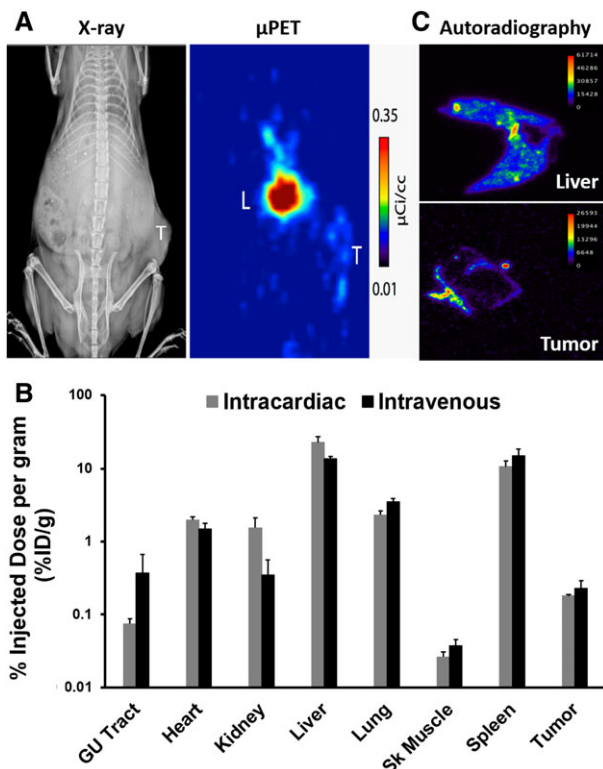


Figure 3. In vivo cell tracking of systemically-infused ^{89}Zr -labeled human MSCs in a prostate cancer xenograft model. **(A):** X-ray and μPET imaging documenting accumulation of the radiolabel in the liver and tumor (PC3) at 7 days post-IV infusion. **(B):** Biodistribution of ^{89}Zr -labeled MSCs at 7 days post-IV or -IC infusion determined by ex vivo scintigraphy. **(C):** Autoradiography detailing sub-organ distribution of ^{89}Zr -labeled MSCs, confirming localization restricted to the tumor periphery. Abbreviation: μPET , microPET.

for example, >90% of MSCs injected into the iliac artery were found acutely arrested at the precapillary level in downstream microvessels (7 μm diameter) of the cremaster muscle [23]. To date, there have been limited studies addressing the relative importance of active versus passive arrest in the lungs or other tissues; however, it is likely that both mechanisms are important and can be manipulated to increase homing efficiency to sites of interest.

In our own studies, we have identified MSCs in benign and malignant human prostate tissue [32]. These observations led us to initiate studies characterizing MSC biodistribution, kinetics, and trafficking toward different prostate cancer xenografts postinfusion, in addition to assessing chemokine and cognate receptor profiles to identify key pathways mediating MSC tumor tropism in prostate cancer. For example, whole body PET imaging using zirconium-89 (^{89}Zr)-labeled MSCs [33] (Fig. 3A), revealed that $\sim 0.2\%$ of the injected cells trafficked to subcutaneous PC3 prostate cancer xenografts per gram of tissue at 7 days postinfusion (Fig. 3B). This uptake is consistent across MSC administration methods used (intra-cardiac [IC]: 0.18 ± 0.02 vs. IV: $0.23 \pm 0.06\%$ ID/g). Broad biodistribution was observed at this time point with >1% of the injected dose detected in the heart, kidney, liver, lung, and spleen independent of the route of administration (Fig. 3B). Autoradiography confirmed tissue distribution of infiltrating MSCs with tumor localization restricted to the periphery as expected based on the vascular pattern of subcutaneous tumors (Fig. 3C).

Strategies to Overcome Mechanical Perfusion Barriers

Collectively, these findings indicate the vast majority of exogenously introduced MSC-based therapeutics have limited access to target tissue outside of the lung as a result of mechanical entrapment. To partially overcome this barrier and improve targeting, preadministration of vasodilators such as sodium nitroprusside have been used to reduce lung entrapment in mouse models [21, 29]. In addition, multiple investigators have developed ex vivo expansion protocols reported to generate MSC cultures with smaller average cell diameters [34–37].

Recently, Luo et al. generated “synthetic MSCs” (synMSCs) by packaging MSC conditioned media into PLGA microparticles coated with MSC membranes, which demonstrated efficacy in a model of myocardial infarction [38]. In this study, the synMSCs were designed to be equal in size to culture-expanded MSCs for comparison, but this raises the interesting possibility of engineering synMSCs (or microparticles coated with other cell membranes/targeting moieties) with engineered diameters designed to avoid first-pass entrapment in pulmonary capillaries and deliver bioactive molecules based on active targeting mechanisms. A similar alternative approach is to incorporate anti-cancer agents of interest (e.g. drugs, proteins, RNA, etc.) into targeted MSC-derived extracellular vesicles or exosomes via active or passive loading mechanisms [9, 12]. Despite these approaches, lung entrapment remains a critical challenge for MSC-based drug delivery; although evidence suggests this is a surmountable engineering challenge.

METHODS TO TRACK MSC HOMING IN VIVO

Standardization of robust quantitative methods with high sensitivity and resolution along with standardized reporting metrics are essential for cross-study comparisons and validation. Methods to track MSCs have largely been variations of the same core techniques, each with advantages and disadvantages (Table 2). Of these approaches, ex vivo histological analysis is the most common. This is typically performed using MSCs labeled with a fluorescent lipophilic vital dye (e.g. CM-Dil or PKH26) pre-infusion or stained immunohistochemically postinfusion for an exogenously introduced marker such as green fluorescent protein (GFP) followed by counting labeled cells in random fields after tissue processing. A variation of this approach uses in situ hybridization to label DNA sequences such as the Y-chromosome or human Alu sequences in sex- or species-mismatched samples, respectively. These ex vivo methods to quantify MSC homing are cost-effective and do not require specialized equipment; however, tissue collection is highly invasive, not amenable to repeated measurements for kinetic analyses, and highly susceptible to sampling bias because only a small portion of the tissue of interest is typically analyzed, in addition to the potential for false positives as a result of label redistribution by phagocytic monocytes following uptake of cellular debris from dying MSCs.

PCR-based techniques are another commonly used method to quantify MSC homing. Frequently, these techniques take advantage of species-mismatched donor/recipient pairs to detect species-specific sequences (e.g. GAPDH or Alu sequences) [28]. Conventional PCR-based methods have an estimated threshold of detection of $\sim 50,000$ cells [39], which does not achieve the sensitivity required to accurately quantify

Table 2. Advantages and disadvantages of common in vivo and ex vivo cell tracking methodologies

Technique	Common imaging agents	Limit of detection	Depth of penetration	Spatial resolution	Temporal resolution	Useful applications advantages	Limitations	References
In vivo techniques								
BLI	D-luciferin/Firefly luciferase, Coelenterazine/Renilla luciferase	10–10,000 cells (depending on tissue depth)	~3 cm (~10-fold loss of signal intensity per cm)	50 µm	1 min	Whole-body imaging; Reporter enzyme expressed only in metabolically active live cells; Cheap; Ease of use	2D image; Limited to small animal studies; Signal attenuation in deeper tissues; Signal quantitation not comparable across tissues; Susceptible to vascular disrupting agents	[21, 56, 65, 76, 95, 102, 106]
MRI	Ferumoxide; Ferumoxytol; Ferritin; Gd chelates	1,000–10,000 cells (depending on imaging agent and instrumentation)	No limit	100–200 µm	1 min	Whole-body imaging; Anatomical imaging; Ferritin reporter gene enables detection exclusively of live cells; Clinical integration	T2 hypointensity indistinguishable from tumor hemorrhage; False positives due to macrophage uptake; 2D image; Label diluted with each cell division; Potential cytotoxicity and ROS generation; Sophisticated equipment and expertise needed	[26, 55, 56]
PET	¹⁸ F-FDG; Hsv-TK + ¹⁸ F-FDG; ⁶⁴ Cu-PTSM; ⁸⁹ Zr; ¹²⁴ I	100–25,000 cells (depending on imaging agent and instrumentation)	No limit	1–2 mm	15 min	Whole-body imaging; 3D imaging; Multiple radioisotopes and labeling chemistries available; Hsv-TK reporter gene enables detection exclusively of live cells; Clinical integration	Use of radioisotopes; Hazardous transfection reagents; Potential false positives after cell death/label efflux; Sophisticated equipment and expertise needed	[33, 48]
In vivo microscopy	GFP; Vital dyes (DiD/DiI/DiD/DiR); CFDA/CFSE	Single cell	150–250 µm	Single cell	Video-rate	Imaging in context of natural microenvironment; Visualization of dynamic processes (migration, vascular adhesion, TEM)	Limited to preselected areas with low required path length; Tissue exteriorization may influence MSC recruitment/retention; Tissue auto-fluorescence; Sophisticated equipment and expertise needed	[18, 23, 46, 58, 60, 61, 99, 100]
In vivo flow cytometry	GFP; Vital dyes (DiD/DiI/DiD/DiR); CFDA/CFSE; PKH26	1–10 cells/mL	150–250 µm	Single cell	Continuous	Enumeration of circulating cells; Tracking dynamic entry and exit from circulation; Detection of cell flow velocities; Analysis of large blood volume; No artifacts from cell isolation and processing	Quantification influenced by flow velocity and vessel size; Tissue auto-fluorescence; Antibody labeling can lead to target cell depletion; Sophisticated equipment and expertise needed	[62–64]

(Continues)

Table 2. Continued.

Technique	Common imaging agents	Limit of detection	Depth of penetration	Spatial resolution	Temporal resolution	Useful applications advantages	Limitations	References
Ex vivo techniques								
Histology	X-gal/ β -gal; Prussian blue/iron oxide	Single cell	N/A	Single cell	Single time point/sample	In situ visualization within contextual tissue structure	Loss of signal from gene silencing or cell division; Sampling bias	[26, 34, 47, 94]
IHC	GFP/anti-GFP; CFDA/ anti-fluorescein; PKH26; Vital dyes (DiI/DiL/DiD/DIR); Quantum dots; Fluc/anti-FLuc	Single cell	N/A	Single cell	Single time point/sample	In situ visualization within contextual tissue structure	Loss of signal from gene silencing or cell division; Sampling bias; Tissue auto-fluorescence; Potential transfer of membrane dyes	[18, 43–46, 56, 71–73, 77]
FISH	Y-Chromosome; Alu sequences	Single cell	N/A	Single cell	Single time point/sample	In situ visualization within contextual tissue structure; No loss of signal	Sampling bias; Tissue auto-fluorescence	[71]
Ex vivo flow cytometry	GFP	1–10 cells/mL	N/A	Single cell	Single time point/sample	Enumeration of circulating cells	Potential artifacts from cell isolation and processing; Cell auto-fluorescence; Sophisticated equipment and expertise needed	[26, 34, 63, 64]
qRT-PCR	Y-Chromosome; Alu sequences	1/600,000 cells (~0.0002%)	N/A	Single cell	Single time point/sample	Quantification from whole tissue	Rare transcripts difficult to detect due to stochasticity of PCR amplification	[25, 28, 40]
ddPCR/ BEAMing	Y-Chromosome; Alu sequences	1/10,000 cells (0.01%)	N/A	Single cell	Single time point/sample	Quantification from whole tissue; Identification of rare transcripts/cell populations	Sophisticated equipment and expertise needed	[41]
Scintigraphy	¹¹¹ In-oxine; ¹⁸ F-FDG; ⁶⁴ Cu-PTSM; ⁵¹ Cr; ¹²⁵ I; ^{99m} Tc-HMPAO	Single cell (depending on labeling efficiency)	N/A	Single cell	Single time point/sample	Quantification from whole tissue	Use of radioisotopes	[20, 26, 33, 47, 51, 52]

Abbreviations: BLI, bioluminescence imaging; FISH, fluorescence in situ hybridization; Gd, gadolinium; Hsv-tk, herpes simplex virus-thymidine kinase; IHC, fluorescence imaging and immunohistochemistry; MRI, magnetic resonance imaging; PET, positron emission tomography; qRT-PCR, quantitative real-time PCR.

the level of MSC homing to most tissues. Although quantitative RT-PCR (qRT-PCR) has been estimated to have a threshold of detection as low as one human MSC in 600,000 murine cells [40], the detection of rare transcripts (i.e., injected MSCs) among a population (i.e., tissue) is still highly problematic for accurate quantification due to the stochastic nature of PCR-based amplification and competition for reagents. More recently developed methodologies such as droplet digital PCR (ddPCR) and BEAMing address this problem by segregating individual transcripts into separate compartments (i.e., droplets/microemulsions) before PCR amplification. This methodology can accurately quantify rare transcripts in the range of 0.01% [41], and new advancements in next generation sequencing (NGS) have pushed the sensitivity even lower depending on the number of genome equivalents analyzed [42].

Whole Body Imaging Methods

Unlike the techniques described earlier, whole-body imaging permits serial imaging over time to determine kinetics of biodistribution in multiple organs simultaneously in live animals. Several approaches have been used including: optical methods such as bioluminescent imaging (BLI) of MSCs expressing firefly luciferase (Fluc) or fluorescent dye-labeled cells; magnetic resonance (MR) imaging using MSCs loaded with superparamagnetic particles; and nuclear imaging techniques (e.g., positron emission tomography [PET] and single photon emission computed tomography [SPECT]) with radiolabeled MSCs.

Of the whole-body imaging techniques, optical methods require the least expensive equipment and have been widely used in proof-of-principle preclinical studies. However, BLI and fluorescence have limited translational application, and for BLI, the signal is dependent on vascular delivery of the luciferase substrate. Consequently, the signal is not necessarily proportional to MSC homing and is highly sensitive to vascular disrupting agents. In addition, both BLI and fluorescent signals have a limited depth of tissue penetration, meaning that signal quantification is not directly comparable for tissues at different depths. In contrast, both nuclear and MR imaging modalities are well-integrated into clinical practice, potentially allowing quantitative *in vivo* tracking of MSCs for clinical trials.

Fluorescence imaging with cell labeling dyes has been widely used in the small animal imaging field to track the distribution of cells labeled *ex vivo* with membrane binding dyes. Light propagation through tissue is heavily dependent on wavelength, and redshifted or near infrared dyes enable visualization of labeled cells through several millimeters of tissue. To that end, membrane-anchored dyes that contain a lipophilic anchor and a near infrared fluorescent component, such as PKH-26 and the Dioctadecyl family of dyes (including DiI, DiD, and DiR), have been used to label MSCs for noninvasive tracking [43–46]. The limited depth of penetration, potential impact of the surface label on MSC behavior, the dilution of the label through cell division, and uptake by phagocytic cells following death are limitations to the use of this technique; however, the fluorescent label does enhance the ability to rapidly detect the presence of the cells in *ex vivo* analyses with the caveat of sampling bias and re-distribution of the tracking label by phagocytic monocytes as described earlier.

In addition, there are a variety of SPECT and PET-compatible radiolabels that have been used for quantitative

in vivo cell tracking of infused MSCs, each with advantages and disadvantages [27, 33, 47–50]. DeGrado et al. recently developed a novel cell labeling methodology using ^{89}Zr , which achieves high labeling efficiency and displays robust stability *in vitro* and *in vivo* with minimal impact on viability [33]. The relatively long half-life of ^{89}Zr ($t_{1/2} = 78.4$ hours) enables *in vivo* cell tracking at high resolution over a 2–3 week period [33]. Another intriguing approach has been to engineer MSCs to express the sodium iodide symporter (NIS), which can be exploited for imaging (^{124}I) or therapeutic (^{131}I) applications [48, 49]. This strategy was recently translated into a phase I/II clinical trial using MSCs infected with an oncolytic measles virus encoding NIS to treat recurrent or chemotherapy-resistant ovarian cancer [NCT02068794]. *Ex vivo* scintigraphy of radiolabeled MSCs is also frequently performed to complement *in vivo* nuclear methods to obtain semi-quantitative counts in tissues of interest.

Although each of these whole-body techniques enable serial imaging for kinetic analyses of MSC homing and biodistribution, it is important to consider the half-life, stability, and cell retention of the particular tracking label selected depending on the specific application and length of study. For example, efflux of ^{111}In -oxine, a commonly used leukocyte labeling agent, from cells is reported to be as high as 70%–80% after just 24–96 hours post labeling [33]. $^{99\text{m}}\text{Tc}$ -hexamethylpropylene amine oxime ($^{99\text{m}}\text{Tc}$ -HMPAO) has a longer retention profile, but is similar to ^{111}In -oxine in that it is a lipophilic complex that can penetrate the cell membrane, which then becomes entrapped once internalized [51]. $^{99\text{m}}\text{Tc}$ -HMPAO labeled MSCs have enabled imaging and quantitation of uptake at sites of brain injury in mice [52] and cardiac damage in rats [47]. Labeling with radioactive sodium chromate ($\text{Na}_2\text{Cr}^{51}\text{O}_4$) involves intracellular reduction of the cell permeable hexavalent chromium (CrO_4^{2-}) to the impermeable trivalent chromic (Cr^{+++}) ion following binding to macromolecules [53]. Alternatively, the novel ^{89}Zr -labeling strategy mentioned earlier also labels macromolecules, but is restricted to primary amines on the cell surface due to poor membrane permeability of the reagents [33]. The fate of such intracellular and membrane-bound radiolabeled proteins following secretion or cell death (e.g., uptake by macrophages/monocytes) and the potential for subsequent redistribution is often not considered but can be monitored. It should be noted that many unbound radionuclides inherently accumulate in the bone and liver when released into systemic circulation. Therefore, significant efforts should be made to confirm that radioactivity or other detection labels observed in tissues of interest is associated with infiltrating MSCs by an independent method whenever possible.

In contrast, ^{125}I -5-iodo-2'-deoxyuridine incorporates into DNA and is only released upon cell death. Furthermore, it is poorly re-used and quickly eliminated following release, meaning that radioactivity is predominantly a direct readout of live cells [54]. Unfortunately, however, ^{125}I SPECT imaging requires a large activity dose, limiting its usefulness for applications with low rates of genome incorporation. The consideration of dose to the cell, which may affect cellular physiology and function, is very important. Ideally, labels are incorporated for tracking in a truly noninvasive setting. As an example, MR imaging provides high spatial and anatomic resolution but relative to nuclear methods a low sensitivity. Thus, MR

approaches using superparamagnetic agents, which have recently been optimized for high labeling efficiency and stability (≥ 21 days), require large mass amounts of cell-internalized particles [55, 56]. Interestingly, Huang et al. found that iron oxide magnetic nanoparticles induced CXCR4 cell surface expression on MSCs in a HIF-1 α -dependent manner and enhanced homing to traumatic brain injury [56]. Collectively, these data suggest that significant care must be taken when selecting an appropriate cell tracking modality, as there may be unintended consequences and varying potential for false positives depending on the application and study design.

Localized Imaging Methods

Confocal, two-photon, or intravital microscopy can be used to visualize fluorescently labeled MSCs in real-time in specific *in vivo* settings. By introducing additional targeted fluorophores, MSCs can be visualized in the context of other labeled structures, such as blood vessels, with high spatial definition. This methodology allows for high resolution quantification down to the single-cell level and can be used to interrogate various stages of the homing cascade, such as MSC rolling, entrapment, and extravasation. However, imaging is limited to preselected areas with penetration up to 250 μm . Due to this limitation, LPS-induced inflammation in the murine ear (~ 200 μm thick) is a commonly used model when employing this technique [57, 58]. *in vivo* microscopy has been used for other applications such as measurement of tumor cell or MSC homing to the bone marrow of murine skulls [59, 60] or MSC passage through blood vessels of an exteriorized cremaster muscle [23]. However, these procedures involve surgery to expose tissues, and such tissue injury may influence recruitment or retention of MSCs. Notably, video-rate two-photon imaging of T-cell infiltration into subcutaneous tumors has been performed at depths of up to 150 μm from the tumor surface [61] and could similarly be used to quantify MSC infiltration.

More recent approaches to quantify MSC homing include *ex vivo* and *in vivo* flow cytometry. Although both techniques are based on the same principles, the former is the more traditional form to analyze cells labeled *ex vivo* with a fluorescent dye or antibody following sample collection, whereas the latter applies transillumination of a narrow slit along an artery with a focused laser to allow detection of circulating cells that are fluorescently labeled before infusion. Like intravital microscopy, arteries within the murine ear are typically used due to accessibility and the low required path length. This approach has been used to quantify circulating cells, including MSC clearance rates from peripheral blood of healthy and tumor-bearing mice [59, 62–64]. Although both *ex vivo* and *in vivo* flow cytometry are able to detect rare populations of cells, ~ 1 –10 cells per ml of blood, *in vivo* flow cytometry is approximately twice as sensitive but significantly more challenging to perform [63].

Each set of methods has advantages and limitations, including the inherent sensitivities of each method (Table 2), that may contribute to the variability often observed between MSC homing studies. In addition, homing efficiency is often reported as a relative measure between experimental and control groups rather than an absolute number. These facts, coupled with the lack of positive controls available for MSC

homing studies, makes standardization and comparison of homing efficiencies across platforms extremely difficult.

IMPLICATIONS FOR CLINICAL TRANSLATION AND EFFICACY

Although clinical efficacy has been observed in several applications despite poor tissue-targeting [2, 14–16], homing efficiency and selectivity are critical for developing MSCs as cell-based delivery vehicles for anti-cancer therapies. Although MSC homing to the tumor microenvironment has been observed [65–67], it is a very inefficient process as discussed earlier with the exception of strategies targeting the lung via entrapment or potentially the liver as a result of clearance. The typical broad biodistribution of systemically infused MSCs in nontarget tissue has significant consequences for potential toxicity to peripheral tissues in drug delivery applications. In addition, MSC infiltration must reach sufficient levels within the tumor microenvironment to deliver a complete tumoricidal dose of the cytotoxic agent, which is dependent upon drug potency, release kinetics, and the amount of drug that can be delivered per cell. Using *in vitro* co-culture assays, Pessina et al. demonstrated that Paclitaxel-primed MSCs needed to represent 2%–33% of the culture to reach 90% cytotoxicity against various cancer cell lines depending on the sensitivity of each line to the drug [68]. In proof-of-principle *in vivo* studies, we have documented that MSCs loaded with microparticles encapsulating a PSA-activated prodrug are required to reach levels of $\sim 1\%$ –10% to achieve a significant anti-tumor effect in a prostate cancer xenograft model [69].

In these preclinical studies, the homing endpoints necessary for efficacy are often not met. For example, only $\sim 0.2\%$ of injected human bone marrow-derived MSCs (i.e., 2,000 cells) per gram of tissue were found in subcutaneous PC3 prostate cancer xenografts at 7 days postinfusion (Fig. 2B). Importantly, our group recently completed a phase 0 pre-prostatectomy clinical trial to quantify homing of IV-infused allogeneic BM-MSCs via BEAMing [41] and NGS haplotype counting [42] to sites of primary prostate cancer [NCT019833709], which documented that MSC homing to prostate tissue was below the level of detection under the conditions and time points tested. In addition, homing of MSCs to the bone marrow, a site of significant disease burden in men with lethal metastatic prostate cancer and other tumor types such as breast cancer, has been analyzed in many studies, often revealing that culture-expanded MSCs have poor bone marrow tropism and are frequently undetectable [20, 70]. Limited tumor tropism was also demonstrated in mouse models of glioma; no eGFP+ MSCs were detected in N29 or N32 glioma xenografts 2 or 7 days after IV injection [71]. In contrast, MSCs were detected in U87, U251, and LN229 glioma xenografts 7 days after local IA injection via the internal carotid artery, and MSCs expressing IFN β extended survival in treated animals, suggesting that $>2.5 \times 10^4$ cells (i.e., 2.5% of injected dose) reached the tumor based on controls [72]. The same group also demonstrated that IFN β -MSCs at fractions as low as 1% of the tumor mass suppressed growth of subcutaneous A375 melanoma xenografts, that MSCs were preferentially localized in the tumor periphery 8 days after IV injection, and that IV-injected IFN β -MSCs significantly prolonged survival in a metastatic melanoma model [73]. Collectively, these studies

highlight the importance of quantifying MSC homing and determining endpoints necessary for efficacy in each application and disease model.

MSC-BASED ANTI-CANCER STRATEGIES

Although the role of MSCs in cancer initiation and progression remains unclear [74], this has not dampened interest in exploiting their (albeit limited) tumor tropism for the delivery of anti-cancer agents (Fig. 1; Table 1). Consequently, delivery of these anti-cancer agents to nontarget tissues and the potential for toxicity are a critical concern for MSC-based drug delivery strategies. Approaches to increase either tumor selective delivery or specificity of the targeted agent are of significant interest. One such strategy has been to infect MSCs with an oncolytic adeno or measles virus that selectively replicates in tumor cells, which has the added advantage of amplifying the anti-tumor effect with subsequent rounds of infection and lysis [75–78]. Another promising approach is the selective activation of prodrugs within the tumor microenvironment. These include engineering MSCs to express cytosine deaminase (CD) or herpes simplex virus-thymidine kinase (Hsv-TK) to convert an inactive systemically injected substrate [5-fluorouracil (5-FU) and ganciclovir, respectively] into their respective active cytotoxic metabolites [79, 80]. Preclinical development of TK-expressing MSCs by Bruns and Nelson et al. led to the landmark TREAT-ME1 study in gastrointestinal adenocarcinomas [NCT02008539], the first clinical trial to use genetically engineered autologous MSCs. Due to the small study size ($n = 6$), conclusions are limited, but it should be noted the treatment was safe and tolerable with no significant adverse events attributed to the MSC infusion product [5, 81].

Prodrug strategies such as these alter pharmacokinetics and limit systemic drug exposure; however, the biodistribution of MSCs in nontarget tissue remains a significant safety concern as this is still the primary determinant of drug activation in peripheral tissue. Furthermore, to enhance specificity, multiple investigators have placed TK under the control of conditionally expressed promoters (e.g. CCL5 or Tie2) to restrict activity to the tumor microenvironment [82, 83]. An alternative approach being explored by our group is the use of prodrugs activated by tissue- or tumor-specific proteases, such as prostate-specific antigen (PSA) to target prostate cancer cells, prostate-specific membrane antigen (PSMA) to target the tumor neovasculature, or fibroblast activation protein (FAP) to target MSCs and the tumor-associated stroma [69, 84–87]. This strategy couples a highly potent nonselective drug or toxin to an activating peptide substrate selectively recognized by a proteolytic enzyme whose expression is restricted to the target site, thereby engineering a tissue- or tumor-specific ‘molecular grenade’ [88].

Another common MSC-based drug delivery approach is to exogenously introduce various immunomodulatory proteins (e.g. type I interferons, chemokines, interleukins, etc.) [57, 73, 89–92]. Similarly, engineering MSCs to express TNF-related apoptosis-inducing ligand (TRAIL) has shown particular promise in multiple preclinical cancer models [93–95]. This preclinical data together with decades of clinical observations regarding MSC biodistribution patterns led to the recently initiated TACTICAL trial, a phase I/II study of MSC-TRAIL in combination

with cisplatin and pemetrexed in non-small cell lung cancer (NSCLC) patients [NCT03298763] [96]. Previous efforts using systemic delivery of TRAIL as an anti-cancer strategy failed clinical testing due to toxicity and poor responses at the administered doses [97]. This provides the rationale for the selective delivery of TRAIL by MSCs within the tumor microenvironment to limit systemic toxicity to non-target peripheral tissues. The rapid entrapment of MSCs in lung capillaries following IV infusion suggests this platform may be uniquely suited to act as a ‘biological micro-factory’ producing an anti-cancer agent (i.e., TRAIL) directly at the target site, at least for this clinical scenario (i.e., NSCLC); although hepatotoxicity may still be of significant concern.

Another potential application for therapeutic MSCs may be in the adjuvant setting for localized treatment of residual disease following surgery or radiotherapy. This could be particularly useful when extensive surgical resection or large radiation fields are difficult or associated with significant risks (e.g. glioblastoma) [50, 95, 98]. Local delivery directly to the site of action obviously circumvents limitations associated with homing efficiency, and the high degree of overall safety observed in clinical trials using MSCs to date in other disease settings make this a feasible strategy.

SYNTHETIC STRATEGIES TO ENHANCE MSC HOMING

Due to the low homing efficiency of MSCs to many tissues of interest, novel methods to synthetically modify MSCs for enhanced targeting are critically needed. Using bone tropism as an example, low homing has been attributed to the lack of chemokine and adhesion molecules such as PSGL-1, CXCR4, and E-selectin ligands, particularly following *ex vivo* expansion in tissue culture [60, 70]. In a seminal paper, Sackstein et al. developed a strategy to mimic hematopoietic stem cell (HSC) selectin-mediated homing to the bone via glycan engineering [60]. Essentially, exogenously introduced fucosyltransferases are used to modify CD44 expressed by MSCs into HCELL (hematopoietic cell E-/L-selectin ligand), a potent E-selectin ligand critical for HSC homing to the bone marrow [60, 99]. This approach is currently being evaluated in two ongoing clinical trials [NCT02566655, NCT03096782], the results of which are eagerly anticipated. Of note, it was recently shown that CD44 expression on MSCs can be transiently increased via culturing on hyaluronic acid (HA)-coated plates [100], potentially providing a simple method to enhance HCELL levels on MSCs and subsequent homing to the bone when used in combination with the fucosylation strategies described earlier.

In addition, Karp et al. have attached the prototypical E-selectin ligand, sialyl Lewis X (sLe^X), to the MSC surface via biotin-streptavidin bridges introduced via a series of techniques with stabilities ranging from 8 hrs to 7 days [101]. The same group has recently used a transient multiplex cell engineering strategy (i.e., triple mRNA transfection) to combine homing modification (PSGL-1 and sLe^X) with delivery of an anti-inflammatory agent (IL-10) [57]. This approach increased MSC homing to γ -irradiation-induced inflammation in the murine ear by 31% and reduced inflammation-induced swelling by 50% compared to unmodified MSCs. Small molecules upregulating the expression of other important homing

ligands, such as those for intracellular adhesion molecule 1 (ICAM-1), have been identified using high-throughput screens [58]. Treating MSCs with the top hit from this screen resulted in 5-fold increased expression of CD11a, an important ICAM-1 ligand, which resulted in an ~2-fold increase in homing toward LPS-induced inflammation in the ear [58].

The biotin-streptavidin bridge concept is a versatile technique that could be adapted for modification of MSCs with many readily-available biotinylated molecules. Similar techniques using palmitated protein A/G or bi-specific antibodies have also been developed for decorating MSCs with a variety of ligands or receptors [102, 103]. Recently, Won et al. optimized conjugation chemistry for attaching lipid-PEG to CXCR4 for noninvasive and rapid insertion into the cell membrane [104]. Another approach has been developed using a NHS-PEG₂-maleimide linker to conjugate thiol-containing molecules to amine residues in native MSC cell surface proteins [105]. Other studies suggest that relatively simple preconditioning regimens can be used to enhance tumor tropism, including hypoxia, estrogen exposure, and incubation with conditioned media from irradiated cancer cells [106–109]. In aggregate, techniques such as these have the potential to optimize synthetically engineered MSCs for homing to specific targets of interest; however, the breadth and diversity of modification techniques being applied to MSC homing presents a significant challenge for standardization across studies. Furthermore, the usefulness of these modifications may be mitigated in the absence of strategies to overcome first-pass entrapment, which would potentiate active homing mechanisms by providing a window of operation.

CONCLUSION

As excitement for the promise of MSC-based therapies, and synthetic biology approaches in general, continues to build and as these therapies increasingly undergo evaluation in the clinic, this review represents a sobering reminder of the broad biodistribution and poor homing efficiency to most target tissues observed using current methodologies (i.e., the ugly). This fact has potentially significant implications for clinical efficacy

and toxicity depending on the application (i.e., the bad). MSC-based drug delivery strategies are particularly sensitive to this challenge and will require clever bioengineering strategies to enhance the therapeutic index between benign and malignant tissue. Furthermore, rational study design regarding the choice of MSC populations, culture conditions for ex vivo expansion, in vivo tracking methodologies, and cell modification strategies is crucial. Employing robust, quantitative methodologies with standardized reporting metrics will facilitate accurate comparisons across studies and enable more rapid and efficient translation of the platforms that are most likely to succeed in the clinic (i.e., the good). Fortunately, there are multiple synthetic strategies in active development that will hopefully enable innovative MSC-based strategies to reach the full promise of their potential.

ACKNOWLEDGMENTS

We acknowledge the expert assistance of Dr. Kenneth Valkenburg and Marie-France Penet for their help with IC and IV injections, respectively. This work was supported by the following sources: Prostate Cancer Foundation Young Investigator Award (W.N.B. and D.L.J.T.), Patrick C. Walsh Prostate Cancer Research Fund (W.N.B. and D.L.J.T.), SKCCC CCSG developmental funds [P30 CA006973, (W.N.B.)], NIH-Prostate SPORE [P50 CA058236, (S.R.D. and J.T.I.)], Department of Defense Prostate Cancer Research Program [W81XWH-16-1-0410, (J.T.I.) and W81XWH-17-1-0528, (W.N.B.)], and NCI [R01CA201035, (D.L.J.T.)].

AUTHOR CONTRIBUTIONS

T.E.G.K., D.L.J.T., S.R.D., J.T.I., and W.N.B.: conception and design; T.E.G.K., D.L.J.T., and W.N.B.: collection and/or assembly of data; T.E.G.K., D.L.J.T., S.R.D., J.T.I., and W.N.B.: data analysis and interpretation; T.E.G.K., D.L.J.T., S.R.D., J.T.I., and W.N.B.: manuscript writing; T.E.G.K., D.L.J.T., S.R.D., J.T.I., and W.N.B.: final approval of manuscript.

DISCLOSURE OF POTENTIAL CONFLICTS OF INTEREST

The authors indicated no potential conflicts of interest.

REFERENCES

- Phinney DG. Functional heterogeneity of mesenchymal stem cells: Implications for cell therapy. *J Cell Biochem* 2012;113:2806–2812. <https://doi.org/10.1002/jcb.24166>
- Caplan AI. Adult mesenchymal stem cells: When, where, and how. *Stem Cells Int* 2015;2015:628767–628766. <https://doi.org/10.1155/2015/628767>
- Brennen WN, Denmeade SR, Isaacs JT. Mesenchymal stem cells as a vector for the inflammatory prostate microenvironment. *Endocr Relat Cancer* 2013;20:R269–R290. <https://doi.org/10.1530/ERC-13-0151>
- D'Souza N, Rossignoli F, Golinelli G et al. Mesenchymal stem/stromal cells as a delivery platform in cell and gene therapies. *BMC Med* 2015;13:186. <https://doi.org/10.1186/s12916-015-0426-0>
- Hagenhoff A, Bruns CJ, Zhao Y et al. Harnessing mesenchymal stem cell homing as an anticancer therapy. *Expert Opin Biol Ther* 2016;16:1079–1092. <https://doi.org/10.1080/14712598.2016.1196179>
- Ankrum J, Karp JM. Mesenchymal stem cell therapy: Two steps forward, one step back. *Trends Mol Med* 2010;16:203–209. <https://doi.org/10.1016/j.molmed.2010.02.005>
- Prockop DJ, Oh JY. Mesenchymal stem/stromal cells (MSCs): Role as guardians of inflammation. *Mol Ther* 2012;20:14–20. <https://doi.org/10.1038/mt.2011.211>
- Phinney DG, Pittenger MF. Concise review: MSC-derived exosomes for cell-free therapy. *STEM CELLS* 2017;35:851–858. <https://doi.org/10.1002/stem.2575>
- Crivelli B, Chlapanidas T, Perteghella S et al. Mesenchymal stem/stromal cell extracellular vesicles: From active principle to next generation drug delivery system. *J Control Release* 2017;262:104–117. <https://doi.org/10.1016/j.jconrel.2017.07.023>
- Galleu A, Riffo-Vasquez Y, Trento C et al. Apoptosis in mesenchymal stromal cells induces in vivo recipient-mediated immunomodulation. *Sci Transl Med* 2017;9:eaarn7828. <https://doi.org/10.1126/scitranslmed.aam7828>
- de Witte SFH, Luk F, Sierra Parraga JM et al. Immunomodulation by therapeutic mesenchymal stromal cells (MSC) is triggered through phagocytosis of MSC by monocytic cells. *STEM CELLS* 2018;36:602–615. <https://doi.org/10.1002/stem.2779>
- Luan X, Sansanaphongpricha K, Myers I et al. Engineering exosomes as refined biological nanoplateforms for drug delivery. *Acta Pharmacol Sin* 2017;38:754–763. <https://doi.org/10.1038/aps.2017.12>

- 13 De Becker A, Riet IV. Homing and migration of mesenchymal stromal cells: How to improve the efficacy of cell therapy? *World J Stem Cells* 2016;8:73–87. <https://doi.org/10.4252/wjsc.v8.i3.73>
- 14 English K, Mahon BP. Allogeneic mesenchymal stem cells: Agents of immune modulation. *J Cell Biochem* 2011;112:1963–1968. <https://doi.org/10.1002/jcb.23119>
- 15 Prockop DJ. Concise review: Two negative feedback loops place mesenchymal stem/stromal cells at the center of early regulators of inflammation. *STEM CELLS* 2013;31:2042–2046. <https://doi.org/10.1002/stem.1400>
- 16 Caplan AI, Sorrell JM. The MSC curtain that stops the immune system. *Immunol Lett* 2015;168:136–139. <https://doi.org/10.1016/j.imlet.2015.06.005>
- 17 Spaeth E, Klopp A, Dembinski J et al. Inflammation and tumor microenvironments: Defining the migratory itinerary of mesenchymal stem cells. *Gene Ther* 2008;15:730–738. <https://doi.org/10.1038/gt.2008.39>
- 18 Ruster B, Gottig S, Ludwig RJ et al. Mesenchymal stem cells display coordinated rolling and adhesion behavior on endothelial cells. *Blood* 2006;108:3938–3944. <https://doi.org/10.1182/blood-2006-05-025098>
- 19 Nitzsche F, Müller C, Lukomska B et al. Concise review: MSC adhesion cascade—insights into homing and transendothelial migration. *STEM CELLS* 2017;35:1446–1460. <https://doi.org/10.1002/stem.2614>
- 20 Gao J, Dennis JE, Muzic RF et al. The dynamic in vivo distribution of bone marrow-derived mesenchymal stem cells after infusion. *Cells Tissues Organs* 2001;169:12–20. <https://doi.org/10.1159/000047856>
- 21 Schrepfer S, Deuse T, Reichenspurner H et al. Stem cell transplantation: The lung barrier. *Transplant Proc* 2007;39:573–576. <https://doi.org/10.1016/j.transproceed.2006.12.019>
- 22 Brennen WN, Kisteman LN, Isaacs JT. Rapid selection of mesenchymal stem and progenitor cells in primary prostate stromal cultures. *Prostate* 2016;76:552–564. <https://doi.org/10.1002/pros.23145>
- 23 Toma C, Wagner WR, Bowry S et al. Fate of culture-expanded mesenchymal stem cells in the microvasculature: in vivo observations of cell kinetics. *Circ Res* 2009;104:398–402. <https://doi.org/10.1161/CIRCRESAHA.108.187724>
- 24 Koc ON, Gerson SL, Cooper BW et al. Rapid hematopoietic recovery after coinfection of autologous-blood stem cells and culture-expanded marrow mesenchymal stem cells in advanced breast cancer patients receiving high-dose chemotherapy. *J Clin Oncol* 2000;18:307–316. <https://doi.org/10.1200/JCO.2000.18.2.307>
- 25 Devine SM, Cobbs C, Jennings M et al. Mesenchymal stem cells distribute to a wide range of tissues following systemic infusion into nonhuman primates. *Blood* 2003;101:2999–3001. <https://doi.org/10.1182/blood-2002-06-1830>
- 26 Kraitchman DL, Tatsumi M, Gilson WD et al. Dynamic imaging of allogeneic mesenchymal stem cells trafficking to myocardial infarction. *Circulation* 2005;112:1451–1461. <https://doi.org/10.1161/CIRCULATIONAHA.105.537480>
- 27 Gholamrezaezhad A, Mirpour S, Bagheri M et al. In vivo tracking of 111In-oxine labeled mesenchymal stem cells following infusion in patients with advanced cirrhosis. *Nucl Med Biol* 2011;38:961–967. <https://doi.org/10.1016/j.nucmedbio.2011.03.008>
- 28 Lee RH, Pulin AA, Seo MJ et al. Intravenous hMSCs improve myocardial infarction in mice because cells embolized in lung are activated to secrete the anti-inflammatory protein TSG-6. *Cell Stem Cell* 2009;5:54–63. <https://doi.org/10.1016/j.stem.2009.05.003>
- 29 Fischer UM, Harting MT, Jimenez F et al. Pulmonary passage is a major obstacle for intravenous stem cell delivery: The pulmonary first-pass effect. *STEM CELLS DEV* 2009;18:683–692. <https://doi.org/10.1089/scd.2008.0253>
- 30 Dutly AE, Kugathasan L, Trogadis JE et al. Fluorescent microangiography (FMA): An improved tool to visualize the pulmonary microvasculature. *Lab Invest* 2006;86:409–416. <https://doi.org/10.1038/labinvest.3700399>
- 31 Lipowsky HH, Bowers DT, Banik BL et al. Mesenchymal stem cell deformability and implications for microvascular sequestration. *Ann Biomed Eng* 2018;46:640–654. <https://doi.org/10.1007/s10439-018-1985-y>
- 32 Brennen WN, Zhang B, Kulac I et al. Mesenchymal stem cell infiltration during neoplastic transformation of the human prostate. *Oncotarget* 2017;8:46710–46727
- 33 Bansal A, Pandey MK, Demirhan YE et al. Novel (89)Zr cell labeling approach for PET-based cell trafficking studies. *EJNMMI Res* 2015;5:19. <https://doi.org/10.1186/s13550-015-0098-y>
- 34 Zanetti A, Grata M, Etling EB et al. Suspension-expansion of bone marrow results in small mesenchymal stem cells exhibiting increased transpulmonary passage following intravenous administration. *Tissue Eng Part C Methods* 2015;21:683–692. <https://doi.org/10.1089/ten.TEC.2014.0344>
- 35 Sekiya I, Larson BL, Smith JR et al. Expansion of human adult stem cells from bone marrow stroma: Conditions that maximize the yields of early progenitors and evaluate their quality. *STEM CELLS* 2002;20:530–541. <https://doi.org/10.1634/stemcells.20-6-530>
- 36 Alimperti S, Lei P, Wen Y et al. Serum-free spheroid suspension culture maintains mesenchymal stem cell proliferation and differentiation potential. *Biotechnol Prog* 2014;30:974–983. <https://doi.org/10.1002/btpr.1904>
- 37 Baksh D, Zandstra PW, Davies JE. A non-contact suspension culture approach to the culture of osteogenic cells derived from a CD49 α subpopulation of human bone marrow-derived cells. *Biotechnol Bioeng* 2007;98:1195–1208. <https://doi.org/10.1002/bit.21556>
- 38 Luo L, Tang J, Nishi K et al. Fabrication of synthetic mesenchymal stem cells for the treatment of acute myocardial infarction in mice. *Circ Res* 2017;120:1768–1775. <https://doi.org/10.1161/circresaha.116.310374>
- 39 Pittenger MF, Martin BJ. Mesenchymal stem cells and their potential as cardiac therapeutics. *Circ Res* 2004;95:9–20. <https://doi.org/10.1161/01.RES.0000135902.99383.6f>
- 40 Iso Y, Spees JL, Serrano C et al. Multipotent human stromal cells improve cardiac function after myocardial infarction in mice without long-term engraftment. *Biochem Biophys Res Commun* 2007;354:700–706. <https://doi.org/10.1016/j.bbrc.2007.01.045>
- 41 Diehl F, Li M, Dressman D et al. Detection and quantification of mutations in the plasma of patients with colorectal tumors. *Proc Natl Acad Sci USA* 2005;102:16368–16373. <https://doi.org/10.1073/pnas.0507904102>
- 42 Debeljak M, Mocci E, Morrison MC et al. Haplotype counting for sensitive chimerism testing: Potential for early leukemia relapse detection. *J Mol Diagn* 2017;19:427–436. <https://doi.org/10.1016/j.jmoldx.2017.01.005>
- 43 Tatebe M, Nakamura R, Kagami H et al. Differentiation of transplanted mesenchymal stem cells in a large osteochondral defect in rabbit. *Cytotherapy* 2005;7:520–530. <https://doi.org/10.1080/14653240500361350>
- 44 Weir C, Morel-Kopp MC, Gill A et al. Mesenchymal stem cells: Isolation, characterization and in vivo fluorescent dye tracking. *Heart Lung Circ* 2008;17:395–403. <https://doi.org/10.1016/j.hlc.2008.01.006>
- 45 Polzer H, Volkmer E, Saller MM et al. Long-term detection of fluorescently labeled human mesenchymal stem cell in vitro and in vivo by semi-automated microscopy. *Tissue Eng Part C Methods* 2012;18:156–165. <https://doi.org/10.1089/ten.TEC.2011.0275>
- 46 Perez JR, Ybarra N, Chagnon F et al. Tracking of mesenchymal stem cells with fluorescence endomicroscopy imaging in radiotherapy-induced lung injury. *Sci Rep* 2017;7:40748. <https://doi.org/10.1038/srep40748>
- 47 Barbash IM, Chouraqui P, Baron J et al. Systemic delivery of bone marrow-derived mesenchymal stem cells to the infarcted myocardium: Feasibility, cell migration, and body distribution. *Circulation* 2003;108:863–868. <https://doi.org/10.1161/01.CIR.0000084828.50310.6A>
- 48 Knoop K, Kolokythas M, Klutz K et al. Image-guided, tumor stroma-targeted 131I therapy of hepatocellular cancer after systemic mesenchymal stem cell-mediated NIS gene delivery. *Mol Ther : J Am Soc Gene Ther* 2011;19:1704–1713. <https://doi.org/10.1038/mt.2011.93>
- 49 Dwyer RM, Ryan J, Havelin RJ et al. Mesenchymal Stem Cell-mediated delivery of the sodium iodide symporter supports radionuclide imaging and treatment of breast cancer. *STEM CELLS* 2011;29:1149–1157. <https://doi.org/10.1002/stem.665>
- 50 Martinez-Quintanilla J, Bhere D, Heidari P et al. Therapeutic efficacy and fate of bimodal engineered stem cells in malignant brain tumors. *STEM CELLS* 2013;31:1706–1714. <https://doi.org/10.1002/stem.1355>
- 51 Ell PJ, Hocknell JM, Jarritt PH et al. A 99Tcm-labelled radiotracer for the investigation of cerebral vascular disease. *Nucl Med Commun* 1985;6:437–441
- 52 Park BN, Shim W, Lee G et al. Early distribution of intravenously injected mesenchymal stem cells in rats with acute brain trauma evaluated by (99m)Tc-HMPAO labeling. *Nucl Med Biol* 2011;38:1175–1182. <https://doi.org/10.1016/j.nucmedbio.2011.05.009>
- 53 Rajam PC, Jackson AL. Distribution and valence state of radiochromium in intracellularly labeled ehrlich mouse ascites carcinoma cells. *Proc Soc Exp Biol Med* 1958;99:210–213

- 54 Fidler IJ. Metastasis: Quantitative analysis of distribution and fate of tumor emboli labeled with 125 I-5-iodo-2'-deoxyuridine. *J Natl Cancer Inst* 1970;45:773–782
- 55 Kim KS, Park W, Na K. Gadolinium-chelate nanoparticle entrapped human mesenchymal stem cell via photochemical internalization for cancer diagnosis. *Biomaterials* 2015;36:90–97. <https://doi.org/10.1016/j.biomaterials.2014.09.014>
- 56 Huang X, Zhang F, Wang Y et al. Design considerations of iron-based nanoclusters for noninvasive tracking of mesenchymal stem cell homing. *ACS Nano* 2014;8:4403–4414. <https://doi.org/10.1021/nn4062726>
- 57 Levy O, Zhao W, Mortensen LJ et al. mRNA-engineered mesenchymal stem cells for targeted delivery of interleukin-10 to sites of inflammation. *Blood* 2013;122:e23–e32. <https://doi.org/10.1182/blood-2013-04-495119>
- 58 Levy O, Mortensen LJ, Boquet G et al. A small-molecule screen for enhanced homing of systemically infused cells. *Cell Rep* 2015;10:1261–1268. <https://doi.org/10.1016/j.celrep.2015.01.057>
- 59 Sipkins DA, Wei X, Wu JW et al. In vivo imaging of specialized bone marrow endothelial microdomains for tumour engraftment. *Nature* 2005;435:969–973. <https://doi.org/10.1038/nature03703>
- 60 Sackstein R, Merzaban JS, Cain DW et al. Ex vivo glycan engineering of CD44 programs human multipotent mesenchymal stromal cell trafficking to bone. *Nat Med* 2008;14:181–187. <https://doi.org/10.1038/nm1703>
- 61 Boissonnas A, Fetler L, Zeelenberg IS et al. In vivo imaging of cytotoxic T cell infiltration and elimination of a solid tumor. *J Exp Med* 2007;204:345–356. <https://doi.org/10.1084/jem.20061890>
- 62 Novak J, Georgakoudi I, Wei X et al. In vivo flow cytometer for real-time detection and quantification of circulating cells. *Optics Lett* 2004;29:77–79
- 63 Fan ZC, Yan J, Liu GD et al. Real-time monitoring of rare circulating hepatocellular carcinoma cells in an orthotopic model by in vivo flow cytometry assesses resection on metastasis. *Cancer Res* 2012;72:2683–2691. <https://doi.org/10.1158/0008-5472.Can-11-3733>
- 64 Xie C, Yang Z, Suo Y et al. Systemically infused mesenchymal stem cells show different homing profiles in healthy and tumor mouse models. *STEM CELLS TRANSLATIONAL MEDICINE* 2017;6:1120–1131. <https://doi.org/10.1002/sctm.16-0204>
- 65 Kidd S, Spaeth E, Dembinski JL et al. Direct evidence of mesenchymal stem cell tropism for tumor and wounding microenvironments using in vivo bioluminescent imaging. *STEM CELLS* 2009;27:2614–2623. <https://doi.org/10.1002/stem.187>
- 66 Brennen WN, Chen S, Denmeade SR et al. Quantification of mesenchymal stem cells (MSCs) at sites of human prostate cancer. *Oncotarget* 2013;4:106–117
- 67 Pessina A, Leonetti C, Artuso S et al. Drug-releasing mesenchymal cells strongly suppress B16 lung metastasis in a syngeneic murine model. *J Exp Clin Cancer Res* 2015;34:82. <https://doi.org/10.1186/s13046-015-0200-3>
- 68 Pessina A, Bonomi A, Coccè V et al. Mesenchymal stromal cells primed with paclitaxel provide a new approach for cancer therapy. *PLoS One* 2011;6:e28321. <https://doi.org/10.1371/journal.pone.0028321>
- 69 Levy O, Brennen WN, Han E et al. A prodrug-doped cellular Trojan Horse for the potential treatment of prostate cancer. *Biomaterials* 2016;91:140–150. <https://doi.org/10.1016/j.biomaterials.2016.03.023>
- 70 Rombouts WJ, Ploemacher RE. Primary murine MSC show highly efficient homing to the bone marrow but lose homing ability following culture. *Leukemia* 2003;17:160–170. <https://doi.org/10.1038/sj.leu.2402763>
- 71 Bexell D, Gunnarsson S, Tormin A et al. Bone marrow multipotent mesenchymal stroma cells act as pericyte-like migratory vehicles in experimental gliomas. *Mol Ther : J Am Soc Gene Ther* 2009;17:183–190. <https://doi.org/10.1038/mt.2008.229>
- 72 Nakamizo A, Marini F, Amano T et al. Human bone marrow-derived mesenchymal stem cells in the treatment of gliomas. *Cancer Res* 2005;65:3307–3318. <https://doi.org/10.1158/0008-5472.Can-04-1874>
- 73 Studeny M, Marini FC, Champlin RE et al. Bone marrow-derived mesenchymal stem cells as vehicles for interferon-beta delivery into tumors. *Cancer Res* 2002;62:3603–3608
- 74 Klopp AH, Gupta A, Spaeth E et al. Concise review: Dissecting a discrepancy in the literature: Do mesenchymal stem cells support or suppress tumor growth? *STEM CELLS* 2011;29:11–19. <https://doi.org/10.1002/stem.559>
- 75 Stoff-Khalili MA, Rivera AA, Mathis JM et al. Mesenchymal stem cells as a vehicle for targeted delivery of CRAds to lung metastases of breast carcinoma. *Breast Cancer Res Treat* 2007;105:157–167. <https://doi.org/10.1007/s10549-006-9449-8>
- 76 Hakkarainen T, Särkioja M, Lehenkari P et al. Human mesenchymal stem cells lack tumor tropism but enhance the antitumor activity of oncolytic adenoviruses in orthotopic lung and breast tumors. *Human Gene Ther* 2007;18:627–641. <https://doi.org/10.1089/hum.2007.034>
- 77 Dembinski JL, Spaeth EL, Fueyo J et al. Reduction of nontarget infection and systemic toxicity by targeted delivery of conditionally replicating viruses transported in mesenchymal stem cells. *Cancer Gene Ther* 2010;17:289–297. <https://doi.org/10.1038/cgt.2009.67>
- 78 Castleton A, Dey A, Beaton B et al. Human mesenchymal stromal cells deliver systemic oncolytic measles virus to treat acute lymphoblastic leukemia in the presence of humoral immunity. *Blood* 2014;123:1327–1335. <https://doi.org/10.1182/blood-2013-09-528851>
- 79 Kucerova L, Altanerova V, Matuskova M et al. Adipose tissue-derived human mesenchymal stem cells mediated prodrug cancer gene therapy. *Cancer Res* 2007;67:6304–6313. <https://doi.org/10.1158/0008-5472.Can-06-4024>
- 80 Cavarretta IT, Altanerova V, Matuskova M et al. Adipose tissue-derived mesenchymal stem cells expressing prodrug-converting enzyme inhibit human prostate tumor growth. *Mol Ther : J Am Soc Gene Ther* 2010;18:223–231. <https://doi.org/10.1038/mt.2009.237>
- 81 von Einem JC, Sylvia P, Christine G et al. Treatment of advanced gastrointestinal cancer with genetically modified autologous mesenchymal stem cells - TREAT-ME-1 – A phase I, first in human, first in class trial. *Oncotarget* 2017;8:80156–80166. <https://doi.org/10.18632/oncotarget.20964>
- 82 Zischek C, Niess H, Ischenko I et al. Targeting tumor stroma using engineered mesenchymal stem cells reduces the growth of pancreatic carcinoma. *Annals Surg* 2009;250:747–753. <https://doi.org/10.1097/SLA.0b013e3181b6d62d0>
- 83 Conrad C, Hüsemann Y, Niess H et al. Linking transgene expression of engineered mesenchymal stem cells and angiopoietin-1-induced differentiation to target cancer angiogenesis. *Annals Surg* 2011;253:566–571. <https://doi.org/10.1097/SLA.0b013e3181fcb5d8>
- 84 Denmeade SR, Jakobsen CM, Janssen S et al. Prostate-specific antigen-activated thapsigargin prodrug as targeted therapy for prostate cancer. *J Natl Cancer Inst* 2003;95:990–1000
- 85 Williams SA, Merchant RF, Garrett-Mayer E et al. A prostate-specific antigen-activated channel-forming toxin as therapy for prostatic disease. *J Natl Cancer Inst* 2007;99:376–385. <https://doi.org/10.1093/jnci/djk065>
- 86 Brennen WN, Rosen DM, Wang H et al. Targeting carcinoma-associated fibroblasts within the tumor stroma with a fibroblast activation protein-activated prodrug. *J Natl Cancer Inst* 2012;104:1320–1334. <https://doi.org/10.1093/jnci/djs336>
- 87 Denmeade SR, Mhaka AM, Rosen DM et al. Engineering a prostate-specific membrane antigen-activated tumor endothelial cell prodrug for cancer therapy. *Sci Transl Med* 2012;4:140ra186. <https://doi.org/10.1126/scitranslmed.3003886>
- 88 Denmeade SR, Isaacs JT. Engineering enzymatically activated “molecular grenades” for cancer. *Oncotarget* 2012;3:666–667. <https://doi.org/10.18632/oncotarget.562>
- 89 Stagg J, Lejeune L, Paquin A et al. Marrow stromal cells for interleukin-2 delivery in cancer immunotherapy. *Human Gene Ther* 2004;15:597–608. <https://doi.org/10.1089/104303404323142042>
- 90 Xin H, Kanehira M, Mizuguchi H et al. Targeted delivery of CX3CL1 to multiple lung tumors by mesenchymal stem cells. *STEM CELLS* 2007;25:1618–1626. <https://doi.org/10.1634/stemcells.2006-0461>
- 91 Ren C, Kumar S, Chanda D et al. Cancer gene therapy using mesenchymal stem cells expressing interferon-beta in a mouse prostate cancer lung metastasis model. *Gene Ther* 2008;15:1446–1453. <https://doi.org/10.1038/gt.2008.101>
- 92 Seo SH, Kim KS, Park SH et al. The effects of mesenchymal stem cells injected via different routes on modified IL-12-mediated antitumor activity. *Gene Ther* 2011;18:488–495. <https://doi.org/10.1038/gt.2010.170>
- 93 Luetzkendorf J, Mueller LP, Mueller T et al. Growth inhibition of colorectal carcinoma by lentiviral TRAIL-transgenic human mesenchymal stem cells requires their substantial intratumoral presence. *J Cell Mol Med* 2010;14:2292–2304. <https://doi.org/10.1111/j.1582-4934.2009.00794.x>

- 94** Loebinger MR, Eddaoudi A, Davies D et al. Mesenchymal stem cell delivery of TRAIL can eliminate metastatic cancer. *Cancer Res* 2009;69:4134–4142. <https://doi.org/10.1158/0008-5472.Can-08-4698>
- 95** Sasportas LS, Kasmieh R, Wakimoto H et al. Assessment of therapeutic efficacy and fate of engineered human mesenchymal stem cells for cancer therapy. *Proc Natl Acad Sci USA* 2009;106:4822–4827. <https://doi.org/10.1073/pnas.0806647106>
- 96** Sage EK, Thakrar RM, Janes SM. Genetically modified mesenchymal stromal cells in cancer therapy. *Cytotherapy* 2016;18:1435–1445. <https://doi.org/10.1016/j.jcyt.2016.09.003>
- 97** von Karstedt S, Montinaro A, Walczak H. Exploring the TRAILS less travelled: TRAIL in cancer biology and therapy. *Nat Rev Cancer* 2017;17:352–366. <https://doi.org/10.1038/nrc.2017.28>
- 98** Duebgen M, Martinez-Quintanilla J, Tamura K et al. Stem cells loaded with multi-mechanistic oncolytic herpes simplex virus variants for brain tumor therapy. *J Natl Cancer Inst* 2014;106:dju090. <https://doi.org/10.1093/jnci/dju090>
- 99** Dykstra B, Lee J, Mortensen LJ et al. Glycoengineering of E-selectin ligands by intracellular versus extracellular fucosylation differentially affects osteotropism of human mesenchymal stem cells. *STEM CELLS* 2016;34:2501–2511. <https://doi.org/10.1002/stem.2435>
- 100** Corradetti B, Taraballi F, Martinez JO et al. Hyaluronic acid coatings as a simple and efficient approach to improve MSC homing toward the site of inflammation. *Sci Rep* 2017;7:7991. <https://doi.org/10.1038/s41598-017-08687-3>
- 101** Sarkar D, Spencer JA, Phillips JA et al. Eng. Cell Homing. *Blood* 2011;118:e184–e191. <https://doi.org/10.1182/blood-2010-10-311464>
- 102** Ko IK, Kim BG, Awadallah A et al. Targeting improves MSC treatment of inflammatory bowel disease. *Mol Ther : J Am Soc Gene Therapy* 2010;18:1365–1372. <https://doi.org/10.1038/mt.2010.54>
- 103** Lee RJ, Fang Q, Davol PA et al. Antibody targeting of stem cells to infarcted myocardium. *STEM CELLS* 2007;25:712–717. <https://doi.org/10.1634/stemcells.2005-0602>
- 104** Won YW, Patel AN, Bull DA. Cell surface engineering to enhance mesenchymal stem cell migration toward an SDF-1 gradient. *Biomaterials* 2014;35:5627–5635. <https://doi.org/10.1016/j.biomaterials.2014.03.070>
- 105** Cheng H, Byrska-Bishop M, Zhang CT et al. Stem cell membrane engineering for cell rolling using peptide conjugation and tuning of cell-selectin interaction kinetics. *Biomaterials* 2012;33:5004–5012. <https://doi.org/10.1016/j.biomaterials.2012.03.065>
- 106** Klopp AH, Spaeth EL, Dembinski JL et al. Tumor irradiation increases the recruitment of circulating mesenchymal stem cells into the tumor microenvironment. *Cancer Res* 2007;67:11687–11695. <https://doi.org/10.1158/0008-5472.CAN-07-1406>
- 107** Das R, Jahr H, van Osch GJ et al. The role of hypoxia in bone marrow-derived mesenchymal stem cells: Considerations for regenerative medicine approaches. *Tissue Eng Part B Rev* 2010;16:159–168. <https://doi.org/10.1089/ten.TEB.2009.0296>
- 108** Mirzamohammadi S, Aali E, Najafi R et al. Effect of 17beta-estradiol on mediators involved in mesenchymal stromal cell trafficking in cell therapy of diabetes. *Cytotherapy* 2015;17:46–57. <https://doi.org/10.1016/j.jcyt.2014.06.009>
- 109** Smith CL, Chaichana KL, Lee YM et al. Pre-exposure of human adipose mesenchymal stem cells to soluble factors enhances their homing to brain cancer. *STEM CELLS TRANSLATIONAL MEDICINE* 2015;4:239–251. <https://doi.org/10.5966/sctm.2014-0149>

The what, when, and why of human prostate cancer xenografts

W. Nathaniel Brennen | John T. Isaacs

Department of Oncology, Prostate Cancer Program, The Sidney Kimmel Comprehensive Cancer Center at Johns Hopkins, The Johns Hopkins University School of Medicine, Baltimore, Maryland

Correspondence

John T. Isaacs, Department of Oncology, Prostate Cancer Program, The Sidney Kimmel Comprehensive Cancer Center at Johns Hopkins, The Johns Hopkins University School of Medicine, Baltimore, MD 21231.
Email: isaacsj@jhmi.edu

Background: Presently, ~85 serially transplantable human prostate cancer xenografts spanning the phenotypic, epigenetic, and genetic heterogeneity seen clinically are available in a variety of laboratories throughout the world. If distributed to the prostate cancer research community, these can provide an experimental platform for resolving the specificity versus generalizability of basic cancer biology principles (eg, credentialing of therapeutic molecular targets) and for validating translational approaches for prevention, diagnosis, and therapy. Thus, there is an urgent need to distribute the already established serially transplantable human prostate cancer xenografts and to develop robust methods for establishing new ones.

Methods: To accelerate the development of such additional xenografts, particularly from patients treated with the newer standard of care agents (ie, abiraterone, enzalutamide, cabazitaxel, alpharadin, etc), a historic review of the field will be presented.

Results: Over the last 50 years, multiple groups throughout the world have developed methods for the successful establishment of serially transplantable human prostate cancer xenografts using a variety of immune deficient mice. These are summarized chronologically.

Conclusions and Future: With the ever growing appreciation of the value of personalized medicine (aka precision medicine), methods need to be developed that allow efficient and timely growth of primary patient derived prostate cancer xenografts (PDXs), which can be used as “avatars” for defining optimal therapy for that specific patient. Such development should be based upon the leads obtained from the successful establishment of serially transplantable prostate cancer xenografts described in this review.

1 | INTRODUCTION

Well characterized serially transplantable human prostate cancer xenografts spanning the full phenotypic, epigenetic, and genetic heterogeneity seen in the clinic need to be widely distributed to the prostate cancer research community to accelerate development of effective approaches for the prevention, detection, and treatment of prostate cancer. Based upon this need, the Movember Foundation in 2014

launched the Global Action Plan (GAP) for an international collaborative program for the development of prostate cancer xenografts to model human prostate cancer. This international collaborative program had two major goals. The first is to provide the prostate cancer community with a summary of the basic characteristics and appropriate contact information for requesting starter inoculum for any of the 85 presently available serially transplantable human prostate cancer xenografts. This information will be available shortly in a joint publication by the international group.¹

The second goal of the GAP xenograft program is to develop and characterize additional prostate cancer xenografts, particularly from patients treated with the newer standard of care agents (ie, abiraterone, enzalutamide, cabazitaxel, alpharadin, etc). Along these lines and with an ever growing appreciation of the value of personalized medicine (aka precision medicine), there is clearly a hope that methods can be developed to allow efficient and timely growth of primary patient-derived prostate cancer xenografts (PDXs), which can be used as “avatars” for defining optimal therapy for that specific patient. To achieve this second goal, it is

critically important to build upon the knowledge obtained over the last 50 years by the global cancer research community, which will be reviewed chronologically herein (Figure 1).

1.1 | Athymic nude mice and initiation of human cancer xenografts

In the early 1960's, neonatal thymectomy of rodents was documented to result in loss of T-cell dependent adaptive immune competence, and



FIGURE 1 Chronology of significant events in prostate cancer xenograft development

thus survival of non-syngeneic tissues increased when xenografted into such thymectomized hosts.² Fortuitously, this realization coincided with the spontaneous development of a mutant hairless (ie, "nude") mouse in 1962 in N.R. Grist's laboratory at the Virus Laboratory, Ruchill Hospital in Glasgow, Scotland.³ The mutation arose in a closed but not deliberately inbred albino stock. Dr. Grist sent these mutant mice to the Institute of Animal Genetics Edinburgh for investigation, where SP Flanagan studied the genetics of the nude mutation.⁴ In addition to being hairless, these nude mice also suffered from recessive thymic aplasia.⁵ Such thymic aplasia is due to a homozygous null mutation in the nuclear transcription factor *FOXN1* gene which produces an immune deficient phenotype due to loss of adaptive mature T-cell function (Table 1).⁶ Due to the loss of functional CD4+ T-cells, mature B-cells are partially defective as well.

At the end of 1968, Jergen Rygaard of the Pathological Anatomical Institute, Kommunehospitalet, Copenhagen Denmark obtained two heterozygous (nu/+) pairs of breeding mice from the Institute for Animal Genetics in Edinburgh, Scotland. Due to poor viability and fertility of the homozygous nude mice from these breeding pairs, Dr. Rygaard backcrossed these mice onto the NMRI outbred stock (ie, derived from a colony of Swiss mice⁷) to produce the homozygous (nu/nu) outbred stock now known as: NMRI-*Foxn1*^{nu/nu} (ie, NMRI-nude mice).⁸ Subsequently in 1969, Jergen Rygaard and Carl O. Povlsen documented that due to such loss of mature T-cell function, these outbred NMRI-nude mice could be successfully xenografted with human cancers.⁹ Since the NMRI-nude mice are an outbred stock, multiple academic laboratories and commercial providers transferred the mutant nude allele homozygously onto various inbred backgrounds by repeated backcrossing. Thus, NIH(S), C57BL/6, and BALB/c inbred strains of homozygous nude mice quickly became available in the 1970's. These inbred athymic nude mice were used in attempts to produce serially transplantable human prostate cancer xenografts by multiple groups throughout the world.

1.2 | Prostate cancer xenograft development using nude mice

One of the earliest groups to initiate a prostate cancer xenograft program using inbred nude mice was led by Gordon H. Sato at the University of California-San Diego.¹⁰ These pioneering efforts in the early 1970's were continued in the late 1970's by Fritz Schroeder, who had been a fellow with Professor Sato at San Diego, when he became the head of the Experimental Urology Research Group of the Department of Urology of Erasmus University Rotterdam.¹¹ Around the same time period, Don D. Mickey and George H. Mickey at Duke University, Durham, North Carolina, and John F. Lechner and M. Edward Kaign at the Pasadena Foundation for Medicinal Research, Pasadena, California, and Julius S. Horoszewicz, Avery A. Sandberg and Gerald P. Murphy at Roswell Park Memorial Institute, Buffalo New York also initiated programs to establish prostate cancer xenografts. In 1977, the Duke group reported establishing the DU145 line in inbred nude intact male mice as a serially transplantable, androgen-independent PDX from a castration-resistant metastatic brain lesion.¹²

Two years later in 1979, the Pasadena Foundation for Medicinal Research group reported upon establishing the PC3 line in inbred nude intact male mice as a serially transplantable, androgen-independent PDX from a castration-resistant lumbar vertebra metastasis.¹³ In 1980, the Roswell Park group reported upon establishing the LNCaP line in inbred nude intact male mice as a serially transplantable, androgen-responsive xenograft from a castration-resistant superclavicular lymph node.¹⁴

Also in 1980, the Rotterdam group reported success in establishing for the first time a serially transplantable, androgen-responsive, primary prostate cancer xenograft (ie, PC-82 line) in nude intact male mice from a hormonally naïve patient.¹⁵ Overall, however, the Rotterdam group subsequently reported that from 1968 to 1988 using their own breeding colony of BALB/c nude mice (originally derived from a colony of Castle's mice⁷), only three xenografts were successfully established out of over 150 specimens of prostatic carcinomas xenografted for an overall success rate of only 2%.¹⁶ They further reported that from 1988 to 1990, 35 prostatic cancer specimens were xenografted subcutaneously in BALB/c nude intact male mice with only one PDX being established from a grafted pelvic lymph node metastases.¹⁶ Based upon this low success rate, the Rotterdam group now led by Wytske van Weerden switched to using outbred NMRI-nude intact male mice, which resulted in six new xenografts out of 16 attempts for a success rate of 38%.¹⁶

The high success rates reported by the Rotterdam group raises the issue of why the outbred NMRI-nude intact male mice are apparently a better host for initial success in xenografting prostate cancer tissue. Relevant to this issue is the observation by the Rotterdam group that once a xenograft is established and growing in the initial NMRI-nude intact male mice, it can be serially transplanted into either outbred NMRI or the inbred BALB/c nude intact male mice.¹⁶ A possible explanation for the enhanced initial success rate in NMRI versus BALB/c nude intact male mice may lie in the fact that while immune deficient, nude mice retain a degree of humoral adaptive immune response coupled with an intact innate immune system, which includes significantly elevated natural killer (NK) cell activity; thus limiting xenograft engraftment. Significantly, such NK activity is lowest in young (ie, 3 week old) BALB/c nude intact male mice but increases rapidly reaching its maximum by 10 weeks of life. At 10 weeks of age, nude intact mice have a three- to four-fold higher level of NK cytolytic activity compared to non-nude BALB/c mice.^{17,18} Significantly, however, NMRI-nude intact male mice have the same high level of NK activity as adult BALB/c mice.¹⁹ Thus, additional factors, host background (Swiss vs Castle's) or possible B-cell dependent humoral adaptive responses, must be involved to explain the difference in success rate between NMRI- and BALB/c-nude intact male mice.

1.3 | Role of Matrigel co-inoculation in prostate cancer xenografts

In the mid-1980's, Pamela J. Russel and Derek Raghaven at the University of Sydney, Australia initiated attempts to establish serially transplantable xenografts in BALB/c nude intact male mice. From 29

TABLE 1 Immune competency of genetically-defective mice commonly used for xenografting

Common name	Gene mutation	Innate immune system				Adaptive immune system				Leakiness	Notes
		NK cells	Dendritic cells	Macrophages	Complement function	Mature B-cells	Mature T-cells	Mature B-cells	Mature T-cells		
Immunodeficiency											
Nude	Foxl1	Present (+ ++)	Present	Present	Present	Partially defective	Absent	Absent	Common	Older mice become "leaky", producing small numbers of mature T- and B-cells; Adaptive antibody responses primarily IgM	
<i>scid</i>	Prkdc	Present (+)	Present	Present	Present	Absent	Absent	Absent	Low	Older mice can become "leaky", incidence is higher on C57BL6 and BALB/c backgrounds; Radiation sensitive due to defective DNA repair; Develop thymic lymphomas	
<i>Rag1/2^{-/-}</i>	<i>Rag1/2</i>	Present (+)	Present	Present	Present	Absent	Absent	Absent	Absent	Unlike scid mutants, considered "non-leaky"; Radiation resistant	
NOD (non-obese diabetic)	NOD*	Defective (+/-)	Defective	Defective	Impaired	Present	Present	Present	Very low	Develop diabetes mellitus	
NOD- <i>scid</i>	NOD*/Prkdc	Defective (+/-)	Defective	Defective	Impaired	Absent	Absent	Absent	Low	Least "leaky" of any scid strain; Decreased lifespan and thymic lymphomas; Radiation sensitive	
NOD-RAG1 ^{-/-}	NOD*	Defective (+/-)	Defective	Defective	Impaired	Absent	Absent	Absent	Absent	Decreased lifespan and thymic lymphomas; "Non-leaky"	
NSG (NOD <i>scid</i> gamma)	NOD*/Prkdc/IL2rgnull	Absent (-)	Defective	Defective	Absent	Absent	Absent	Absent	Very low	Extremely immunodeficient; Deficient in IL-2, -4, -7, -9, -15, and -21 signaling	

Adapted from information available on the Jackson Laboratories website and references (Schultz LD, et al Nat Rev Immunol. 2007 Feb; 7(2): 118-30. Koboziev I, et al Inflamm Bowel Dis. 2015 July; 21(7): 1652-73).
 *NOD: non-obese diabetic strain is polygenic (ie, *Cdh23^{del}*, *Gpr84^{del}*, *H2^{g7}*, *Hc⁰*, *Il2^{mi}*, *mt-T^{mi}*).

attempts, only three new xenografts were established, one of which was subsequently replaced by a mouse fibrosarcoma (ie, success rate of <10%).²⁰ At the end of the 1980's, Thomas G. Pretlow at Case Western Reserve University, Cleveland, Ohio likewise initiated a program to establish xenografts in nude intact male mice inoculated with localized human prostate cancer tissue with the innovation of embedding the xenografted tissue in gelled basement membrane (ie, Matrigel).²¹ Matrigel is the trade name for a gelatinous basic membrane protein mixture secreted by Engelbreth-Holm-Swarm (EHS) mouse sarcoma cells produced and marketed by Corning Life Sciences. Trevigen, Inc. markets their own version under the trade name Cultrex BME. Regardless of the commercial source, this material is approximately 60% laminin, 30% collagen IV, and 8% entactin. Entactin is a bridging molecule that interacts with laminin and collagen IV; thereby, contributing to the structural organization of these extracellular matrix molecules, which occurs rapidly to form a gel above 4°C.

Therefore, this Matrigel co-inoculum gel provides an initial barrier to the infiltration of host adaptive and innate immune cells optimizing the possibility of initial cancer cell growth in mice. In addition to this initial barrier function, standard Corning Matrigel contains a series of growth factors, including ~3 ng/mL of Transforming Growth Factor- β (TGF- β) with the growth factor reduced (GFR) Corning Matrigel still containing ~2 ng/mL of TGF- β (as per Corning specification sheet). This is significant because T-, B-, and NK cells express TGF- β type I and II receptors and at 1-2 ng/mL of TGF- β ligand, the binding of this ligand to its cognate receptors highly suppresses both the adaptive and innate immune system via inhibition of T-, B-, and NK cell cytolytic activities.^{22,23} Importantly, multiple groups have also documented that localized and metastatic prostate cancers characteristically down-regulate expression of both type I and II TGF- β receptors, thereby losing the growth suppression normally induced in epithelial cells by TGF- β .²⁴⁻²⁶

Thus, the combination of an initial barrier to the infiltration of cytolytic host cells and the local TGF- β -dependent immunosuppressive responses that are present once cytolytic hosts cells do eventually infiltrate the Matrigel co-inoculum provides a rationale for why the Case Western Reserve group reported a 20% success rate (4 out of 20 attempts) when using Matrigel co-inoculation for establishing serially transplantable PDXs from primary prostate cancers.²⁷

1.4 | Prostate cancer xenograft development using SCID mice

Based upon the results of the 1980s, multiple groups initiated attempts in the early 90's to establish xenografts directly from living patients using biopsy material from localized disease, in addition to soft tissue and bone metastatic prostate cancer tissue from both hormonally naïve and androgen ablated patients. One of the successful groups was led by Nora M. Navone and Patricia Troncoso, working with Christopher Logothetis and Andrew von Eschenbach at the M D Anderson Cancer Center, Houston, Texas. Initially, the MD Anderson group used nude intact male mice as the host with no Matrigel co-inoculation. However,

as discussed above nude intact male mice retain a degree of humoral adaptive immune responses and an intact innate immune system, including high NK cell activity. Based upon these limitations, the MD Anderson group switched to using the more immune deficient T- and B-cell deficient severe combined immune deficient (ie, *scid*) intact male mice (Table 1), which do not have elevated NK activity,²⁸ but again with no Matrigel co-inoculation.²⁹ Such severe immune deficiency is due to a homozygous nonsense mutation in the carboxy-terminal region that creates a premature stop codon in the *PRKDC* gene, which encodes the DNA-PK catalytic subunit involved in DNA repair via non-homologous end joining (NHEJ).³⁰ V(D)J recombination, which rearranges the genetic components of antibodies (ie, immunoglobulins) and T-cell receptors during B- and T-cell maturation, respectively; requires NHEJ for proper function. Therefore, loss of the *PRKDC* functional protein prevents maturation of both B- and T-cells, which are essential for adaptive immune responses. This defect in DNA repair also renders *scid* strains sensitive to radiation-induced DNA damage, and it should be noted that *scid* strains have a propensity to generate functional B- and T-cells with increasing age; a phenomenon known as "leakiness."³¹

A recent paper summarizing the 25 year MD Anderson experience reported that 34 serially transplantable prostate cancer xenografts were established from 24 different patients.²⁹ Another group led by Charles L. Sawyers and Owen N. Witte, at UCLA, Los Angeles, California also started a prostate cancer xenograft program in the early 90's. This ULCA group used *scid* intact male mice in combination with Matrigel co-inoculation to establish the LAPC-3, -4, and -9 xenografts from eight attempts.³² More recently, the group at the University of Melbourne, Australia led by Elizabeth D. Williams was also able to establish an androgen sensitive serially transplantable xenograft (ie, BM18) using Matrigel co-inoculation into *scid* intact male mice.³³

1.5 | Prostate cancer xenograft development using sub-renal capsule (SRC) inoculation of NOD-SCID mice

All of the previously presented results used subcutaneous inoculation as the site of initial xenografting. In contrast, the Living Tumor Laboratory (LTL) at the University of British Columbia, Canada led by Yuzhuo Wang, has used sub-renal capsule (SRC) inoculation without Matrigel into androgen supplemented NOD-*scid* intact male mice (Table 1). This approach takes advantage of the highly vascular nature of the kidney coupled with the use of NOD-*scid* mice as the host. These animals have been developed by transferring the *scid* mutation onto a non-obese diabetic (ie, NOD) background, which is also originally derived from a Swiss colony.⁷ Animals homozygous for the *scid* mutation have impaired T- and B-cell lymphocyte maturation as described above, and the NOD animals have deficiencies in innate immunity, including defective NK, dendritic, and macrophage cell function, in addition to the loss of C5, a critical component of the hemolytic complement cascade. Using these NOD-*scid* mice, fresh primary or metastatic prostate cancer samples from 18 patients were transplanted into the SRC of NOD-*scid* male mice supplemented with

testosterone.³⁴ Tumors from 2 of 18 patients were terminated because of development of B-cell lymphoma (ie, a problem in immune deficient mice that will be discussed later), whereas 9 of remaining 16 were viable but static for >2 years after grafting. From the remaining 7 patients, they established and expanded 12 transplantable tumor lines for a minimum of five generations of serial passaging. Nine of these transplantable xenografts were developed from primary tumors (5 different patients). Furthermore, 7 of these lines were derived from needle biopsies (3 different patients), the first-time needle biopsies were established as xenografts.

1.6 | Xenograft development from metastatic, castration-resistant prostate cancers obtained from rapid autopsies

While it is not clear from all of the groups that successfully established at least one xenograft exactly how many attempts failed using tissue directly from living patients, based upon the Rotterdam and Case Western Reserve reported experiences, the cumulative success rate is limited. In addition to insufficient suppression of the host's adaptive and innate immune systems, this limited success rate could be due to the fact that the previous attempts used either small biopsy samples from metastatic sites or localized prostate cancers from radical prostatectomy specimens which did not allow validation of their aggressive nature (ie, lethality). To allow a more diverse sampling of different lethal metastatic sites, including bone metastases, and to allow a more optimally standardized tissue yield and viability protocol, Robert L. Vessella and Paul H. Lange at the University of Washington, Seattle initiated a rapid autopsy program in the early 90's to harvest lethal prostate cancer tissue from a variety of metastatic sites from each patient.³⁵ During the period from 1991 to 2005, the University of Washington group collected 261 prostate cancer samples from 156 patients and implanted them subcutaneously into immune deficient intact male mice without Matrigel. Initially this involved the use of nude intact male mice. This group later switched to using the more immune deficient *scid* intact male mice, but again did not use Matrigel co-inoculation. Eva Corey now leads this program and has reported that 26 xenografts have been successfully propagated beyond three passages.³⁵

Based upon the leads of the University of Washington, a similar rapid autopsy program began in 1995 at Johns Hopkins School of Medicine, Baltimore, MD led by G. Steven Bova and William B. Isaacs.³⁶ By 1997, 117 metastatic tissue samples from multiple organ sites obtained from 22 castration-resistant prostate cancer (mCRPC) patients were co-inoculated in Matrigel into *scid* intact male mice supplemented with exogenous testosterone (John T. Isaacs, unpublished data). While only 5 (ie, ~4%) of these first passage xenografts produced macroscopically (ie, >200 mm³ in size) growing tumors during a one year observation period, ~25% of the static xenografts contained viable (ie, AR, PSA, and Ki67 positive) cancer cells when the harvested tissue was examined histologically. When the five first passage growing xenografts were subsequently passaged with Matrigel co-inoculation into *scid* intact male mice supplemented

with exogenous testosterone only two grew, and only one of these made it to the 3rd passage, but not beyond.

A similar low success rate for establishing serially transplantable prostate cancer xenografts from mCRPC tissues was also reported from the warm autopsy program starting in 1996 at the University of Michigan led by Kenneth J. Pienta and Mark Rubin. This group reported an overall success rate of ~5% when multiple metastatic sites per autopsy from the first 14 patients were co-inoculated with Matrigel subcutaneously into *scid* intact male mice.³⁷ These efforts resulted in the VCaP line from a lumbar vertebrae metastasis.³⁸

1.7 | Different levels of androgen are optimal for establishing xenografts from hormonal naïve versus castration resistant prostate cancer patients

The circulating blood level of testosterone (T) varies by more than 150-fold from less than 0.3 ng/mL (ie, 1 nM) to >45 ng/mL (ie, 155 nM) in intact adult males of both outbred and inbred immune competent as well as immune deficient (eg, nude) strains of mice. This results in a mean serum T of less than 2 ng/mL (ie, 7 nM) with a standard error of the mean (SEM) of 1-2 ng/mL (ie, 3-7 nM).³⁹ This extreme variation in serum T occurs even if all of the animals are cross-sectionally sampled at the same time of day, or if the same animal is longitudinally sampled at multiple times throughout the day.³⁹ These observations are not a methodological artifact, because these extreme daily variations in serum T are detectable using radioimmunoassay, ELISA, or liquid chromatography-electrospray ionization-tandem mass spectrometry.³⁹

Indeed, early studies by the Rotterdam group documented that BALB/c nude intact male mice have low and highly variable circulating levels of serum T.⁴⁰ In adult BALB/c nude intact male mice, serum T ranges from 0.1 to 45 ng/mL (ie, 0.3-138 nM) with a mean of 1.7 ± 1.2 ng/mL (ie, 5.8 ± 4.1 nM) and a median of 0.25 ng/mL (ie, 0.9 nM).⁴⁰ A major reason for this wide variation in serum T is due to the fact that mice do not express Sex Hormone Binding Globulin (SHBG) in their blood.³⁹ By contrast, in adult human males which express SHBG, serum T does not normally fluctuate by more than 20% during the day with the mean ranging from 4.2 to 5.4 ng/mL (ie, 19-15 nM) between the ages 40 to 80 years.³⁹ Thus, the Rotterdam group routinely provided exogenous androgen supplemental to elevate and stabilize serum T >3 ng/mL (ie, 10 nM) in adult intact male mice used for xenografting.¹⁶ This is very reasonable when xenografting prostate cancer from a hormonally-naïve patient. However, CRPC from androgen ablated hosts consistently express a >30-fold elevated level of Androgen Receptor (AR) protein compared to normal prostate luminal epithelial cells.⁴¹ While this adaptive increase in AR facilitates their continuous growth in a castrate level of serum T (ie, <0.2 ng/mL or <0.7 nM), this paradoxically sensitizes CRPC cells to growth inhibition and death when these cancer cells are rapidly switched from a low castration level to a high (ie, >3 ng/mL or >10 nM) level of androgen. Indeed, this is the basis for clinical trials using Bipolar Androgen Therapy (ie, BAT), which cycles metastatic castration-resistant patients rapidly between short episodic periods of pharmacologically high serum T back to castrate levels of low serum T.⁴¹⁻⁴³

Thus, since circulating serum T in adult intact male mice is already essentially equivalent to that of castrated adult human males,³⁹ supplementing these animals with exogenous T when xenografting CRPCs may not be optimal, since this could potentially suppress their growth and induce cell death. This realization could provide an explanation for the poor success obtained by the Hopkins group when they xenografted mCRPC obtained at rapid autopsy into androgen supplemented adult intact male scid mice during their initial series of attempts.

1.8 | Prostate cancer xenograft development using NOD scid gamma (aka NSG) mice

NOD scid gamma (aka NSG) mice were developed by Leonard Shultz at The Jackson Laboratory and are among the most immune deficient mice presently available (Table 1). The mice carry two homozygous mutations on the NOD genetic background; severe combined immune deficiency (*scid*) and complete null alleles of the IL2 receptor common gamma chain (ie, *IL2rg*). The NOD background carries significant deficiencies in innate immunity, and the homozygous *scid* mutation renders the mice deficient in mature B- and T-cell adaptive function as described above. The homozygous mutation in the *IL2rg* alleles prevents cytokine signaling (ie, IL-2, -4, -7, -9, -15, and -21) through multiple receptors. Signaling through these high affinity cytokine receptors is required for functional B-, T-, and NK cell development. Like NSG mice, NOG animals also lack functional T-, B-, and NK cells. However, rather than the null mutation present in NSG mice, NOGs have a truncated form of the gamma chain that still binds the cytokines but does not signal through the receptor because it lacks the cytoplasmic domain; thus, producing the same severely compromised immunodeficient phenotype. Using these triple immune deficient NSG mice, a second xenograft program was initiated at Johns Hopkins School of Medicine led by Angelo M. DeMarzo starting at the end of 2009 using tissue obtained from a rapid autopsy program of metastatic CRPC patients. From the first 9 autopsies, 9 serially transplantable prostate cancer xenografts were established by subcutaneous Matrigel co-inoculation of 27 metastatic sites (ie, bone, liver, lung, lymph node, and skin) into these triple immune deficient NSG adult male mice not supplemented with exogenous T (ie, an overall success rate of 30%). The genetic, phenotypic, and growth characteristics of these new xenografts will be published shortly (John T. Isaacs, W. Nathaniel Brennen, Angelo M. De Marzo et al, unpublished results).

1.9 | The outgrowth of EBVtransformed human lymphomas from prostate cancer xenografts

When immune deficient mice are used as human tissue xenograft recipients, human B-cell lymphomas can develop from latent Epstein Barr Virus (EBV) infected B-cells that were initially present within the original human tissue are implanted. Indeed, as discussed earlier, the Vancouver Prostate Cancer group reported that from their 20 human prostate cancer xenograft "takes" in NOD-*scid* mice, 2 were not prostate cancer, but B-cell lymphomas.³⁴ A later Swiss collaboration

between Cyril A. Rentsch and Lukas Bubendorf, University Hospital Basel, and Marco Cecchini and George N. Thalmann, University of Bern, also documented this EBV-lymphoma issue. This latter group reported that from 48 patients, prostate cancer tissue was transplanted either subcutaneously or into the SRC in NSG mice supplemented with testosterone. From the 10 "takes" which grew, 8 were identified as human donor-derived lymphomas, including seven EBV-positive diffuse large B-cell lymphomas and one EBV-negative peripheral T-cell lymphoma.⁴⁴ This group concluded that up to 80% of the tumors that arise within the first 3 months after prostate cancer xenografting when using triple immune deficient NSG mice are patient-derived EBV-positive lymphomas.

Similarly, the prostate cancer xenograft cooperative program led by Anna T. Collins and Gabri van der Pluijn between the University of York/University of Leeds, UK and Leiden University Medical School, The Netherlands reported their results from primary prostate cancer fragments inoculated subcutaneously into immune deficient RAG-2 gamma mice.⁴⁵ Since the recombination-activating gene (RAG)-1 and -2 proteins are involved in V(D)J recombination, these homozygous RAG1/2 null mice, like *scid* mice, do not make mature B- or T-cells, but do not develop "leakiness" with age as occurs in the *scid* background (Table 1). The homozygous *IL2rg* null mutation prevents cytokine signaling through multiple receptors, leading to a deficiency in functional NK cells as described above. Using these triple immune deficient RAG2 gamma mice, xenografts were established from 47 out of 147 primary prostate cancer inoculated (ie, 32%).⁴⁵ Of these, only 20 were serially transplantable. Unfortunately, however, only three of the 20 established lines were confirmed as prostate cancer; one line was comprised of mouse stroma, and 16 were verified as human donor-derived EBV positive B-cell lymphomas. Thus, their overall success rate of establishing serially transplantable prostate cancer xenografts was 2% (3 out of 147 attempts).⁴⁵ Significantly, two out of the three serially transplantable prostate cancer xenograft lines were established from CRPC tissue inoculated subcutaneously in intact mice not receiving exogenous androgen supplementation.

These combined results document that when using triple immune deficient mice to generate serially transplantable xenografts from prostate cancer fragments, it is critical to evaluate the nature of primary outgrowths to document whether they are prostate cancer versus EBV-transformed lymphomas.

1.10 | Future focus on primary patient derived prostate cancer xenografts (PDXs) for personalized medicine

With an ever growing appreciation for the value of personalized medicine (aka precision medicine), there is clearly a hope that methods can be developed to allow efficient and timely growth of patient-derived prostate cancer xenografts (PDXs), which can then be used as "avatars" for defining optimal therapy for that specific patient. Optimizing the individualized establishment of prostate cancer PDXs from localized prostate cancers has been a particular focus of the group led by Renea A. Taylor and Gail P. Risbridger at Monash

University Victoria, Australia. Several technical improvements to the xenografting protocol have increased take rates, including the use of testosterone implants, placement of grafts under the renal capsule, and co-inoculation with murine neonatal inductive mesenchyme.⁴⁶ Using these modification, PDXs were successfully established from localized primary prostate cancers via SRC inoculation into NOG mice from 7 of 10 castration-resistant patients.⁴⁷ Grafts were most successful when the original patient specimens contained high amounts of viable cancer, defined as samples with at least 50% cancer cells, no physical damage due to tissue processing, and a detectable rate of proliferation.

While the Monash group has focused upon establishing individualized PDXs from solid prostate cancer tissue, the group at the Icahn School of Medicine at Mount Sinai, New York led by Joseph Domingo-Domenech has used circulating tumor cells (CTC) in the blood to generate prostate cancer PDXs.⁴⁸ This latter approach is highly promising since it could allow a much larger proportion of patients with metastatic prostate cancer to have access to such an approach. One limitation, however, is that the number of CTC present in such patients is low (ie, <50 cells/mL of blood) until the patient progresses to a quite advanced mCRPC stage. To overcome this limitation, Yu Chen at Memorial Sloan Kettering Cancer Center, New York has championed the use of in vitro organoid culture to expand the low number of CTCs isolated from the blood of prostate cancer patients so that the a sufficient number of malignant cells can be used for in vivo xenografting.⁴⁹ Based upon these leads, the next several years should be quite exciting as personalized medicine for prostate cancer becomes the norm and not the exception.

2 | CONCLUSION

In summary, the past 50 years of research has yielded significant insights into the generation of patient-derived xenografts (PDXs) from men with primary and metastatic prostate cancer. To date, these efforts have produced ~85 serially transplantable human prostate cancer xenografts spanning the phenotypic, epigenetic, and genetic heterogeneity observed clinically, which are to be described in greater detail in an upcoming publication.¹ It is hoped that dissemination of these models to the prostate cancer research community can provide experimental platforms for resolving the specificity versus generalizability of basic cancer biology principles (eg, credentialing of therapeutic molecular targets) and validating translational approaches for prevention, diagnosis, and therapy. Furthermore, it is hoped the insights highlighted in the present article from decades of efforts by laboratories throughout the world can accelerate the development of additional xenograft models, particularly from patients treated with newer standard of care agents such as abiraterone, enzalutamide, cabazitaxel, alfaradin, etc. Ultimately, the goal is to develop optimal methods for the efficient generation of PDX “avatars” from all patients, which can then be used to guide personalized therapeutic approaches that maximize clinical efficacy and reduce unnecessary or ineffective treatment and side effects.

ACKNOWLEDGMENTS

The authors would like to acknowledge the following sources of financial support: Movember Foundation Global Action Plan (GAP) program for development of prostate cancer xenografts to model human prostate cancer (JTI); Prostate Cancer Foundation Young Investigator Award (WNB); Patrick C. Walsh Prostate Cancer Research Fund (WNB); Department of Defense Prostate Cancer Research Program, Award No W81XWH-16-1-0410 (JTI) and W81XWH-17-1-0528 (WNB); NIH-Prostate SPORE grant number P50 CA058236 (JTI); and the NIH-SKCCC CCSG grant number P30 CA006973.

REFERENCES

1. Movember GAP1 PDX Project International Cooperative Group. Prostate Cancer PDXs: *They Do Exist*. Prostate. 2018 (in Press).
2. Grogan JB, Hardy JD. Increased survival of xenogeneic tumors in thymectomized hosts. *J Surgical Res*. 1968;8:7–9.
3. Isaacson JH, Cattanaach BM. Report. *Mouse News Letter*. 1962;27:31.
4. Flanagan SP. 'Nude', a new hairless gene with pleiotropic effects in the mouse. *Genet Res*. 1966;8:295–309.
5. Pantelouris EM. Observations on the immunobiology of 'Nude' Mice. *Immunology*. 1971;20:247–249.
6. Vaidya HJ, Briones Leon A, Blackburn CC. FOXN1 in thymus organogenesis and development. *Eur J Immunol*. 2016;46:1826–1837.
7. Beck JA, Lloyd S, Hafezparast M, et al. Genealogies of mouse inbred strains. *Nat Genet*. 2000;24:23–25.
8. Rygaard J. Immunobiology of the mouse mutant “Nude”. *Acta Path Microbiol Scand*. 1969;77:761–762.
9. Rygaard J, Povlson CO. Heterotransplantation of a human Malignant Tumor to “nude” mice. *Acta Path Microbiol Scand*. 1969;77:758–760.
10. Sato G, Desmond W, Kelly F. Human prostatic tumors in conditioned animals and culture. *Cancer Chemother Rep*. 1975;59:47–49.
11. Schroeder FH, Okada K, Jellinghaus W, Wullstein HK, Heinemeyer HM. Human prostatic adenoma and carcinoma. Transplantation of cultured cells and primary tissue fragments in “nude” mice. *Invest Urol*. 1976;13:395–403.
12. Mickey DD, Stone KR, Wunderli H, Mickey GH, Vollmer RT, Paulson DF. Heterotransplantation of a Human Prostatic Adenocarcinoma Cell Line in Nude Mice. *Cancer Res*. 1977;37:4049–4058.
13. Kaighn ME, Narayan KS, Ohnuki Y, Lechner JF, Jones LW. Establishment and characterization of a human prostatic carcinoma cell line (PC-3). *Invest Urol*. 1979;17:16–23.
14. Horoszewicz JS, Leong SS, Chu TM, et al. The LNCaP cell line—a new model for studies on human prostatic carcinoma. *Prog Clin Biol Res*. 1980;37:115–132.
15. Hoehn W, Schroeder FH, Reimann JF, Joebis AC, Hermanek P. Human prostatic adenocarcinoma: some characteristics of a serially transplantable line in nude mice (PC 82). *Prostate*. 1980;1:95–104.
16. van Weerden WM, de Ridder CM, Verdaasdonk CL, et al. Development of seven new human prostate tumor xenograft models and their histopathological characterization. *Am J Pathol*. 1996;149:1055–1062.
17. Hanna N, Davis TW, Fidler IJ. Environmental and genetic factors determine the level of NK activity of nude mice and affect their suitability as models for experimental metastasis. *Int J Cancer*. 1982;30:371–376.
18. Herberman RB, Nunn ME, Lavrin DH. Natural cytotoxic reactivity of mouse lymphoid cells against syngeneic acid allogeneic tumors. I. Distribution of reactivity and specificity. *Int J Cancer*. 1975;16:216–229.
19. Steerenberg PA, Korenromp EL, van Loveren H, Mol DQ, Geerse L, de Grijl FR. Natural killer cell activity during UVR-induced skin tumor formation in the Skh hairless mouse. *Photochem Photobiol*. 1997;65:150–154.

20. Russell PJ, Russell P, Rudduck C, Tse BW, Williams ED, Raghavan D. Establishing prostate cancer patient derived xenografts: lessons learned from older studies. *Prostate*. 2015;75:628–636.
21. Pretlow TG, Wolman SR, Micale MA, et al. Xenografts of primary human prostatic carcinoma. *J Natl Cancer Inst*. 1993;85:394–398.
22. Kehrl JH, Alvarez-Mon M, Fauci AS. Type β transforming growth factor suppresses the growth and differentiation of human B and T lymphocytes. *Clin Res*. 1985;33:610–615.
23. Rook AH, Kehrl JH, Wakefield LM, et al. Effects of transforming growth factor beta on the functions of natural killer cells: depressed cytolytic activity and blunting of interferon responsiveness. *J Immunol*. 1986;136:3916–3920.
24. Kim IY, Ahn HJ, Zelter DJ, et al. Loss of expression of transforming growth factor beta type I and type II receptors correlates with tumor grade in human prostate cancer tissues. *Clin Cancer Res*. 1996;2:1255–1261.
25. Williams RH, Stapleton AM, Yang G, et al. Reduced levels of transforming growth factor beta receptor type II in human prostate cancer: an immunohistochemical study. *Clin Cancer Res*. 1996;2:635–640.
26. Guo Y, Jacobs SC, Kyprianou N. Down-regulation of protein and mRNA expression for transforming growth factor-beta (TGF-beta1) type I and type II receptors in human prostate cancer. *Int J Cancer*. 1997;71:573–579.
27. Wainstein MA, He F, Robinson D, et al. CWR22: androgen-dependent xenograft model derived from a primary human prostatic carcinoma. *Cancer Res*. 1994;54:6049–6052.
28. Dorshkind K, Pollack SB, Bosma MJ, Phillips RA. Natural killer (NK) cells are present in mice with severe combined immunodeficiency (scid). *J Immunol*. 1985;134:3798–3801.
29. Kleb B, Estéicio MR, Zhang J, et al. Differentially methylated genes and androgen receptor re-expression in small cell prostate carcinomas. *Epigenetics*. 2016;11:184–193.
30. Blunt T, Gell D, Fox M, et al. Identification of a nonsense mutation in the carboxyl-terminal region of DNA-dependent protein kinase catalytic subunit in the scid mouse. *Proc Natl Acad Sci U S A*. 1996;93:10285–10290.
31. Busman GC, Fried M, Custer RP, Carroll A, Gibson DM, Bosma MJ. Evidence of functional lymphocytes in some (leaky) scid mice. *J Exp Med*. 1988;167:1016–1033.
32. Klein KA, Reiter RE, Redula J, et al. Progression of metastatic human prostate cancer to androgen independence in immunodeficient SCID mice. *Nat Med*. 1997;3:402–408.
33. McCulloch DR, Opeskin K, Thompson EW, Williams ED. BM18: a novel androgen-dependent human prostate cancer xenograft model derived from a bone metastasis. *Prostate*. 2005;65:35–43.
34. Lin D, Wyatt AW, Xue H, et al. High fidelity patient-derived xenografts for accelerating prostate cancer discovery and drug development. *Cancer Res*. 2014;74:1272–1283.
35. Nguyen HM, Vessella RL, Morrissey C, et al. LuCaP Prostate Cancer Patient-Derived Xenografts Reflect the Molecular Heterogeneity of Advanced Disease and Serve as Models for Evaluating Cancer Therapeutics. *Prostate*. 2017;77:654–667.
36. Suzuki H, Freije D, Nusskern DR, et al. Interfocal heterogeneity of PTEN/MMAC1 gene alterations in multiple metastatic prostate cancer tissues. *Cancer Res*. 1998;58:204–209.
37. Rubin MA, Putzi M, Mucci N, et al. Rapid (“warm”) autopsy study for procurement of metastatic prostate cancer. *Clin Cancer Res*. 2000;6:1038–1045.
38. Korenchuk S, Lehr JE, McLean L, et al. VCaP, a cell-based model system of human prostate cancer. *In Vivo*. 2001;15:163–168.
39. Sedelaar JPM, Dalrymple SS, Isaacs JT. Of mice and men-warring: intact versus castrated adult male mice as xenograft hosts are equivalent to hypogonadal versus abiraterone treated aging human males, respectively. *Prostate*. 2013;73:1316–1325.
40. van Steenbrugge GJ, Groen M, de Jong FH, Schroeder FH. The use of steroid-containing silastic implants in male nude mice: Plasma hormone levels and the effect of implantation on the weights of ventral prostate and seminal vesicles. *Prostate*. 1984;5:639–647.
41. Isaacs JT, D’Antonio JM, Chen S, et al. Adaptive auto-regulation of androgen receptor provides a paradigm shifting rationale for bipolar androgen therapy (BAT) for castrate resistant human prostate cancer. *Prostate* 2012;72:1491–1505.
42. Schweizer MT, Antonarakis ES, Wang H, et al. Effect of bipolar androgen therapy for asymptomatic men with castration-resistant prostate cancer: results from a pilot clinical study. *Sci Transl Med*. 2015;7:269ra2.
43. Teply BA, Wang H, Lubber B, et al. Bipolar androgen therapy in men with metastatic castration-resistant prostate cancer after progression on enzalutamide: an open-label, phase 2, multicohort study. *Lancet Oncol*. 2018;19:76–86.
44. Wetterauer C, Vlajnic T, Schüler J, et al. Early development of human lymphomas in a prostate cancer xenograft program using triple knock-out immunocompromised mice. *Prostate*. 2015;75:585–592.
45. Taurozzi AJ, Beekharri R, Wantoch M, et al. Spontaneous development of Epstein-Barr virus associated human lymphomas in a prostate cancer xenograft program. *PLoS ONE*. 2017;12:e0188228.
46. Lawrence MG, Taylor RA, Toivanen R, et al. A preclinical xenograft model of prostate cancer using human tumors. *Nat Protoc*. 2013;8:836–848.
47. Lawrence MG, Pook DW, Wang H, et al. Establishment of primary patient-derived xenografts of palliative TURP specimens to study castrate-resistant prostate cancer. *Prostate*. 2015;75:1475–1483.
48. Williams ES, Rodriguez-Bravo V, Chippada-Venkata U, et al. Generation of prostate cancer patient derived xenograft models from circulating tumor cells. *J Vis Exp*. 2015;105:53182.
49. Gao D, Chen Y. Organoid development in cancer genome discovery. *Curr Opin Genet Dev*. 2015;30:42–48.

How to cite this article: Brennen WN, Isaacs JT. The what, when, and why of human prostate cancer xenografts. *The Prostate*. 2018;78:646–654. <https://doi.org/10.1002/pros.23510>

Review Article

Resolving the Coffey Paradox: what does the androgen receptor do in normal vs. malignant prostate epithelial cells?

John T Isaacs^{1,2}

¹Department of Oncology, Prostate Cancer Program, The Sidney Kimmel Comprehensive Cancer Center at Johns Hopkins, Baltimore, MD 21231, USA; ²The Brady Urologic Institute, Department of Urology, The Johns Hopkins University School of Medicine, Baltimore, MD 21231, USA

Received March 12, 2018; Accepted March 19, 2018; Epub April 1, 2018; Published April 15, 2018

Abstract: Donald Straley Coffey completed his 85 year life's journey on November 9, 2017. In his wake, he left a legion of inspired and loyal students, fellows, and faculty colleagues from all over the world to carry on his passion both for life in general and his 50 year quest to conquer cancer. Early in his career, Dr. Coffey developed a series of animal models to study how androgen regulates the growth of both normal and abnormal prostatic epithelium. As part of these early studies, Dr. Coffey uncovered a paradox in that anti-androgen treatment given at the "wrong" time paradoxically enhanced, not inhibited, normal prostate growth. Advances over the last several years concerning the paracrine-dependent stem cell organization of the prostate provide a mechanistic explanation for this "Coffey Paradox". This is based upon the realization that the normal function of the Androgen Receptor (AR) in the paracrine-dependent stem cell organization of the prostate is to induce terminal differentiation of normal prostate epithelial cells while suppressing their growth, despite the presence of high levels of stromal cell-derived paracrine growth factors. Such growth suppression involves ligand-dependent AR binding to the Tcf-4/ β -catenin 3'c-Myc enhancer in prostate epithelial cells, which inhibits c-Myc transcription needed for proliferation. Therefore, if anti-androgen is given at the wrong time, it prevents such AR-dependent c-Myc down regulation, and thus paradoxically enhances epithelial regrowth (i.e. the Coffey Paradox) induced by exogenous androgen replacement in the castration regressed prostate. In contrast to the normal prostate epithelium, in prostate cancer cells retaining AR expression, androgen-induced AR signaling no longer reduces c-Myc transcription but instead up-regulates c-Myc translation and protein stability to stimulate malignant growth. Thus, in these AR expressing prostate cancer cells, AR signaling is converted from a growth suppressor to an oncogene, which involves a gain of function to upregulate c-Myc protein expression. Such a gain of function "addicts" these prostate cancer cells to AR signaling for their proliferation and survival, which provides the rationale for therapy targeted at inhibiting such AR signaling. While therapies targeted at maximally decreasing the level of androgen ligand are the most commonly used, recent studies have documented that a subset of patients progressing on such androgen ablation (i.e. castration-resistant disease) due to their adaptive increase in AR protein expression respond positively to rapid cycling between pharmacologically high and castration low levels of circulating androgen. [i.e. Bipolar Androgen Therapy (BAT)].

Keywords: Prostate, castration, prostate cancer, androgen receptor, stem cells, andromedins

Introduction to the "Coffey Paradox"

In the late 1960s, Donald S. Coffey reported his seminal studies on the biochemical changes in prostate tissue associated with androgen-induced DNA synthesis [1]. These studies, using the androgen-induced proliferative regrowth of the 2 week castration regressed rat prostate as the experimental model, documented that proliferative regrowth of the prostatic epithelium occurred over a 10-14 day period with

the maximal rate of proliferative DNA synthesis occurring between 2-3 days post-exogenous androgen replacement [1]. Dr. Coffey went on to document in 1972 that anti-androgens, like cyproteroneacetate or flutamide, could prevent such proliferative regrowth of the regressed prostate if given simultaneously with exogenous androgen replacement to the castrated animals (Detailed in **Figure 1**, replicated from reference [2]). Paradoxically, however, if the castrated rats were given 54 hours of treat-

Normal vs. malignant AR activity

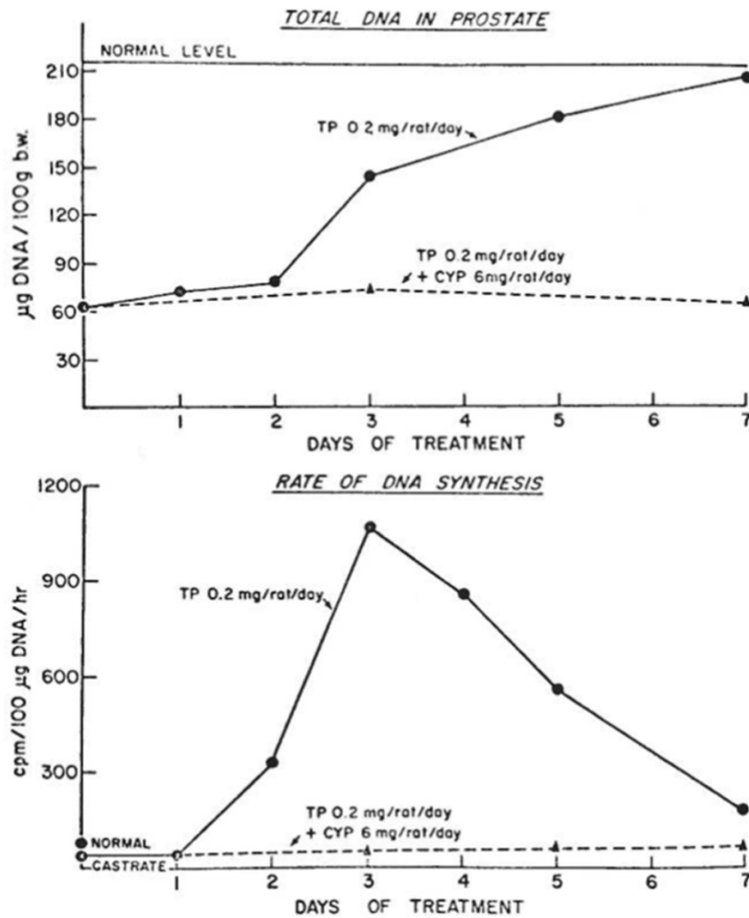


Figure 1. The effect of the anti-androgen cyproterone acetate (6 mg/rat/day) in blocking the exogenous androgen replacement (0.2 mg testosterone propionate/rat/day)-induced regrowth of the ventral prostate of a 2-week previously castrated rat based upon total DNA content expressed as $\mu\text{g DNA}/100$ grams of body weight (upper panel) and DNA synthesis expressed as tritiated thymidine incorporation/ $100 \mu\text{g DNA/hr}$ (lower panel). Figure replicated from reference [2], with permission.

ment with exogenous androgen alone followed by 18 hours of co-treatment with exogenous androgen plus anti-androgen, the rate of proliferative prostatic DNA synthesis was significantly enhanced by ~50% as compared to when the animals received 72 hours of androgen replacement alone (Detailed in **Figure 2**, replicated from reference [2]).

Androgen regulation of stem cell organization in normal prostate and the Coffey Paradox

The mechanism for this “Coffey Paradox” has only recently been resolved based upon several additional seminal observations. The first, discovered and championed by Gerry Cunha, is that in the normal prostate, epithelial cell number is dependent upon the level of ligand bind-

ing to the androgen receptor (AR) within prostate stromal cells, which stimulates their production and secretion of androgen-regulated stromal cell-derived paracrine peptide factors (i.e. andromedins) [3]. These andromedins then diffuse into the epithelial compartment and bind to cognate receptors to initiate signaling pathways that promote epithelial cell growth and survival. The second, discovered more than 30 years ago in collaboration with Dr. Coffey, is that the normal prostate can undergo successive cycles of androgen deprivation and replacement without diminishing its ability for continued regeneration [4]. Since then, a large number of independent groups have clarified how the human prostate is organized into prostate stromal and epithelial adult stem cell units, **Figure 3**, and how androgen-sensitive reciprocal paracrine interactions between these two compartments allows such profound cyclic regenerative growth capacity [4-9]. In the stromal compartment, adult mesenchymal stem cells (MSCs) respond to paracrine factors (e.g. SHH) secreted by prostate basal epithelial cells for their self-renewal and the generation of stromal progeny cells, which have a limited proliferative ability before differentiating into a variety of proliferatively quiescent stromal cell types (e.g. smooth muscle cells, adipocytes, fibroblasts, pericytes, etc.), a subset of which express the AR [10-12]. When adequate levels of androgen are present to efficiently bind to and thus activate AR transcriptional signaling, these AR expressing stromal cells secrete andromedins that diffuse throughout the immediate microenvironment until binding their cognate receptors on specific cell types within the epithelial and stromal compartments to induce compartment-specific differentiation programs, **Figure 3** [8].

Normal vs. malignant AR activity

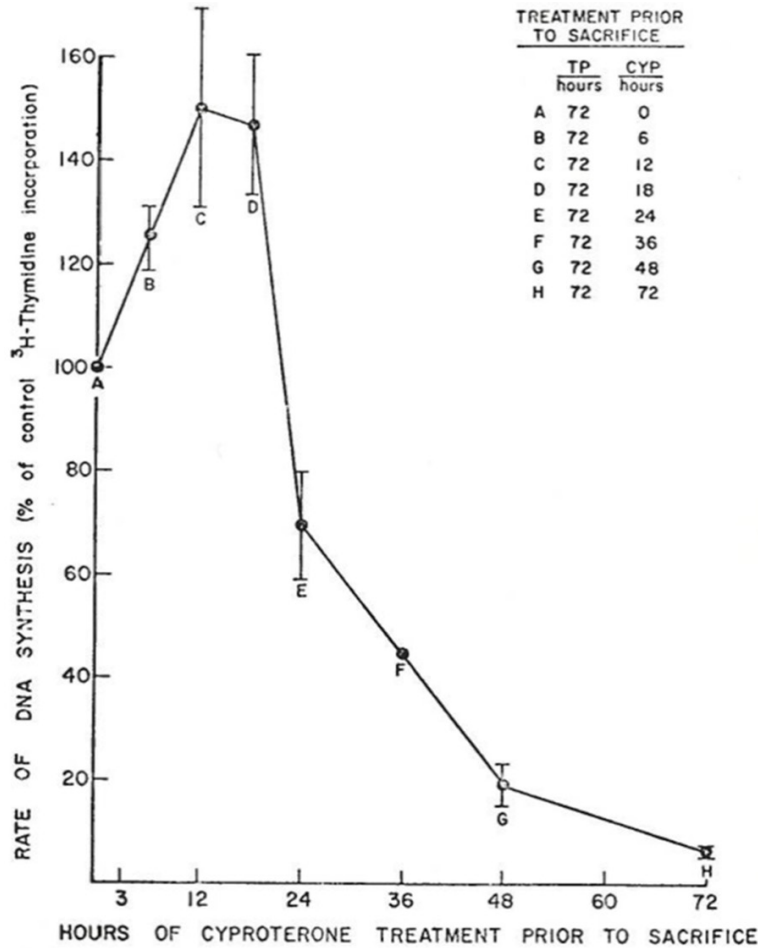


Figure 2. The effect of delaying treatment with anti-androgen (i.e. 6 mg cyproterone acetate) on its ability to block the stimulated rate of regenerative DNA synthesis in the 2-week regressed ventral prostate of rats after 3 days exogenous androgen replacement (i.e. 0.2 mg of testosterone propionate/day). Figure replicated from reference [2], with permission.

The human prostate epithelial compartment is a tubuloalveolar structure containing a simple stratified epithelium composed of a continuous basal layer underneath a luminal layer. Functionally, this epithelial compartment is organized by epithelial adult stem cell units [8]. These prostate epithelial adult stem cells are located in niches in the basal layer of the proximal epithelial ducts, **Figure 3** [7-9]. These prostate epithelial adult stem cells are androgen independent as documented by the classic tissue recombination studies of Gerry Cunha, which proved that epithelial morphogenesis and growth occurs even when AR protein is not expressed by any prostate epithelial cells, including adult stem cells, as long as there is ligand-dependent AR paracrine signaling in the supporting stromal cells [3, 5]. The mechanism

for this epithelial growth in the absence of epithelial AR expression is related to the hierarchical expansion and maturation of AR-negative epithelial adult stem cells and their progeny, **Figure 3**. E. Lynette Wilson et al. documented that these androgen insensitive epithelial stem cells are located in niches that control their survival and self-renewal, which are positioned in the basal epithelial layer at the opening of the proximal ducts as they enter the urethra [7, 9]. AR-negative epithelial adult stem cells within these proximal duct basal niches undergo self-renewal division in which one daughter remains in the niche as a stem cell and the other daughter cell migrates out of the niche and undergoes differentiation. Though this migrating daughter occasionally differentiates into a non-proliferating, AR-negative neuroendocrine (NE) cell, the much more prevalent pathway is differentiation into a Δ Np63-positive/basal cytokeratin-positive/AR-negative proliferating progenitor cell. Using *in situ* lineage tracing on human prostate tissues, Rakesh Heer et al. documented these basal progenitor cells undergo a limited number of amplifying proliferations while they migrate in streams in the basal layer along the proximal-distal ductal axis, **Figure 3** [9]. Such basal progenitor proliferation requires the androgen regulated production and secretion of diffusible stromal-derived paracrine andromedins [8]. These paracrine secreted andromedins diffuse from the stroma into the epithelial compartment where their binding to cognate receptors stimulates progenitor cell proliferation and subsequent maturation of a subset of these cells into Δ Np63-negative basal and luminal cytokeratin-positive (i.e. intermediate) basal cells, initially documented by Schalken et al. [6]. These intermediate basal cells begin to express an increasing level of AR protein as

Normal vs. malignant AR activity

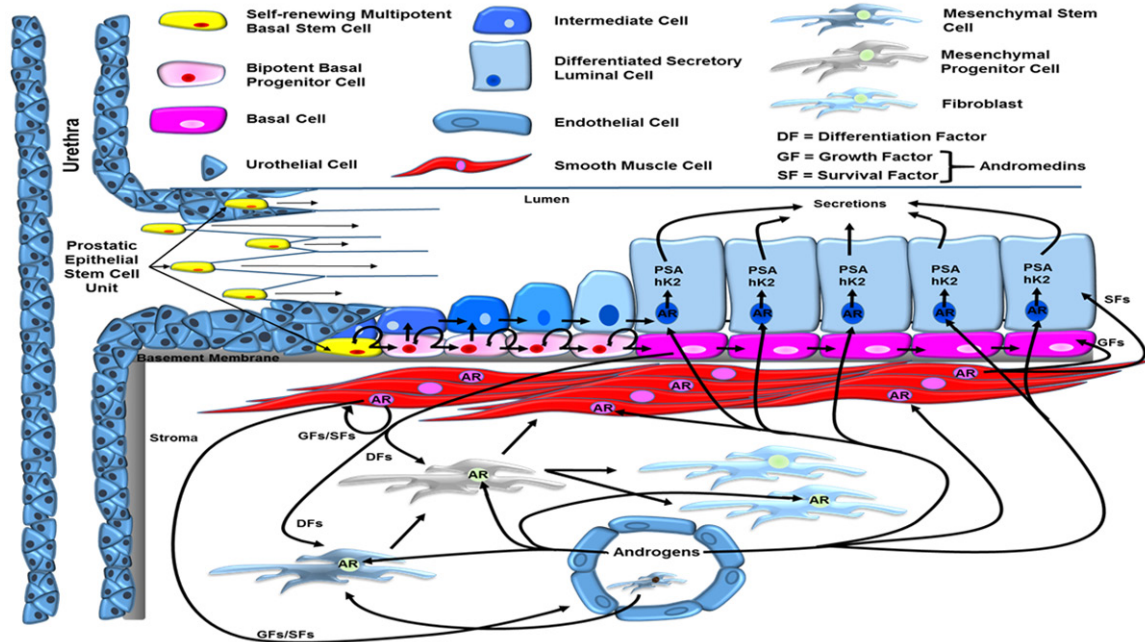


Figure 3. Reciprocal hierarchical expansion of epithelial and stromal adult stem cells in the human prostate. Prostate epithelial stem cells located in niches in the basal layer of the proximal ducts are induced to undergo hierarchical expansion in response to AR-dependent stromal-derived andromedins. This hierarchical expansion produces a stratified epithelium consisting of a continuous layer of Δ Np63-positive/basal cytokeratin-positive/AR-negative basal cells under a layer of Δ Np63-negative/luminal cytokeratin-positive/AR-positive/PSA-expressing secretory luminal cells. Adapted from Isaacs [8] and Moad, et al. [9].

they migrate from the basal to the luminal layer to become luminal intermediate cells during their flow to the more distal ducts. Ligand-dependent AR binding to response elements in the enhancer/promoter of AR target genes (e.g. PSA) induces differentiation of these luminal intermediate cells into Δ Np63-negative/luminal cytokeratin-positive/AR-positive/PSA-expressing secretory luminal cells [13].

While this adult stem cell organization provides a framework for understanding both the paracrine mechanism of androgen action in the normal prostate and how the gland maintains its ability to regenerate through multiple cycles of androgen deprivation and restoration, only recently has there been an understanding of what restricts the continuous overgrowth of normal adult prostate epithelial stem cell units in the continuous presence of high levels of andromedins in the prostate of non-castrated adult males. Immunocytochemical studies document that in the human prostate, the small fraction of proliferating normal prostate epithelial cells is located in the basal compartment and do not express AR protein, while the AR positive secretory-luminal cells are proliferative

quiescent [14]. It has also been demonstrated experimentally that AR signaling activated by androgen binding in prostate epithelial cells induces their growth arrest and eventual differentiation into secretory-luminal cells [15, 16]. Likewise, transgenic mouse studies have documented that when the AR gene is knocked out selectively in secretory-luminal cells within the prostate, then only these AR-deficient cells become hyper-proliferative and do not terminally differentiate [17-19]. These data document that AR-induced epithelial cell growth arrest limits the positive feed-forward proliferative stromal-driven paracrine loop. Thus, preventing continuous prostatic epithelial hyperplasia in the presence of high levels of stromal andromedins that are chronically maintained by physiological levels of androgen in an intact male [15, 16]. The mechanism for such growth suppression is due to ligand occupied AR binding to the β -catenin/TCF-4 complex located at the c-Myc 3' TCF-4 enhancer, which prevent transcription of c-Myc [15, 16].

When previously castrated hosts with a regressed prostate are given physiologic androgen replacement, adequate ligand occupancy of

nuclear AR re-occurs within the prostatic stromal cells to re-stimulate their production and secretion of an adequate level of andromedins to enter the epithelial compartment and stimulate the proliferation of initially AR-negative/p63-positive basal epithelial cells. The progeny of these initially AR-negative epithelial cells now express AR protein to which the replaced androgen binds. This ligand occupancy allows AR to bind to specific gene enhancers and promoters as a transcription factor inducing increased expression of NKX3.1, PSA, HK2, and luminal cytokeratins (e.g. CK18) coupled with down regulation of p63 and basal cytokeratins (e.g. CK14); thus differentiating these cells into intermediate cells. The ligand occupied AR in these intermediate cells also binds the β -catenin/TCF-4 complex located at the c-Myc 3' TCF-4 enhancer preventing transcription of c-Myc and thus completing their terminal differentiation into non-proliferating secretory-luminal cells. On the other hand, if such castrated hosts are given androgen replacement alone for a sufficient amount of time to produce adequate levels of stromal andromedins to stimulate proliferation and differentiation of AR-negative basal cells into AR-positive intermediate progeny before initiating anti-androgen treatment, then anti-androgen prevents AR from binding to the β -catenin/TCF-4 complex at the c-Myc 3' TCF-4 enhancer, which allows c-Myc expression and thus their continued proliferation. Thereby, explaining the Coffey Paradox.

AR acquires oncogenic functions during prostatic carcinogenesis

During prostatic carcinogenesis, stromal AR expression is not required for prostate cancer growth since there is a conversion from the normal AR-dependent stromal paracrine to a cell autonomous autocrine mechanism for AR-stimulated malignant growth [20]. Such a conversion is characterized by a lack of AR expression in the tumor stromal cells surrounding AR-positive human prostate primary cancer and their metastases [21]. During this molecular conversion from stromal dependent paracrine to cell autonomous autocrine AR signaling pathways, the prostate cancer cells become "addicted" to such cell autonomous AR oncogenic signaling [20, 21]. Such cell autonomous AR-dependent growth stimulation involves secretion, extracellular binding, and signaling by

autocrine growth factors that stimulate prostate cancer growth, not the andromedins secreted by normal prostate stromal cells [21]. Such cell autonomous extracellular autocrine signaling is necessary but not sufficient for the optimal growth of prostate cancer cells [21]. Thus, AR-induced growth stimulation of human prostate cancer also requires AR-dependent intracellular pathways to regulate the expression of critical transcription factors, like c-Myc [15, 16, 21]. For example, this oncogenic conversion involves a differential loss of AR suppression of c-Myc transcription coupled with a gain of AR up-regulation of c-Myc translation and protein stability that stimulates prostate cancer growth as documented by inhibition of both of these responses following treatment with an AR antagonist, such as bicalutamide [16, 22].

Conclusions

In normal prostate epithelial cells, AR signaling induces both differentiation and growth suppression. During prostatic carcinogenesis, AR signaling loses its growth suppressive ability either by its lack of expression (i.e. in AR-negative PCa) or by molecular changes that prevent its suppressor function in cancer cells that continue to express AR [22-24]. Under this latter situation, continued AR expression can also undergo a gain of oncogenic function to stimulate prostate cancer cell growth via stimulating c-Myc expression [16, 20-22]. Such a gain of function "addicts" prostate cancer cells to AR signaling for their proliferation and survival, providing the rationale for therapy targeted at inhibiting such AR signaling. While therapies targeted at maximally decreasing the level of androgen ligand are the most commonly used, recent studies have documented that a subset of patients progressing on such androgen ablation (i.e. castration resistance) due to their adaptive increase in AR protein expression respond positively to sequential cycles alternating rapidly between periods of acute supraphysiologic androgen followed by acute ablation to take advantage of a vulnerability produced by adaptive auto-regulation and binding of AR [25-29]. Resolving the mechanism (s) for the effectiveness of such Bipolar Androgen Therapy (BAT) is presently an active area of study with AR functioning in DNA replication and DNA damage repair being leading candidates.

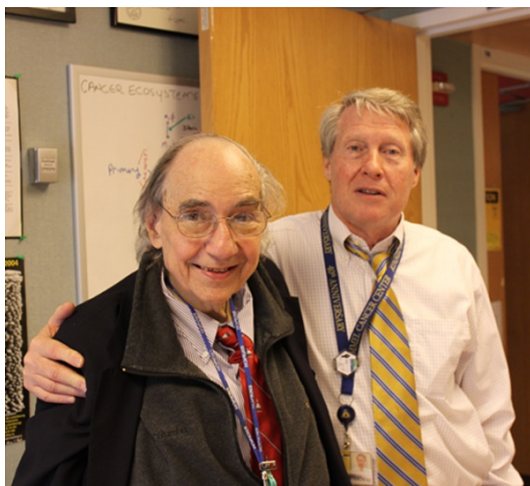


Figure 4. The author standing on the shoulder of a giant (i.e. Donald Straley Coffey).

Postscript

In a letter to Robert Hooke in 1675, Sir Isaac Newton stated that “If I have seen further, it is by standing on ye shoulders of Giants”. I have had the privilege and the joy to have stood on the shoulders of Donald Straley Coffey, **Figure 4**.

Acknowledgements

The author would like to acknowledge the following sources of financial support: SKCCC Cancer Center Support Grant (P30 CA006973), Department of Defense Prostate Cancer Research Program (Award No W81XWH-16-1-0410), and NIH-Prostate SPORE Grant (P50 CA0582-36).

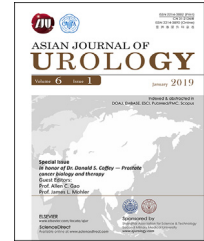
Address correspondence to: John T Isaacs, Department of Oncology, Prostate Cancer Program, The Sidney Kimmel Comprehensive Cancer Center at Johns Hopkins, Baltimore, MD 21231, USA; The Brady Urologic Institute, Department of Urology, The Johns Hopkins University School of Medicine, Baltimore, MD 21231, USA. E-mail: isaacjo@jhmi.edu

References

- [1] Coffey DS, Shimazaki J, Williams-Ashman HG. Polymerization of deoxyribonucleotides in relation to androgen-induced prostatic growth. *Arch Biochem Biophys* 1968; 124: 184-198.
- [2] Carter MF, Chung LWK, Coffey DS. The temporal requirements for androgen during the cell cycle of the prostate gland. In *Urologic Research*, edited by LR King and GP Murphy, New York, Plenum Press, 1972, pp. 27-28.
- [3] Cunha GR, Chung LW, Shannon JM, Taguchi O, Fujii H. Hormone-induced morphogenesis and growth: role of mesenchymal-epithelial interactions. *Recent Prog Horm Res* 1983; 39: 559-98.
- [4] Isaacs J, Coffey DS. Etiology and disease process of benign prostatic hyperplasia. *Prostate Suppl* 1989; 2: 33-50.
- [5] Wang Y, Hayward S, Cao M, Thayer K, Cunha G. Cell differentiation lineage in the prostate. *Differentiation* 2001; 68: 270-279.
- [6] Schalken JA, van Leenders G. Cellular and molecular biology of the prostate: stem cell biology. *Urology* 2003; 62: 11-20.
- [7] Goto K, Salm SN, Coetzee S, Xiong X, Burger PE, Shapiro E, Lepor H, Moscatelli D, Wilson EL. Proximal prostatic stem cells are program to regenerate a proximal-distal ductal axis. *Stem Cells* 2006; 24: 1859-1868.
- [8] Isaacs JT. Prostate stem cells and benign prostatic hyperplasia. *Prostate* 2008; 68: 1025-1034.
- [9] Moad M, Hannezo E, Buczacki SJ, Wilson L, El-Sherif A, Sims D, Pickard R, Wright NA, Williamson SC, Turnbull DM, Taylor RW, Greaves L, Robson CN, Simons BD, Heer R. Multipotent basal stem cells, maintained in localized proximal niches, support directed long-ranging epithelial flows in human prostates. *Cell Rep* 2017; 20: 1609-1622.
- [10] Lamm ML, Catbagan WS, Laciak RJ, Barnett DH, Hebner CM, Gaffield W, Walterhouse D, Iannaccone P, Bushman W. Sonic hedgehog activates mesenchymal Gli1 expression during prostate ductal bud formation. *Dev Biol* 2002; 249: 349-366.
- [11] Karhadkar SS, Bova GS, Abdallah N, Dhara S, Gardner D, Maitra A, Isaacs JT, Berman DM, Beachy PA. Hedgehog signalling in prostate regeneration, neoplasia and metastasis. *Nature* 2004; 431: 707-712.
- [12] Peng YC, Levine CM, Zahid S, Wilson EL, Joyner AL. Sonic hedgehog signals to multiple prostate stromal stem cells that replenish distinct stromal subtypes during regeneration. *Proc Natl Acad Sci U S A* 2013; 110: 20611-20616.
- [13] Vander Griend DJ, Karthaus WL, Dalrymple S, Meeker A, DeMarzo AM, Isaacs JT. The role of CD133 in normal human prostate stem cells and malignant cancer-initiating cells. *Cancer Res* 2008; 68: 9703-9711.
- [14] De Marzo AM, Meeker AK, Epstein JI, Coffey DS. Prostate stem cell compartments: expression of the cell cycle inhibitor p27Kip1 in normal, hyperplastic, and neoplastic cells. *Am J Pathol* 1998; 153: 911-9.
- [15] Antony L, van der Schoor F, Dalrymple SL, Isaacs JT. Androgen receptor (AR) suppresses normal human prostate epithelial cell proliferation.

Normal vs. malignant AR activity

- tion via AR/beta-catenin/TCF-4 complex inhibition of c-MYC transcription. *Prostate* 2014; 74: 1118-1131.
- [16] Vander Griend DJ, Litvinov IV, Isaacs JT. Conversion of androgen receptor signaling from a growth suppressor in normal prostate epithelial cells to an oncogene in prostate cancer cells involves a gain of function in c-Myc regulation. *Int J Biol Sci* 2014; 10: 627-42.
- [17] Wu CT, Altuwajiri S, Ricke WA, Huang SP, Yeh S, Zhang C, Niu Y, Tsai MY, Chang C. Increased prostate cell proliferation and loss of cell differentiation in mice lacking prostate epithelial androgen receptor. *Proc Natl Acad Sci U S A* 2007; 104: 12679-84.
- [18] Simanainen U, Allan CM, Lim P, McPherson S, Jimenez M, Zajac JD, Davey RA, Handelsman DJ. Disruption of prostate epithelial androgen receptor impedes prostate lobe-specific growth and function. *Endocrinology* 2007; 148: 2264-72.
- [19] Simanainen U, McNamara K, Gao YR, Handelsman DJ. Androgen sensitivity of prostate epithelium is enhanced by postnatal androgen receptor inactivation. *Am J Physiol Endocrinol Metab* 2009; 296: E1335-43.
- [20] Gao J, Arnold JT, Isaacs JT. Conversion from a paracrine to an autocrine mechanism of androgen-stimulated growth during malignant transformation of prostatic epithelial cells. *Cancer Res* 2001; 61: 5038-5044.
- [21] Vander Griend DJ, D'Antonio J, Gurel B, Antony L, Demarzo AM, Isaacs JT. Cell-autonomous intracellular androgen receptor signaling drives the growth of human prostate cancer initiating cells. *Prostate* 2010; 70: 90-9.
- [22] Litvinov IV, De Marzo AM, Isaacs JT. Is the Achilles' heel for prostate cancer therapy a gain of function in androgen receptor signaling? *J Clin Endocrinol Metab* 2003; 88: 2972-82.
- [23] Brennen WN, Isaacs JT. Cellular origin of androgen receptor pathway-independent prostate cancer and implications for therapy. *Cancer Cell* 2017; 32: 399-401.
- [24] D'Antonio JM, Vander Griend DJ, Antony L, Ndikuyeze G, Dalrymple SL, Koochekpour S, Isaacs JT. Loss of androgen receptor-dependent growth suppression by prostate cancer cells can occur independently from acquiring oncogenic addiction to androgen receptor signaling. *PLoS One* 2010; 5: e11475.
- [25] Denmeade SR, Isaacs JT. Bipolar androgen therapy: the rationale for rapid cycling of supraphysiologic androgen/ablation in men with castration resistant prostate cancer. *Prostate* 2010; 70: 1600-7.
- [26] Isaacs JT, D'Antonio JM, Chen S, Antony L, Dalrymple SP, Ndikuyeze GH, Luo J, Denmeade SR. Adaptive auto-regulation of androgen receptor provides a paradigm shifting rationale for bipolar androgen therapy (BAT) for castrate resistant human prostate cancer. *Prostate* 2012; 72: 1491-505.
- [27] Schweizer MT, Antonarakis ES, Wang H, Ajiboye AS, Spitz A, Cao H, Luo J, Haffner MC, Yegnasubramanian S, Carducci MA, Eisenberger MA, Isaacs JT, Denmeade SR. Effect of bipolar androgen therapy for asymptomatic men with castration-resistant prostate cancer: results from a pilot clinical study. *Sci Transl Med* 2015; 7: 269ra2.
- [28] Isaacs JT, Brennen WN, Denmeade SR. Rationale for bipolar androgen therapy (BAT) for metastatic prostate cancer. *Cell Cycle* 2017; 16: 1639-1640.
- [29] Teply BA, Wang H, Luber B, Sullivan R, Rifkind I, Bruns A, Spitz A, DeCarli M, Sinibaldi V, Pratz CF, Lu C, Silberstein JL, Luo J, Schweizer MT, Drake CG, Carducci MA, Paller CJ, Antonarakis ES, Eisenberger MA, Denmeade SR. Bipolar androgen therapy in men with metastatic castration-resistant prostate cancer after progression on enzalutamide: an open-label, phase 2, multicohort study. *Lancet Oncol* 2018; 19:76-86.



Review

Albumin-linked prostate-specific antigen-activated thapsigargin- and niclosamide-based molecular grenades targeting the microenvironment in metastatic castration-resistant prostate cancer



Emmanuel S. Akinboye, W. Nathaniel Brennen, Samuel R. Denmeade, John T. Isaacs*

Department of Oncology, Prostate Cancer Program, The Sidney Kimmel Comprehensive Cancer Center at Johns Hopkins, The Johns Hopkins University School of Medicine, Baltimore, MD, USA

Received 22 May 2018; accepted 6 September 2018
Available online 28 November 2018

KEYWORDS

Albumin-linked prodrug;
Maleimide coupled albumin delivery;
Thapsigargin;
Niclosamide

Abstract Localized prostate cancer is curable via annihilation of the entire cancer neighborhood by surgery or local radiation. Unfortunately, once metastatic, no available therapy is curative. The vast majority will die despite aggressive systemic combinational androgen-ablation therapies. Thus, there is an urgent need for effective systemic therapeutics that sterilize the entire microenvironment in metastatic castration-resistant prostate cancer (mCRPC). To accomplish this goal, advantage can be taken of the unique biology of mCRPC cells. Like their normal cell of origin, mCRPCs retain expression of the prostate-specific differentiation protein, prostate-specific antigen (PSA), which they abundantly secrete into their extracellular fluid (ECF). This unique, and essentially universal, secretion of enzymatically active PSA into the ECF by mCRPCs creates an exploitable therapeutic index for activation of systemically delivered highly lipophilic toxins as “molecular grenades” covalently linked to cysteine-34 of human serum albumin (HSA) via a stable maleimide containing PSA cleavable peptide such that PSA-dependent hydrolysis (*i.e.*, “detonation”) releases the grenades restrictively within the ECF of mCRPC. This approach decreases dose-limiting host toxicity while enhancing plasma half-life from minutes to days (*i.e.*, pharmacokinetic effect) and increasing the tissue concentration of the maleimide coupled albumin delivery (MAD) in the ECF at sites of cancer due to the enhanced permeability of albumin at these sites (*i.e.*, enhanced permeability and

* Corresponding author.

E-mail address: isaacjo@jhmi.edu (J.T. Isaacs).

Peer review under responsibility of Second Military Medical University.

retention effect). This allows the MAD-PSA detonated grenades to circulate throughout the body in a non-toxic form. Only within sites of mCRPC is there a sufficiently high level of enzymatically active PSA to efficiently “pull the pin” on the grenades releasing their lipophilic cell-penetrant toxins from HSA. Thus, if a sufficient level of “detonation” occurs, this will kill mCRPC cells, and sterilize the entire PSA-rich metastatic sites via a bystander effect. In this review, two examples of such MAD-PSA detonated molecular grenades are presented—one based upon thapsigargin and the other on niclosamide.

© 2019 Editorial Office of Asian Journal of Urology. Production and hosting by Elsevier B.V. This is an open access article under the CC BY-NC-ND license (<http://creativecommons.org/licenses/by-nc-nd/4.0/>).

1. Introduction

Donald S. Coffey spent more than 50 years in a quest to conquer cancer, particularly prostate cancer. Along the way, one of the most insightful challenges that Don asked each of the legion of his loyal inspired students, fellows, and faculty colleagues was whether they wanted “to study or cure cancer”. Don realized that this was a loaded question since in order to cure cancer, one needs to be armed with sufficient basic science knowledge about cancer to acquire the “wisdom” needed to identify unique vulnerabilities and thus enable more than a simple empiric approach to the development of novel curative therapies. In addition, Don was a champion for the fact that each organ site-specific cancer presents both unique biological problems and opportunities. This realization led Don to be a strong proponent of organ site-specific basic and translational science. Based upon his inspiration and mentoring, after an initial 2 decades of “studying” prostate cancer to acquire sufficient knowledge, our group has spent the last 2 decades translating this basic science wisdom into novel, rational therapeutic approaches.

2. Problems with metastatic castration-resistant prostate cancer (mCRPC) — Low therapeutic index for standard drugs and tumor heterogeneity

There is an urgent need to develop effective systemic therapeutics for mCRPC patients. Obviously the goal for such therapeutics is to produce death of mCRPC cells without an unacceptable amount of killing or injury to the non-malignant cells in normal host tissues. This is a daunting engineering challenge. Remarkably, modest successes, and even cures, are achieved through the use of non-selective, proliferation-dependent chemotherapeutic poisons in a limited number of cancer types due to their high proliferative rate and low cell death threshold compared to normal tissues [1]. The price for such non-selectivity, however, is dose-limiting host toxicities, particularly myelosuppression, which greatly limits therapeutic efficacy against the more slowly proliferating mCRPC cells. This is particularly relevant since we documented more than 20 years ago that while mCRPC cells have the lowest proliferation rate of any type of human cancer cells (*i.e.*, <5% of these malignant cells are proliferating per

day), they are still eventually lethal since their death rate is even lower (*i.e.*, <3% of cells die per day) [2]. Since the cells of multiple vital normal organs (*e.g.*, skin, bone marrow, and gut) have proliferation rates of >20% of cells per day, there is almost no therapeutic index for standard proliferation-dependent cytotoxic chemotherapy drugs for the systemic treatment of mCRPCs. Over the last 2 decades, two rapid autopsy studies, one at Johns Hopkins University [3] and the other at the University of Michigan [4] have confirmed our earlier cell kinetic data. In our study at Hopkins, the median growth fraction in 117 individual mCRPC sites was 3% and the mean was $(7 \pm 1)\%$ [3]. For the Michigan study, the median growth fraction in 103 individual mCRPC sites was 5% and the mean was $(5 \pm 5)\%$ [4]. These characteristic cell kinetic limitations have led to a profound re-thinking about therapeutic strategies that can activate the proliferation-independent death of mCRPC cells.

Along these lines, cancer cells often acquire an addiction to specific oncogenic signaling pathways that control both their survival and proliferation. For mCRPC, intracellular signaling by nuclear androgen receptor (AR) is the most validated of such oncogenic addictions [5,6]. Thus, novel approaches to block AR signaling are being developed by many investigators in the field. While this is entirely reasonable, there are limitations to such an approach based upon the heterogeneity of AR expression within metastatic sites in individual mCRPC patients. For example, autopsy studies document that AR expression varies widely across mCRPC samples ($n = 265$) with only 31% of tumor samples having >50% of the malignant cells expressing AR while 42% have <10% and 20% have <1% of the malignant cells expressing AR [4]. Overall, this translates to a median of only 20% of the mCRPC cells expressing AR with a mean of $(28 \pm 34)\%$ [4]. These results make the sobering prediction that any treatment which completely inhibits intracellular signaling by nuclear AR will be clinically useful, but probably not curative for the vast majority of mCRPC patients.

3. Rationale for prostate-specific antigen (PSA) targeting of mCRPC

To overcome the curative limitation due to the heterogeneity of AR expression, advantage can be taken of the unique biology of prostate cancer cells. Like their normal cell of origin, prostate cancer cells retain expression of the

prostate-specific differentiation protein, PSA, which they abundantly secrete into their extracellular fluid (ECF) [7]. Autopsy studies document that within 265 samples of metastatic sites from 30 mCRPC patients, none lacked detectable expression of PSA and in half of the samples; at least 50% of the cancer cells express PSA with a median expression of 39% and a mean of $(43 \pm 35)\%$ [4]. PSA is a 33 kD single-chain glycoprotein that is synthesized and uniquely secreted in large quantities by prostate epithelial cells (*i.e.*, expression is nearly 3 log orders higher in prostate than any other tissue in the human body) [8]. PSA is a serine protease with chymotrypsin-like substrate specificity that is found in 100 $\mu\text{mol/L}$ concentrations in the seminal plasma where its major proteolytic substrates are the seminal gel-forming proteins, semenogelin I and II [9]. In collaboration with Dr. Hans Lilja, we used the PSA cleavage map for the semenogelins to identify a peptide with the amino acid sequence His-Ser-Ser-Lys-Leu-Gln-//X (HSSKLQ//X) in which hydrolysis between the carboxyl group of Gln (Q) and the amine of the C-terminal amino acid (*i.e.*, Q//X) is highly restricted to PSA recognition (*i.e.*, PSA >2 logs better hydrolysis rate for this substrate than chymotrypsin or any other known cancer-associated proteinases including elastase, matrix metalloproteinase (MMP)-2, MMP-9, urokinase, plasmin, tissue plasminogen activator, thrombin, human kallikrein 1 (HK1), human kallikrein 2 (HK2), and fibroblast activation protein (FAP) [9]. We used this HSSKLQ//X substrate to document that prostate cancer cells secrete extremely large (*i.e.*, 1.6–2.1 $\mu\text{mol/L}$) amounts of enzymatically active PSA into their ECF [7]. Once in the ECF, PSA eventually enters the blood. However, in the blood, PSA is enzymatically inactivated via covalent binding to the serum protease inhibitors α -1-antichymotrypsin and α -2-macroglobulin, which are present in vast molar (*i.e.*, mmol/L) excess [9]. Importantly, a high level of enzymatically active PSA continues to be secreted into the ECF by prostate cancer cells even in patients with high Gleason grade and/or late-stage mCRPC patients [10]. In fact, it is the continuous increase in the serum level of α -1-antichymotrypsin covalently bound PSA (*i.e.*, “complexed” PSA), which requires enzymatically active PSA, that is used as one of the main markers of clinical progression in such lethal patients [10]. Along these lines, a study from MD Anderson documented that $<3\%$ of metastatic patients (*i.e.*, 100 out of 4145) treated for prostate cancer had disease progression without an elevation in complexed PSA in the serum [11].

The essentially universal secretion of enzymatically active PSA into the ECF by mCRPC cells creates an exploitable therapeutic index for activation of a combination of systemically delivered “molecular grenades” designed so that their hydrolysis (*i.e.*, “detonation”) releases potent lipophilic toxins (*i.e.*, grenades) restrictively within the ECF of mCRPC sites. The chemical engineering requirements for such a combinational PSA-detonated molecular grenade platform is that the individual toxins must be: 1) highly cell penetrant (*i.e.*, lipophilic) when liberated, 2) a potent (*i.e.*, nmol/L) inhibitor of vital, but complementary, intracellular targets (*e.g.*, endoplasmic reticulum [ER] and mitochondria), whose inhibition induces the proliferation-independent death by all cell types, and 3) capable of peptide bond formation with the C-terminal

carboxyl group of Gln (Q) in the HSSKLQ//PSA peptide to form a prodrug (*i.e.*, molecular grenade) that is not toxic until hydrolyzed by PSA. Thus, following systemic dosing, such PSA-detonated molecular grenades circulate throughout the body in an inactive state, but only within sites of mCRPC is there a sufficiently high level of enzymatically active PSA to efficiently “pull the pin” on the grenades releasing the cell penetrant toxins from the peptide. Since this hydrolysis occurs in the ECF, the toxins once liberated rapidly penetrate all cell types in the immediate vicinity due to their lipophilicity and do not re-enter systemic circulation. Thus, if a sufficient level of “detonation” occurs, this will not only kill the mCRPC cells, but sterilize the entire PSA-rich metastatic sites including all of the tumor-infiltrating host cells which are stimulating the lethal cancer growth (*i.e.*, tumor endothelial cells, cancer associated fibroblasts [CAFs] and immunosuppressive mesenchymal stem cells [MSCs], myeloid derived suppressor cells [MDSCs], and regulatory T-cells [Tregs]) [12–14]. An additional advantage of such selective extracellular hydrolysis is that only a fraction of the cells within the tumor microenvironment need to express PSA since its continuous enzymatic activity amplifies the level of cell penetrant toxin liberated in the ECF within the metastatic site. This stoichiometric amplification negates the problem of tumor cell heterogeneity by inducing a substantial “bystander effect” in which, like a detonated grenade, all cells within the tumor site including both malignant and infiltrating host supporting cells are killed, including those that do not express PSA. Thus, development of resistance is retarded without simultaneously producing non-selective toxicity within normal tissue sites. In addition, unlike many other therapeutic strategies in which expression of the molecular target is assumed, but not validated individually, clinical use of such PSA detonated molecular grenades is “personalized” based upon the detection of α -1-antichymotrypsin bound PSA target in the patient’s serum, thereby, validating this precision medicine approach.

4. First generation PSA-activated thapsigargin (TG) molecular grenade

As the first example of this innovative molecular grenade strategy, a chemically-modified analog of the naturally occurring sesquiterpene γ -lactone, TG was chosen. TG (Fig. 1A) isolated from the *Thapsia garganica* plant is highly lipophilic and thus cell permeable [15]. Once inside the cell, TG is a potent inhibitor (IC_{50} 10 nmol/L) of the ER calcium ATPase (*i.e.*, ATP2A2 a. k.a. SERCA 2b) pumps [16]. Our group initially discovered that sustained exposure of human mCRPC cells to TG induces rapid inhibition of their SERCA pumps, resulting in the depletion of the high (*i.e.*, $>500 \mu\text{mol/L}$) Ca^{2+} in their ER, inducing both an ER stress response and a “capacitance entrance” of extracellular Ca^{2+} [17]. This leads to an initial increase in the intracellular free Ca^{2+} (Ca_i) from ~ 40 to >300 nmol/L within minutes followed by a return to baseline over 9–12 h, which is then followed by a delayed sustained increase in Ca_i to $>1 \mu\text{mol/L}$ over the next 18–36 h [18]. The combination of ER stress and a sustained elevation of Ca_i eventually results

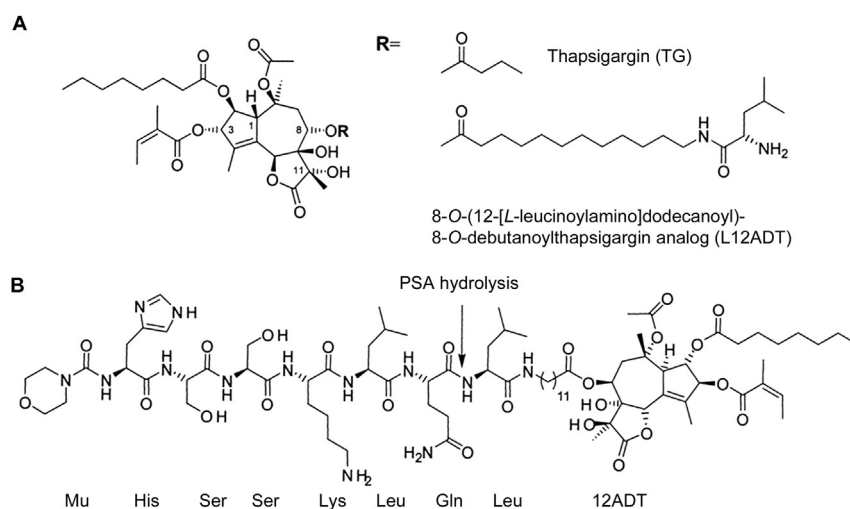


Figure 1 Chemical structures of thapsigargin (TG) and TG prodrug. (A) Structures of TG and L12ADT; (B) Structure of Mu-HSSKLQ//L12ADT. The arrow indicates the site of prostate-specific antigen (PSA) hydrolysis.

within several days in the apoptotic death of mCRPC with a lethal dose which causes 50% cell death (LD_{50}) of <50 nmol/L [17–20]. As part of the death response, TG treatment rapidly depletes AR protein expression in AR-positive mCRPC cells [20]. Importantly, unlike drugs like doxorubicin or taxanes which are much more effective in killing proliferating cells, TG is equally effective in killing both non-proliferating and proliferating cells [20]. Furthermore, TG even kills multidrug resistant cells lacking apoptotic Bak and Bax proteins [21]. Such potent TG-induced killing, however, is not cancer cell specific (*i.e.*, TG kills normal cells equally well) [19]. In particular, TG at <100 nmol/L not only kills human umbilical vascular endothelial cells (HUVECs), but also inhibits sprouting by the surviving cells needed for tumor angiogenesis, as documented using a 3-dimensional HUVEC sprouting assay as we have described previously [22]. Thus, if targeted to sites of mCRPC, TG is an ideal agent to annihilate all the cell types present within the cancer neighborhood (*i.e.*, microenvironment).

To target TG's cell proliferation-independent toxicity to cancer neighborhoods, our group has collaborated with Dr. Søren Brøgger Christensen, one of the original discoverers of TG [15]. Initially, we used an iterative medicinal chemistry approach in which individual side chains of the TG molecule were selectively modified. We determined that position 8 of TG could be modified without significantly affecting SERCA binding. Based upon a combination of enzyme assays, protein crystallography, and *in vitro* efficacy, we determined that a primary amine-containing 8-O-(12-aminododecanoyl)-8-O-debutanoyl thapsigargin analog (12ADT) has an optimal-length side chain for inhibitory binding to the SERCA pump (IC_{50} 10 nmol/L) and is only slightly less lipophilic than TG, and thus has a cytotoxic potency only slightly less (LD_{50} 55 ± 12 nmol/L) than TG (LD_{50} 13 ± 3 nmol/L) [20,23,24]. The advantage of 12ADT, however, is that it can be covalently coupled via a peptide bond between its primary amine to the C-terminal carboxylic acid of Q in the HSSKLQ PSA-hydrolysable peptide. Direct coupling, however, resulted in a conjugate that is not hydrolyzed efficiently by PSA [19]. Subsequently, we

discovered that 12ADT coupled to the C-terminal of leucine (L) to produce L12ADT (Fig. 1A) is more lipophilic and thus more potent (LD_{50} 14 ± 8 nmol/L) than 12ADT. In addition, when the N-terminus of leucine in L12ADT is coupled to the C-terminus of Q in the PSA peptide, the resulting HSSKLQ//L12ADT peptide conjugate (Fig. 1B) is efficiently hydrolyzed (*i.e.*, k_{cat}/K_m ratio of 22) by PSA to liberate L12ADT [19]. Thus, this HSSKLQ//L12ADT peptide conjugate is stable in human plasma and selectively toxic (LD_{50} 74 ± 3 nmol/L) to PSA-producing prostate cancer cells *in vitro* [19].

Pharmacokinetic/pharmacodynamic (PK/PD) and tumor efficacy analyses of human mCRPC xenografts in nude mice documented that this first-generation peptide conjugation (*i.e.*, molecular grenade) functions to solubilize the lipophilicity of TG to allow aqueous systemic intravenous (IV) delivery of the peptide conjugate, and to decrease its penetration into cells at sites lacking enzymatic PSA, thus limiting host toxicity [19]. In fact, the maximum tolerated dose (MTD) for this first generation peptide conjugation was shifted from <1 μ mol/kg for TG to >12 μ mol/kg. A single IV dose of 12 μ mol/kg resulted in a peak serum concentration of 15 ± 1 μ mol/L and a half-life ($t_{1/2}$) of approximately 3 h. Over 24 h, less than 0.5% of the administered peptide–drug conjugate was observed in plasma in the free (*i.e.*, toxic) L12ADT form. When mice bearing growing human mCRPC xenografts were IV dosed daily for 3 days with 12 μ mol/kg, the level of liberated L12ADT in the cancer tissues was 170 ± 58 nmol/L, which is 13 times higher than its *in vitro* LD_{50} [19]. A regimen of five daily IV injections with 12 μ mol/kg dose every 2 weeks resulted in >75% inhibition of the growth of human mCRPC xenografts in mice over a 40 day period without substantial host toxicity, but had no effect on non-PSA producing human renal carcinoma xenografts [19]. However, the therapeutic index for this first generation compound is narrower than anticipated from the *in vitro* studies. While multiple daily doses of 12 μ mol/kg are tolerated, a single dose of 36 μ mol/kg is lethal to mice. Similar non-specific toxicity is observed when this first generation PSA detonated TG molecular grenade was evaluated in a preclinical cynomolgus monkey

toxicology screen. These studies also documented unexpected dose-limiting toxicity. We recently discovered the mechanism for this toxicity is due to the inability of the 6 amino acid PSA carrier peptide to sufficiently neutralize the high lipophilicity of TG, which allows non-selective permeation of the non-hydrolyzed grenade into normal cells in noncancerous tissues. This result is consistent with our protein crystallization studies, which documented that once inside a cell, potent (*i.e.*, nmol/L) binding to and thus inhibition of the SERCA pump occurs even if the amino-dodecanoyl side chain in position 8 of TG is coupled to small peptides [25].

5. Rationale for maleimide coupled albumin delivery (MAD) for PSA-activated TG molecular grenade

To overcome the problem with the first generation TG-molecular grenade's promiscuous cellular uptake, we are taking advantage of the fact that human serum albumin (HSA) has a single reactive free cysteine (cys-34) whose reactivity is so efficient that it has been used to produce albumin-coupled prodrugs for clinical trials [26]. Based upon this realization, a second generation molecular grenade has been designed in which cys-34 of HSA is covalently bound to a "stabilized" maleimide (*i.e.*, 2-fluoro-5-maleimidobenzoate) linker covalently coupled to the N-terminus of the PSA-activated peptide ending in L12ADT, (Fig. 2). As we have reported previously, using 2-fluoro-5-maleimidobenzoate for sulfhydryl coupling to HSA produces a much more stable succinamic acid thioether linkage than compared to the more commonly used N-alkyl maleimides that produce a succinimide thioether ring linkage which undergoes significant spontaneous cleavage by a retro-Michael reaction under physiologic conditions [27]. When this spontaneous succinimide thioether ring cleavage reaction occurs *in vivo*, it results in dose-limiting systemic toxicity as the therapeutic agent is spontaneously released to circulate in the blood to form adducts with other sulfhydryl containing species like glutathione, cysteine, *etc.*; thereby, generating a systemically toxic molecule. In contrast, opening of the succinimide-thioether ring (succinimidyl hydrolysis) to form the succinamic acid thioether results in the generation of a stable drug-protein conjugation with a very long half-life of up to 2 years [27].

Using this specific 2-fluoro-5-maleimidobenzoate strategy for production of a "stabilized" MAD-conjugated second generation PSA detonated grenade accomplishes four goals. First, coupling to HSA prevents non-selective cell permeation to minimize side effects (*i.e.*, toxicity) to non-PSA producing host tissues outside of sites of mCRPC. Second, this coupling greatly increases the serum half-life of the second generation grenade from hours to days (pharmacokinetic effect). Third, blood vessels in sites of cancer are much more permeable to albumin than in normal tissues, and thus coupling to albumin enhances the extracellular concentration of the grenade specifically at sites of mCRPC via a tumor site-specific process known as the enhanced permeability and retention (EPR) effect [28]. Fourth, this MAD approach creates a modular platform for the production of a "family" of PSA-detonated molecular grenades attacking different, but complementary, critical intracellular targets.

6. MAD for PSA-activated nicosamide molecular grenade

While this MAD approach for second generation PSA-activated TG molecular grenades should significantly increase its anti-prostate cancer efficacy, it is unknown whether it will be curative when used as monotherapy. What is clear, however, is that this general MAD approach provides a modular platform for the creation of other PSA-detonated molecular grenades to induce proliferation-independent cell death selectively within sites of mCRPC via complementary, but SERCA pump inhibition independent, intracellular targets. As a complementary target, we have focused on the unique vulnerability of mCRPC cells via their dependence upon "parasitic" co-option of nutrients from their supporting tumor stroma. This occurs because despite activation of tumor angiogenesis, the metabolic needs of the cancer cells eventually exceed the nutrient level provided by the tumor blood supply, producing a compromised tumor microenvironment. Under this stress, the infiltrating stroma cells composed of endothelial cells, macrophages, fibroblasts, and adipocytes undergoes autophagy/mitophagy to liberate energy-rich nutrients like fatty acids and metabolic intermediates like glutamine and lactic acid into the tumor ECF [29]. These metabolites are efficiently parasitized from the ECF due to enhanced expression of the specific plasma membrane transports for

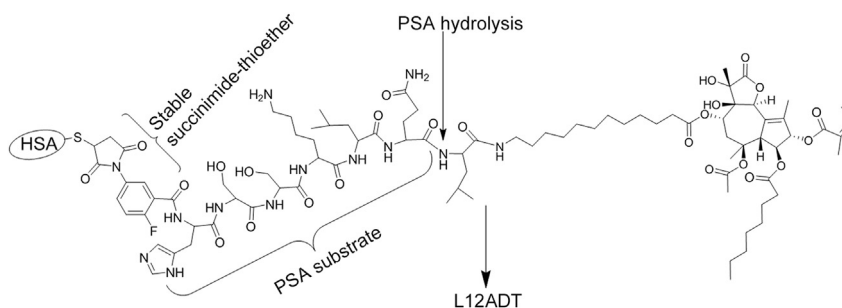


Figure 2 Structure of prostate-specific antigen (PSA) activated prodrug of 8-O-(12-[L-leucinoylamino]dodecanoyl)-8-O-debutanoylthapsigargin analog (L12ADT) with 2-fluoro-5-maleimidobenzamide covalently coupled to the N-terminal of PSA substrate histidine-serine-serine-lysine-leucine-glutamic acid (HSSKLQ).

these substrates by the mCRPC cells [30–32]. In contrast, expression of the plasma membrane glucose transporters is characteristically low in mCRPC cells consistent with their low rate of glucose uptake [33,34]. These results provide a mechanistic explanation for why mCRPC cells characteristically have a low rate of glycolysis and instead derive the majority of their ATP generation from mitochondrial oxidation using a combination of free fatty acid, lactate/pyruvate, and glutamine/glutamate as substrates [35–37]. For these reasons, [^{18}F]-fluorodeoxy glucose (FDG) positron emission tomography (PET) imaging is typically not used in prostate cancer patients due to the frequent presence of FDG-negative metastatic sites. This parasitic nutrient cooption of mCRPC is thus unique compared to other solid malignancies since it is not characteristically driven by a high level of aerobic glycolysis (*i.e.*, lacks the Warburg effect), but instead shunts glucose carbons toward lipogenesis [36]. This is also consistent with why prostate cancer cells have a striking increase in the number and pleomorphism of mitochondria [38–40].

These results support the hypothesis that additional PSA-detonated grenades targeted at inhibiting mitochondria function provides a highly rational target based upon mCRPC cells' unique dependence on "parasitic" nutrient co-option, particularly when combined with ER-targeted PSA-detonated TG grenades. Thus, we are synthesizing a mitochondrial-targeted PSA-detonated grenade based upon the FDA-approved salicylanilide anti-helminthic, niclosamide (Fig. 3A). This lipophilic cell-penetrant compound was originally approved for human use 50 years ago based upon its ability to uncouple oxidative phosphorylation and stimulate ATPase activity in the mitochondria of cestodes (*e.g.*, tapeworms), thus killing these parasites [41]. Subsequently, over the last 5 years, niclosamide had been documented to kill mammalian cells, including mCRPC cells, with an $\text{LC}_{50} < 1 \mu\text{mol/L}$ [41,42]. The mechanism for such cell death includes its ability to collapse the outer mitochondrial membrane potential; thereby, uncoupling oxidative phosphorylation [43–45]. This uncoupling is due to niclosamide's high lipophilicity and thus cell penetration, where it

enters mitochondria to collapse the proton gradient needed for ATP synthesis [46]. This protonophoric effect is dependent upon the pK_a of the aromatic hydroxyl group of niclosamide, which at physiologic pH allows cycling between a neutral and anionic form (Fig. 3A). This is critical since it enables delocalization of the negative charge of the anionic form to maintain its lipophilicity to allow it to cross the outer mitochondrial membrane where the proton dissociates, releasing the neutral form which re-crosses the outer mitochondrial membrane; thus collapsing the proton gradient [45,46].

Using a 3-(4,5-dimethylthiazol-2-yl)-2,5-diphenyltetrazolium bromide (MTT) growth and clonogenic survival assays combined with *in situ* cell staining, we have confirmed that niclosamide not only kills mCRPC cells (*i.e.*, LD_{50} is 600 nmol/L for LNCaP, 800 nmol/L for CRW22-Rv1, 750 nmol/L for PC-3, and 500 nmol/L for LAPC4 human prostate cancer lines), but that this toxicity involves loss of the mitochondrial outer membrane potential detected as a decrease in mitochondrial ability to convert JC-1 dye from a green to a red fluorescence [47]. The well-established mitochondrial uncoupler, carbonyl cyanide 4-(trifluoromethoxy)phenylhydrazone (FCCP), was used for comparison (Fig. 3B). We have also confirmed that when given at 25 mg/kg per day (*i.e.*, 76 $\mu\text{mol/kg}$ per day) for 2 weeks via intraperitoneal injection in 5% Tween-80/5% ethanol/90% phosphate buffered saline (*i.e.*, a non FDA-approved vehicle), niclosamide inhibits the *in vivo* growth of human mCRPC xenografts in nude mice as reported by Alan Gao's group (Fig. 3C) [42]. This inhibition is due to increased cell death within the site of cancer (Fig. 4).

Niclosamide's potent killing ability is not restricted to malignant cells, but also occurs in normal cells including endothelial cells (*i.e.*, LD_{50} for HUVECs is 500 nmol/L). In addition, using a three-dimensional sprouting assay, as we have described previously [22,48], we documented that niclosamide inhibits HUVEC sprouting with an IC_{50} of 200 nmol/L. This raises the serious issue of the therapeutic index for niclosamide as a cancer drug. In addition, a major problem for the clinical development of niclosamide for

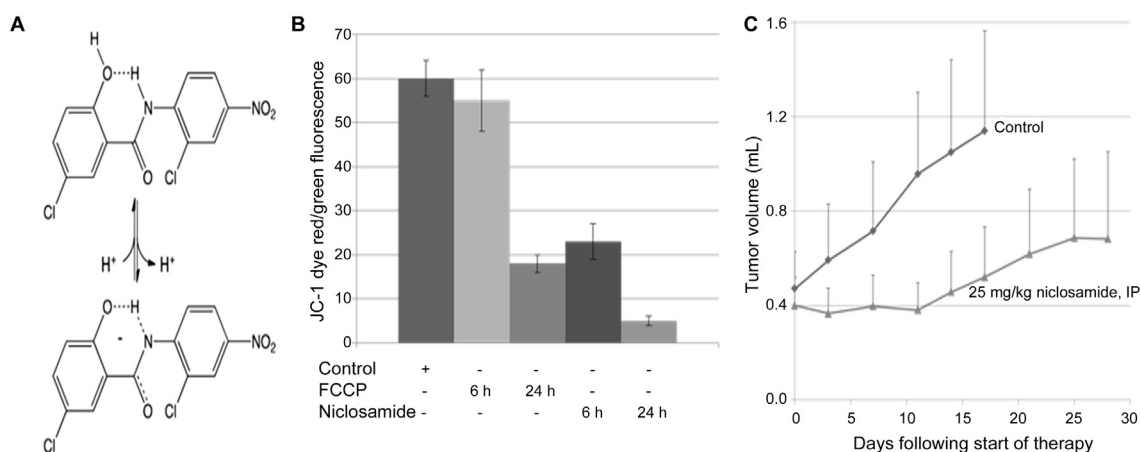


Figure 3 (A) Structure of the anionic vs. neutral form of niclosamide; (B) Loss of mitochondrial outer membrane potential detected as a decrease in JC-1 dye red/green fluorescence ratio; (C) *In vivo* growth inhibition of the CWR-22 human prostate cancer xenograft in nude mice ($n = 10$ per group) by niclosamide given at 25 mg/kg per day (*i.e.*, 76 $\mu\text{mol/kg}$ per day) for 2 weeks via intraperitoneal (IP) injection in 5% Tween-80/5% ethanol/90% phosphate buffered saline. FCCP, 4-(trifluoromethoxy)phenylhydrazone.

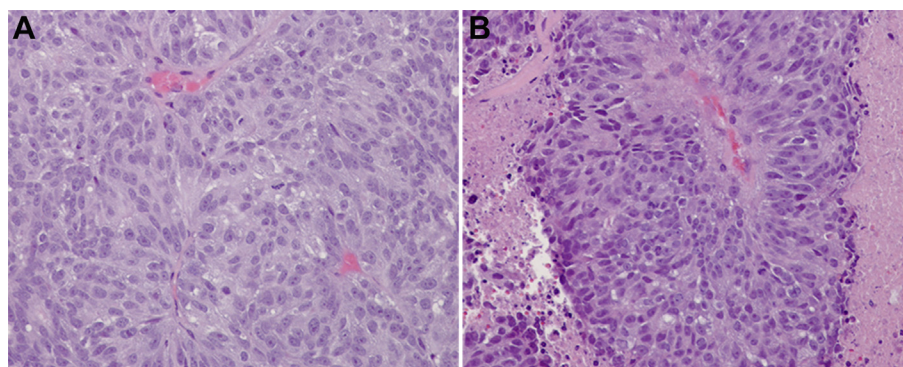


Figure 4 Histology of the CWR-22 human prostate cancer xenograft in vehical control (A) vs. niclosamide (B) treated hosts.

cancer therapy is its poor aqueous solubility (*i.e.*, 0.23 $\mu\text{g}/\text{mL}$ or only 700 nmol/L according to the Merck Index). This is significant as the LD_{50} value for killing cells is essentially equal to niclosamide's water solubility. This makes achieving a therapeutic blood level via IV dosing using FDA-approved vehicles very difficult. To overcome this solubility issue, we coupled a glycyproline (GP) dipeptide (compound 1) to the amine of a self-cleaving linker (SCL), and the resulting compound 2 is then coupled to the critical aromatic hydroxyl group of niclosamide (compound 3) via an ether or carbamate linkage to produce compound 4 [GP-SCL-niclosamide], chemically as described in Fig. 5.

Formation of GP-SCL-niclosamide (compound 4) not only solubilizes niclosamide (*i.e.*, $>100 \mu\text{mol}/\text{L}$) but also prevents anion formation of the aromatic hydroxyl group blocking its protonophoric ability, totally preventing its protonophoric killing ability. In addition, the GP dipeptide-SCL-niclosamide is chosen because it is an excellent substrate for C-terminal cleavage between P and the self-cleaving linker by either dipeptidyl peptidase IV (DPPIV) or FAP expressed within the cancer microenvironment on the plasma membrane of prostate cancer cells [49] or tumor-infiltrating CAFs/MSCs, respectively, as we have documented previously [50–52]. Once compound 4 is hydrolyzed, the liberated SCL-coupled compound undergoes spontaneous self-cleavage; as we have documented previously with other SCL coupled compounds [50,53], liberating

niclosamide with its aromatic hydroxyl group now is able to ionize and thus function as cell penetrant protonophore (Fig. 6). This is documented by the observation that GP-SCL-niclosamide is so efficiently hydrolyzed by DPPIV that it has an essentially identical LD_{50} as niclosamide for killing DPPIV expressing mCRPC cells *in vitro* (600 nmol/L for LNCaP, 800 nmol/L for CRW22-Rv1, and 500 nmol/L for LAPC4 human prostate cancer lines), but no ability to kill normal prostatic basal epithelial cells, which lack DPPIV expression, even at 100 $\mu\text{mol}/\text{L}$.

To further restrict the killing ability of a niclosamide molecular grenade to only sites of mCRPC, we are taking advantage of two additional modifications to compound 4. First, the N-terminal G of compound 4 is being covalently linked to the C-terminal Q in the PSA peptide to produce HSSKLQ//GP-SCL-niclosamide. Since both DPPIV and FAP are endopeptidases and thus require a free N-terminal of G in order to hydrolyze the bond between P and the self-cleaving linker, liberation of niclosamide from HSSKLQ//GP-SCL-niclosamide requires sequential dual hydrolysis by PSA then DPPIV/FAP. Second, as with the thapsigargin approach, the N-terminus of the HSSKLQ//GP-SCL-niclosamide is being covalently linked to cys-34 of HSA via a "stabilized" maleimide (*i.e.*, 2-fluoro-5-maleimidobenzoate) containing linker to produce an HSA-coupled PSA/DPPIV dual-detonated niclosamide grenade (Fig. 7). This is being tested for its systemic anticancer efficacy alone and in combination with the HSA-coupled

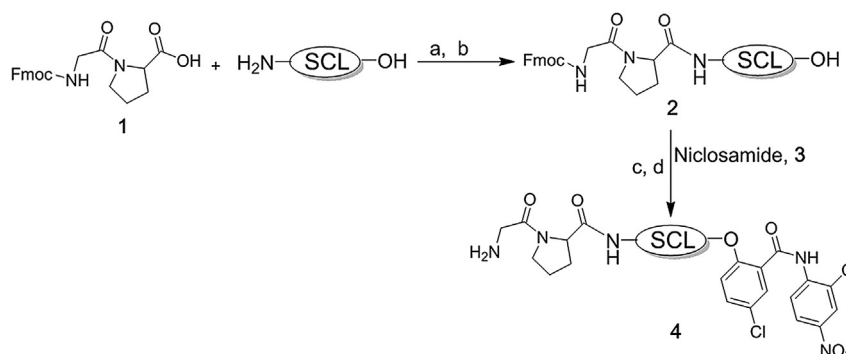


Figure 5 Synthetic scheme for glycyproline (GP) coupling via a self cleaving linkers (SCL) to the aromatic hydroxyl group of niclosamide to produce GP-SCL-niclosamide (*i.e.*, compound 4). SCL, self cleaving linker; a, 2-Ethoxy-1-ethoxycarbonyl-1,2-dihydroquinoline (EEDQ), Dichloromethane N,N-dimethylformamide-dichloromethane (DMF-DCM); b, 25% piperidine in DMF; c, Diisopropyl azodicarboxylate (DIAD), triphenylphosphine (PPh₃), tetrahydrofuran (THF); d, 20% piperidine/DMF.

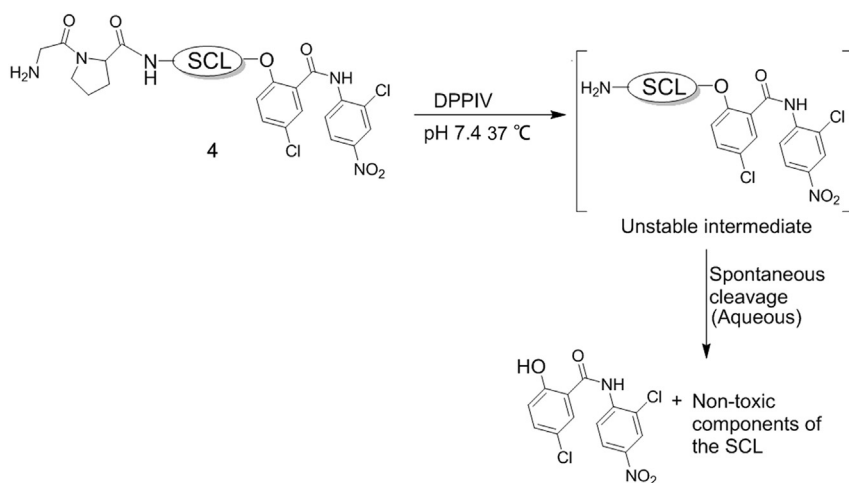


Figure 6 Schematic description of dipeptidyl peptidase IV (DPPIV)/fibroblast activation protein (FAP) activation of compound 4 to liberate niclosamide. SCL, self-cleaving linker.

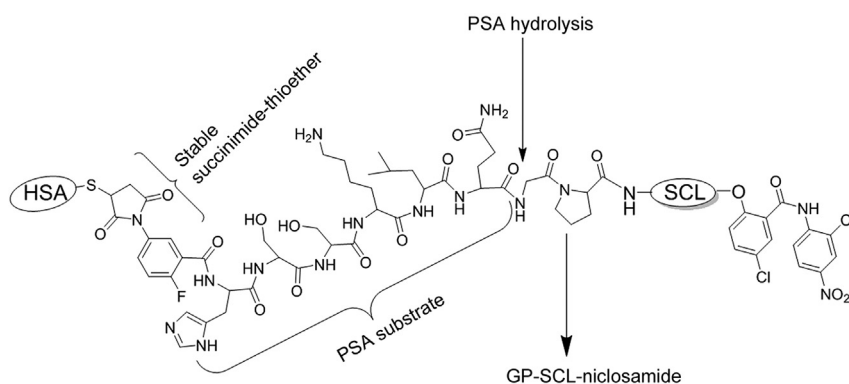


Figure 7 Schematic description of the albumin-linked dual prostate-specific antigen (PSA)/dipeptidyl peptidase IV (DPPIV)-activated niclosamide molecular grenade. HSA, human serum albumin; GP, glycyproline; SCL, self-cleaving linker.

PSA-detonated TG grenade when given intravenously in an FDA-approved vehicle (*i.e.*, saline).

7. Conclusion

While Don Coffey consistently championed the need for continuing expansion of basic science discoveries, he always challenged us to translate basic science discoveries into “cures” for prostate cancer. Along these lines, the rationale for several MAD-linked PSA-activated molecular grenades for targeting metastatic CRPC have been presented. Additional approaches developed by our group using PSA to active recombinant bacterial toxins (*i.e.*, topsalysin) and a prostate specific membrane antigen activated TG prodrug (*i.e.*, mipsagargin) have entered clinical testing [23,54]. Similar approaches exploiting the unique enzymatic activity of other tumor-associated proteases such as FAP are being developed [52].

Author contributions

Study concept and design: Emmanuel S. Akinboye and John T. Isaacs.

Data acquisition: Emmanuel S. Akinboye and John T. Isaacs.

Data analysis: Emmanuel S. Akinboye and John T. Isaacs.

Drafting of manuscript: Emmanuel S. Akinboye and John T. Isaacs.

Critical revision of the manuscript: W. Nathaniel Brennen and Samuel R. Denmeade.

Conflicts of interest

The authors declare no conflict of interest.

Acknowledgments

We would like to acknowledge the Prostate Cancer Foundation, Department of Defense Prostate Cancer Research Program (W81XWH-16-1-0410), NIH Prostate SPORE (P50 CA058236), Patrick C. Walsh Prostate Cancer Research Fund, and the Hopkins-Allegheny Health Network Cancer Research Fund. Also we wish to thank the Cell Imaging Facility, Animal Core Facility, and Tissue Histology Core supported by the SKCCC CCSG (P30 CA006973) for their services and assistance and the Mass Spectrometry and

Proteomics Core facility of the Johns Hopkins School of Medicine.

References

- [1] Shackney SE, McCormack GW, Cuchural GJ. Growth rate patterns of solid tumors and their relation to responsiveness to therapy. *Ann Intern Med* 1978;89:107–21.
- [2] Berges RR, Vukanovic J, Epstein JI, CarMichel M, Cisek L, Johnson DE, et al. Implication of cell kinetic changes during the progression of human prostatic cancer. *Clin Cancer Res* 1995;1:473–80.
- [3] Pinski J, Parikh AG, Bova S, Isaacs JT. Therapeutic implications of enhanced G₀/G₁ checkpoint control induced by coculture of prostate cancer cells with osteoblasts. *Cancer Res* 2001;61:6372–6.
- [4] Shah RB, Mehra R, Chinnaiyan AM, Shen R, Ghosh D, Zhou M, et al. Androgen-independent prostate cancer is a heterogeneous group of diseases: lessons from a rapid autopsy program. *Cancer Res* 2004;64:9209–16.
- [5] Litvinov IV, De Marzo AM, Isaacs JT. Is the Achilles' heel for prostate cancer therapy a gain of function in androgen receptor signaling? *J Clin Endocrinol Metab* 2003;88:2972–82.
- [6] Vander Griend DJ, D'Antonio J, Gurel B, Antony L, Demarzo AM, Isaacs JT. Cell-autonomous intracellular androgen receptor signaling drives the growth of human prostate cancer initiating cells. *Prostate* 2010;70:90–9.
- [7] Denmeade SR, Sokoll LJ, Chan DW, Khan SR, Isaacs JT. Concentration of enzymatically active prostate-specific antigen (PSA) in the extracellular fluid of primary human prostate cancers and human prostate cancer xenograft models. *Prostate* 2001;48:1–6.
- [8] Cunha AC, Weigle B, Kiessling A, Bachmann M, Rieber EP. Tissue-specificity of prostate specific antigens: comparative analysis of transcript levels in prostate and non-prostatic tissues. *Cancer Lett* 2006;236:229–38.
- [9] Denmeade SR, Lou W, Lovgren J, Malm J, Lilja H, Isaacs JT. Specific and efficient peptide substrates for assaying the proteolytic activity of prostate-specific antigen. *Cancer Res* 1997;57:4924–30.
- [10] Schweizer MT, Antonarakis ES, Wang H, Ajiboye AS, Spitz A, Cao H, et al. Effect of bipolar androgen therapy for asymptomatic men with castration-resistant prostate cancer: results from a pilot clinical study. *Sci Transl Med* 2015;7:269ra2.
- [11] Leibovici D, Spiess PE, Agarwal PK, Tu SM, Pettaway CA, Hitzhusen K, et al. Prostate cancer progression in the presence of undetectable or low serum prostate-specific antigen level. *Cancer* 2007;109:198–204.
- [12] Brennen WN, Isaacs JT, Denmeade SR. Rationale behind targeting fibroblast activation protein-expressing carcinoma-associated fibroblasts as a novel chemotherapeutic strategy. *Mol Cancer Ther* 2012;11:257–66.
- [13] Brennen WN, Denmeade SR, Isaacs JT. Mesenchymal stem cells as a vector for the inflammatory prostate microenvironment. *Endocr Relat Cancer* 2013;20:R269–90.
- [14] Brennen WN, Zhang B, Kulac I, Kisteman LN, Antony L, Wang H, et al. Mesenchymal stem cell infiltration during neoplastic transformation of the human prostate. *Oncotarget* 2017;8:46710–27.
- [15] Rasmussen U, Christensen SB, Sandberg F. Thapsigargin and thapsigargin, two new histamine liberators from *Thapsigargin L*. *Acta Pharm Suec* 1978;15:133–40.
- [16] Thastrup O, Cullen PJ, Drøbak BK, Hanley MR, Dawson AP. Thapsigargin, a tumor promoter, discharges intracellular Ca²⁺ stores by specific inhibition of the endoplasmic reticulum Ca²⁺-ATPase. *Proc Natl Acad Sci* 1990;87:2466–70.
- [17] Furuya Y, Lundmo P, Short AD, Gill DL, Isaacs JT. The role of calcium, pH, and cell proliferation in the programmed (apoptotic) death of androgen-independent prostatic cancer cells induced by Thapsigargin. *Cancer Res* 1994;54:6167–75.
- [18] Tombal B, Denmeade SR, Isaacs JT. Assessment and validation of a microinjection method for kinetic analysis of [Ca²⁺]_i in individual cells undergoing apoptosis. *Cell Calcium* 1999;25:19–28.
- [19] Denmeade SR, Jakobsen CM, Janssen S, Khan SR, Garrett ES, Lilja H, et al. Prostate-specific antigen-activated thapsigargin prodrug as targeted therapy for prostate cancer. *J Natl Cancer Inst* 2003;95:990–1000.
- [20] Vander Griend DJ, Antony L, Dalrymple SL, Xu Y, Christensen SB, Denmeade SR, et al. Amino acid containing thapsigargin analogues deplete androgen receptor protein via synthesis inhibition and induce the death of prostate cancer cells. *Mol Cancer Ther* 2009;8:1340–9.
- [21] Janssen K, Horn S, Niemann MT, Daniel PT, Schulze-Osthoff K, Fischer U. Inhibition of ER Ca²⁺ pump forces multidrug-resistant cells deficient in Bak and Bax into necrosis. *J Cell Sci* 2009;122:4481–91.
- [22] Isaacs JT, Antony L, Dalrymple SL, Brennen WN, Gerber S, Hammers H, et al. Tasquinimod is an allosteric modulator of HDAC4 survival signaling within the compromised cancer microenvironment. *Cancer Res* 2014;73:1386–99.
- [23] Jakobsen CM, Denmeade SR, Isaacs JT, Gady A, Olsen CE, Christensen SB. Design, synthesis, and pharmacological evaluation of thapsigargin analogues for targeting apoptosis to prostatic cancer cells. *J Med Chem* 2001;44:4696–703.
- [24] Sohoel H, Jensen AM, Moller JV, Poul Nissen P, Denmeade SR, Isaacs JT, et al. Natural products as starting materials for development of second-generation SERCA inhibitors targeted towards prostate cancer cells. *Bioorg Med Chem* 2006;14:2810–5.
- [25] Denmeade SR, Mhaka AM, Rosen DM, Brennen WN, Dalrymple S, Dach I, et al. Engineering a prostate-specific membrane antigen-activated tumor endothelial cell prodrug for cancer therapy. *Sci Transl Med* 2012;4: 140ra86.
- [26] Kratz F. A clinical update of using albumin as a drug vehicle—a commentary. *J Contr Release* 2014;190:331–6.
- [27] Akinboye ES, Rogers OC, Isaacs JT. 2-fluoro-5-maleimidobenzoic acid-linked albumin drug (MAD) delivery for selective systemic targeting of metastatic prostate cancer. *Prostate* 2018;78:655–63.
- [28] Greish K. Enhanced permeability and retention of macromolecular drugs in solid tumors: a royal gate for targeted anti-cancer nanomedicines. *J Drug Target* 2007;15:457–64.
- [29] Martinez-Outschoorn UE, Pestell RG, Howell A, Tykocinski M, Nagajyothi F, Machado FS, et al. Energy transfer in “parasitic” cancer metabolism. Mitochondria are the powerhouse and Achilles' heel of tumor cells. *Cell Cycle* 2011;10:4208–16.
- [30] Pinthus JH, Lu JP, Bidaisee LA, Lin H, Bryskine I, Gupta RS, et al. Androgen-dependent regulation of medium and long chain fatty acids uptake in prostate cancer. *Prostate* 2007; 1330–8.
- [31] Wang Q, Hardie RA, Hoy AJ, van Geldermalsen M, Gao D, Fazli L, et al. Targeting ASCT2-mediated glutamine uptake blocks prostate cancer growth and tumor development. *J Pathol* 2015;236:278–89.
- [32] Sanita P, Capulli M, Teti A, Galatioto GP, Vicentini C, Chiarugi P, et al. Tumor-stroma metabolic relationship based on lactate shuttle can sustain prostate cancer progression. *BMC Cancer* 2014;14:154.
- [33] Chandler JD, Williams ED, Slavin JL, Best JD, Rogers S. Expression and localization of GLUT1 and GLUT12 in prostate carcinoma. *Cancer* 2003;97:2035–42.

- [34] Jadvar H. Imaging evaluation of prostate cancer with (18)F-fluorodeoxyglucose PET/CT: utility and limitations. *Eur J Nucl Med Mol Imag* 2013;1:s5–10.
- [35] Liu Y, Zuckier LS, Ghesani NV. Dominant uptake of fatty acid over glucose by prostate cells: a potential new diagnostic and therapeutic approach. *Anticancer Res* 2010;30:369–74.
- [36] Zadra G, Photopoulos C, Loda M. The fat side of prostate cancer. *Biochem Biophys Acta* 2013;183:1518–32.
- [37] Panov A, Orynbayeva Z. Bioenergetic and antiapoptotic properties of mitochondria from cultured human prostate cancer cell lines PC-3, DU145, and LNCaP. *PLoS One* 2013;8, e72078.
- [38] Mao P, Nakao K, Angrist A. Human prostatic carcinoma: an electron microscopic study. *Cancer Res* 1966;26:955–73.
- [39] Sun X, Liao NK, YU JJ. Prognostic value of a mitochondrial functional score in prostate cancer. *J Int Med Res* 2012;40:371–6.
- [40] Grupp K, Jedrzejewska K, Tsourlakis MC, Koop C, Wilczak W, Adam M, et al. High mitochondria content is associated with prostate cancer progression. *Mol Cancer* 2013;12:145.
- [41] Li Y, Li PK, Roberts MJ, Arend RC, Samant RS, Buchsbaum DJ. Multi-targeted therapy of cancer by niclosamide: a new application for an old drug. *Cancer Lett* 2014;349:8–14.
- [42] Liu C, Lou W, Zhu Y, Nadiminty N, Schwartz CT, Evans CP, et al. Niclosamide inhibits androgen receptor variants expression and overcomes enzalutamide resistance in castration-resistant prostate cancer. *Clin Cancer Res* 2014;20:3198–210.
- [43] Jin Y, Lu Z, Ding K, Li J, Du X, Chen C, et al. Antineoplastic mechanisms of niclosamide in acute myelogenous leukemia stem cells: inactivation of the NF-kappaB pathway and generation of reactive oxygen species. *Cancer Res* 2010;70:2516–27.
- [44] Park SJ, Shin JH, Kang H, Hwang JJ, Cho DH. Niclosamide induces mitochondria fragmentation and promotes both apoptotic and autophagic cell death. *BMB Rep* 2011;44:517–22.
- [45] Fonseca BD, Diering GH, Bidinosti MA, Dalal K, Alain T, Balgi AD, et al. Structure-activity analysis of niclosamide reveals potential role for cytoplasmic pH in control of mammalian target of rapamycin complex 1 (mTORC1) signaling. *J Biol Chem* 2012;287:17530–45.
- [46] Terada H. Uncouplers of oxidative phosphorylation. *Environ Health Perspect* 1990;87:213–8.
- [47] Reers M, Smiley ST, Mottola-Hartshorn C, Chen A, Lin M, Chen LB. Mitochondrial membrane potential monitored by JC-1 dye. *Methods Enzymol* 1995;260:406–17.
- [48] Brennen WN, Nguyen H, Dalrymple SL, Reppert-Gerber S, Kim J, Isaacs JT, et al. Assessing angiogenic responses induced by primary human prostate stromal cells in a three-dimensional fibrin matrix assay. *Oncotarget* 2016;7:71298–308.
- [49] Wilson MJ, Ruhland AR, Quast BJ, Reddy PK, Ewing SL, Sinha AA. Dipeptidylpeptidase IV activities are elevated in prostate cancers and adjacent benign hyperplastic glands. *J Androl* 2000;21:220–6.
- [50] Akinboye ES, Brennen WN, Rosen MD, Bakare O, Denmeade SR. Iterative design of emetine-based prodrug targeting fibroblast activation protein (FAP) and dipeptidyl peptidase IV (DPPiV) using a tandem enzymatic activation strategy. *Prostate* 2016;76:703–14.
- [51] Aggarwal S, Brennen WN, Kole TP, Schneider E, Topaloglu O, Yates M, et al. Fibroblast activation protein peptide substrates identified from human collagen I derived gelatin cleavage sites. *Biochemistry* 2008;47:1076–86.
- [52] Brennen WN, Rosen DM, Wang H, Isaacs JT, Denmeade SR. Targeting carcinoma-associated fibroblasts within the tumor stroma with a fibroblast activation protein-activated prodrug. *J Natl Cancer Inst* 2012;104:1320–34.
- [53] Kumar SK, Williams SA, Isaacs JT, Denmeade SR, Khan SR. Modulating paclitaxel bioavailability for targeting prostate cancer. *Bioorg Med Chem* 2007;15:4973–84.
- [54] Williams SA, Merchant RF, Garrett-Mayer E, Isaacs JT, Buckley JT, Denmeade SR. A prostate-specific antigen-activated channel-forming toxin as a therapy for prostatic disease. *J Natl Cancer Inst* 2007;99:376–85.